TAMPEREEN TEKNILLINEN YLIOPISTO
TAMPERE UNIVERSITY OF TECHNOLOGY

Anssi Järvinen

Novel Electrical Aerosol Instrumentation for Calibration and Charge Measurement Applications

Julkaisu 1572• Publication 1572

Tampere 2018

Tampereen teknillinen yliopisto. Julkaisu 1572
Tampere University of Technology. Publication 1572

Anssi Järvinen

Novel Electrical Aerosol Instrumentation for Calibration and Charge Measurement Applications

Thesis for the degree of Doctor of Science in Technology to be presented with due permission for public examination and criticism in Tietotalo Building, Auditorium TB109, at Tampere University of Technology, on the 26th of October 2018, at 12 noon.

Tampereen teknillinen yliopisto - Tampere University of Technology
Tampere 2018

Doctoral candidate: Anssi Järvinen, M.Sc.
Laboratory of Physics / Aerosol Physics
Faculty of Natural Sciences
Tampere University of Technology
Finland

Supervisor: Jyrki M. Mäkelä, Professor
Laboratory of Physics / Aerosol Physics
Faculty of Natural Sciences
Tampere University of Technology
Finland

Instructors: Jaakko Yli-Ojanperä, Dr.
Laboratory of Physics / Aerosol Physics
Faculty of Natural Sciences
Tampere University of Technology
Finland

Jorma Keskinen, Professor
Laboratory of Physics / Aerosol Physics
Faculty of Natural Sciences
Tampere University of Technology
Finland

Pre-examiners: M. Matti Maricq, Dr.
Research and Advanced Engineering
Ford Motor Company
United States of America

Juha Kangasluoma, Docent
Institute for Atmospheric and Earth System Research / Physics
University of Helsinki
Finland

Opponent: Alfred Wiedensohler, Professor
Department of Experimental Aerosol and Cloud Microphysics
Leibniz Institute for Tropospheric Research
Germany

ISBN 978-952-15-4195-7 (printed)
ISBN 978-952-15-4220-6 (PDF)
ISSN 1459-2045

Abstract

Aerosol measurements are conducted in several applications, such as in air quality and emission analysis. This thesis focuses on electrical aerosol instrumentation, in which the aerosol detection is achieved by measuring electric current from charged particles. If particle charge is known accurately, the current produced by particles can be used as an accurate and traceable concentration reference in calibration of various aerosol instruments. Additionally, same methods can be applied with small modifications in the measurement of particle charge. These form the main objectives of this thesis, which are to develop particle charge measurement and aerosol instrument calibration methods in a size range from nanometers to micrometers.

In this thesis, the operation of the Electrical Low Pressure Impactor (ELPI+) is introduced. The instrument contains two main components, charger and impactor, which were characterized in calibration measurements. The ELPI+ and the Differential Mobility Analyzer (DMA) were used as a basis of the developed DMA-ELPI particle charge measurement method, in which particles are classified according to their electrical mobility, which is a function of particle size and charge. This is followed by aerodynamic size classification and detection with an ELPI+. The main advantage of the developed method is the wide particle size range compared to other available techniques. The charge measurement was successfully tested using particles with well-defined size distributions and charging states. Additionally, an instrument called BOLAR was developed for studying charge from inhaler-generated particles. The BOLAR is capable of measuring the size fractioned bipolar charging state of aerosol particles. The operation of the instrument was verified with calibration measurements, and the instrument was applied in studying charge of inhaler-generated particles. As a final application of electrical aerosol instrumentation, a new wide size range instrument calibration setup was developed. This included designing and constructing a particle growth unit, an electrical mobility classifier for µm-sized particles and a flow mixing and splitting assembly. All these components were characterized, and the setup was used to calibrate a particle counter traceably in the size range from 3.6 nm to 5.3 µm, which has not previously been possible with any single setup. The introduced high accuracy calibration method can be used as a traceable primary standard for particle number concentration.

Tiivistelmä

Aerosolihiukkasten mittausta tarvitaan useissa sovelluksissa, kuten ilmanlaadun tai päästöjen analysoinnissa. Tässä väitöskirjassa keskitytään sähköisiin aerosolimittausmenetelmiin, joissa varatut hiukkaset mitataan niiden tuottaman sähkövirran avulla. Jos varaustila tunnetaan tarkasti, voidaan hiukkasten tuottamaa virtaa käyttää jäljitettävänä hiukkaspitoisuuden referenssiarvona erilaisten aerosolimittalaitteiden kalibroinneissa. Toisaalta samoja menetelmiä voidaan käyttää hieman muokaten hiukkasten varaustilan tutkimiseen. Näistä tekijöistä muodostuu väitöskirjan päätavoite, joka on kehittää aerosolihiukkasten varausmittausmenetelmiä ja laitteiden kalibrointia nano-mikrometrikokoalueelle.

Tässä väitöskirjassa esitellään sähköisen alipaineimpaktorin (ELPI+) toiminta. Laite koostuu kahdesta pääkomponentista: varaajasta ja impaktorista, joiden toiminta määritettiin kalibrointimittauksilla. ELPI+:n ja differentiaalisen liikkuvuusanalysaattorin (DMA) perustalle kehitettiin DMA-ELPI varausmittausmenetelmä, jossa hiukkaset luokitellaan niiden varauksesta ja koosta riippuvan sähköisen liikkuvuuden mukaisesti ja tämän jälkeen sekä kokoluokitellaan aerodynaamisesti että mitataan sähköisesti ELPI+:lla. Uuden menetelmän suurimpana etuna on erittäin laaja hiukkaskokoalue muihin mittausvaihtoehtoihin verrattuna. Menetelmää testattiin onnistuneesti hiukkasilla, joiden kokojakaumat ja varaustilat olivat tarkasti tiedossa. Väitöskirjatyössä kehitettiin myös laitteistoa inhalaattorien tuottamien hiukkasten varaustilan tutkimiseen. Kyseinen laite, BOLAR, pystyy mittaamaan aerosolihiukkasten bipolaarisen varaustilan kokoluokiteltuna. Laitteen toiminta varmistettiin kalibrointimittauksilla ja laitetta käytettiin myös inhalaattorilla tuotettujen hiukkasten varaustilan tutkimiseen. Työssä kehitettiin lisäksi sähköisiin aerosolimittausmenetelmiin perustuva kalibrointilaitteisto laajalle kokoalueelle. Kalibrointilaitteistoon suunniteltiin ja rakennettiin hiukkasten kasvatusyksikkö, µm-koon hiukkasten sähköinen luokittelija sekä virtausjako. Kaikkien näiden toiminta varmistettiin kokeellisesti ja laitteistoa käytettiin lisäksi hiukkaslaskurin laskentatehokkuuden jäljitettävään primäärikalibrointiin kokoalueella 3,6 nm – 5,3 µm, mikä ei ole aiemmin ollut mahdollista millään yksittäisellä kalibrointilaitteistolla. Kehitetyn kalibrointimenetelmän suuri tarkkuus mahdollistaa sen käyttämisen lukumäärähiukkaspitoisuuden jäljitettävänä primääristandardina.

Preface

Work for this thesis was carried out in the Aerosol Physics research group at Tampere University of Technology under different research projects. I am grateful to Tekes, which funded these projects directly and through the Cluster for Energy and Environment (CLEEN) MMEA-program. I am also grateful to Dekati, GlaxoSmithKline, Pegasor, and the Helsinki Region Environmental Services Authority (HSY), which have been funding and participating in the research projects I have been working with for several years.

Dr. Jaakko Yli-Ojanperä acted as a co-author and instructor in all the included publications. I wish to thank him for guidance from the beginning up to the final stages of this thesis. I also express my gratitude to Prof. Jyrki Mäkelä, who supervised my studies and has always given good advice in various circumstances and to Prof. Jorma Keskinen, who administrated the projects and gave significant contribution to the research work and the article manuscripts. Dr. Matti Maricq and Doc. Juha Kangasluoma pre-examined this thesis and pointed out parts that could be improved. I acknowledge them for the valuable comments they gave.

Co-authors had a significant role in the publications, and I want to thank them for their contribution. Doc. Topi Rönkkö's interest and ambition for science has been vital for acquiring funding for the group, and I am grateful to him for the work he has conducted. This thesis required manufacturing of various custom components. I wish to acknowledge Veli-Pekka Plym, Antti Lepistö and Timo Lindqvist from the workshop for not only manufacturing the components but also guiding me in the mechanical design. I am also grateful to all the Aerosol Physics staff, including Janne Haapanen, my roommate for several years, for creating an encouraging environment to work.

Finally, I would thank my parents for all the support and encouragement, and my friends for bringing other than work-related aspects to my life.

Tampere, August 2018

Anssi Järvinen

Contents

List of Symbols and Abbreviations

Symbols

C_c	Slip correction factor
$C_{c,a}$	Slip correction factor according to aerodynamic diameter
D_a	Particle aerodynamic diameter
D_{50}	Impactor cut diameter
D_p	Particle diameter, particle mobility diameter
e	Elementary charge
E	Impactor collection efficiency
E_i	Impactor stage i collection efficiency
f	Fraction of particles
I	Electric current
I_f	Electric current measured from a filter after an impactor stage
I_i	Electric current measured from an impactor stage
k	Kernel function
L	Length of the DMA classification section
m	Mass
n	Number of elementary charges per particle
N	Particle number concentration
P	Particle penetration
q	Electric charge
Q	Flow rate
Q_{DMA}	DMA inlet flow rate
Q_e	DMA excess flow rate
Q_s	DMA sheath flow rate
R_1	DMA inner radius
R_2	DMA outer radius
s	Impactor collection efficiency curve steepness value
V	Voltage
x	Particle concentration term
Z	Electrical mobility
Z^*	Mean electrical mobility
Z_{FWHM}	Width of the DMA transfer function (Full Width Half Maximum)
β	Bias
η_g	Gas viscosity
η	Detection efficiency
η_{CPC}	CPC detection efficiency
ρ_p	Particle density
ρ_0	Standard density, 1000 kg/m^3

Abbreviations

AD	Analog to Digital
AIST	National Institute of Advanced Science and Technology, Japan
APS	Aerodynamic Particle Sizer
A.U.	Arbitrary Unit
BECU	Bipolar Electrical Collection Unit
BLPI	Berner Low Pressure Impactor
CPC	Condensation Particle Counter
DEHS	Diethylhexyl Sebacate, Dioctyl Sebacate
DMA	Differential Mobility Analyzer
DMPS	Differential Mobility Particle Sizer
DMS	Differential Mobility Spectrometer
DPI	Dry Powder Inhaler
E-SPART	Electrical Single Particle Aerodynamic Relaxation Time Analyzer
EAD	Electrical Aerosol Detector
ECG	Evaporation-Condensation Generator
EEPS	Engine Exhaust Particle Sizer
ELPI	Electrical Low Pressure Impactor
eNGI	Electrical Next Generation Impactor
ESP	Electrostatic Precipitator
FCAE	Faraday Cup Aerosol Electrometer
FCUP	Faraday Cup Filter
FM	Flow Measurement
FMAG	Flow-focusing Monodisperse Aerosol Generator
GSD	Geometric Standard Deviation
HV	High Voltage
IAG	Inkjet Aerosol Generator
METAS	Federal Institute of Metrology, Switzerland
MFC	Mass Flow Controller
NSAM	Nanoparticle Surface Area Monitor
OPC	Optical Particle Counter
PSL	Polystyrene Latex
PTH	Pressure, Temperature, Humidity
SCAR	Single Charged Aerosol Reference
SI	Système International, the International System of Units
SMPS	Scanning Mobility Particle Sizer
VOAG	Vibrating Orifice Aerosol Generator
USP	United States Pharmacopeia

List of Publications

This thesis is based on following peer-reviewed publications:

I. Järvinen A., Aitomaa M., Rostedt A., Keskinen J., and Yli-Ojanperä J. (2014). Calibration of the New Electrical Low Pressure Impactor (ELPI+), Journal of Aerosol Science, 69, 150-159.

II. Järvinen A., Heikkilä P., Keskinen J., and Yli-Ojanperä J. (2017). Particle Charge-size Distribution Measurement Using a Differential Mobility Analyzer and an Electrical Low Pressure Impactor, Aerosol Science and Technology, 51, 20-29.

III. Yli-Ojanperä J., Ukkonen A., Järvinen A., Layzell S., Niemelä V., and Keskinen, J. (2014). Bipolar Charge Analyzer (BOLAR): A New Aerosol Instrument for Bipolar Charge Measurements, Journal of Aerosol Science, 77, 16-30.

IV. Järvinen A., Keskinen J., and Yli-Ojanperä J. (2018). Extending the Faraday Cup Aerosol Electrometer Based Calibration Method up to 5 µm. Aerosol Science and Technology, 52, 828-840.

Author’s Contribution

Author's contribution to the publications included in the thesis:

I. The author and Miika Aitomaa conducted the measurements and wrote significant parts of the manuscript. The author finalized the manuscript and did the improvements that were suggested in the reviewing process.

II. The author planned and performed the measurements, conducted the data-analysis and wrote major part of the publication. Paavo Heikkilä developed the inversion algorithm and the computing code, which solves the charge distribution.

III. The author conducted the impactor and flow splitter measurements, data-analysis for these, and participated in writing the publication. Jaakko Yli-Ojanperä participated in instrument development, tested the collection tubes and wrote a major part of the publication. Ari Ukkonen participated in instrument development, conducted the inhaler measurements, and participated in the writing process.

IV. The author designed the new components of the measurement system including the particle classifier, conducted all the measurements, data-analysis and wrote most of the publication.

1 Introduction

Aerosol particles are solid or liquid material dispersed in a carrier gas. They have both adverse and beneficial characteristics. Aerosol particles have been linked to harmful health effects (Dockery et al. 1993, Beelen et al. 2014). These include for instance respiratory diseases and cardiovascular or cardiopulmonary diseases (Pope et al. 2002, Miller et al. 2007, Badyda et al. 2016, Stockfelt et al. 2017). As a result, limits for outdoor air particle concentrations have been set (e.g. European Commission 2008), and particle emissions from vehicles are tightly regulated (e.g. European Commission 2011). In contrast, while some aerosols have harmful properties, aerosolized pharmaceuticals are frequently used to treat pulmonary diseases (e.g. Ali 2010). In industrial applications, aerosol processes (e.g. Athanassiou et al. 2010) provide means for fast production of engineered nanomaterials in large quantities. In atmosphere, aerosols affect climate directly and through interaction with clouds (Boucher et al. 2013).

Both the scientific community and the regulators need accurate aerosol measurements. Perhaps the most common aerosol measurement is related to particle concentration, typically mass or number concentration. Particle mass concentrations are routinely measured for instance in air quality monitoring stations, whereas the particle number concentrations are often measured in general aerosol research. Particle size is a major factor affecting particle motion and interaction with other particles and surfaces. For instance, deposition into the respiratory track is significantly affected by the particle size. Particle formation process affects the particle size, and different processes often produce particles in different size ranges. The particle size analysis is a basis of typical aerosol research in combination with the concentration measurement.

Particle electric charge is a factor that affects particle motion through electric effects. For instance, the lung deposition of particles depends not only on size but also on electric

charge (Balachandran et al. 1997). Particles may acquire electric charge during the formation process or through interaction with ions. Particle charging is an essential technique especially in electrical size measurement, electrical concentration measurement, and electrostatic precipitation.

The charging state of aerosol particles of known diameter is often measured using a combination of electrical classification and a particle detection instrument. The detection instruments have been limiting the size range of minute-scale measurements to small sub-50 nm particles (Maricq 2004) or to large optically detectable particles (Emets et al. 1991, Vishnyakov et al. 2016). The intermediate size range from approximately 50 to 300 nm has been covered with a method utilizing dual electrical classification (Kim et al. 2005, Maricq 2005), which is a slow method with a measurement duration of tens of minutes. Therefore, a single charge measurement method, which is fast and operates in the size range from nanometers to micrometers, would be highly beneficial.

Inhalers produce charged particles. Advanced measurement methods have been capable of measuring either the size fractioned net charge (Kwok and Chan 2008) or the bipolar charge from the entire aerosol (O'Leary et al. 2008) but not the both polarities as a function of the particle size. The lung deposition is a function of both size and charge. Hence, a method capable of measuring both polarity particles as a function of the particle size would provide the information needed in the development of inhalers and inhalable pharmaceuticals.

Accurate particle concentration measurements are only possible if instruments are calibrated, i.e. the instrument reading is compared to a reference, which is traceable to the base units of the International System of Units (Système International, SI). Aerosol instruments measuring particle concentration operate in a wide size range. Some instruments are capable of measuring particles close to 1 nm in diameter (e.g. Vanhanen et al. 2011, Kangasluoma et al. 2015, Hering et al. 2017) and some instruments measure particles with a diameter exceeding 10 µm (e.g. Baron 1986). Simultaneously, particle number concentration may vary from less than 1 $1/cm^3$ to over 10^8 $1/cm^3$. From the calibration point of view, both the wide size and concentration ranges are challenging.

Calibrations have been traditionally conducted with charged particles in the size range below 100 nm. Particles are introduced to the instrument and to the reference, which is an electrically measured filter. The electric current from the filter is used as a reference signal for the particle number concentration. With careful particle generation, the size range of this electrical method has been previously extended up to 1 µm (Yli-Ojanperä et al. 2012). At sizes above 1 µm, calibrations have been based on optical detection of particles or highly controlled generation of particles (Iida et al. 2014). These methods cannot be used at high particle concentrations. As a result, some instruments cannot be

calibrated using present methods. A single calibration setup operating from nm-range to µm-range with high maximum particle concentration and high accuracy would enable calibration of various types of instruments.

1.1 Research objectives and scope of the thesis

The two major objectives of this thesis were:

- To develop a particle charge measurement technique with a size range from nanometers to micrometers, and an instrument for analyzing bipolar charge from inhaler-generated particles.

- To develop an aerosol instrument calibration method covering a wide size range from nanometers up to micrometers.

The first objective is approached by developing two new charge measurement methods. The method utilizing the Differential Mobility Analyzer (DMA) and the Electrical Low Pressure Impactor (ELPI), was first developed and then evaluated in the size range from 30 to 800 nm (**Paper II**). Such a size range has not been achievable with any single method. The challenge in developing the DMA-ELPI charge measurement method is how to combine the electrical mobility classification to the ELPI size and concentration measurement. The method must be also tested by measuring response to particles of known size and charge. Another new charge measurement technique was developed for µm-sized inhaler-generated particles. A new commercial instrument utilizing this technique, BOLAR, was introduced and characterized (**Paper III**). Previously, there has not been an instrument available for such an application. Inhalers produce particles during short bursts, which requires a fast real-time measurement with parallel measurement channels. These channels contain components that must be characterized experimentally, which is a laborious task.

The second objective of the thesis takes its motivation from the practical need in the calibration of wide size range instruments (e.g. Yli-Ojanperä et al. 2012). Calibration of an aerosol instrument with multiple different reference methods in a conventional way is both challenging and time consuming. This was the case of the ELPI+ calibration (**Paper I**). To simplify the calibration procedure and to increase the calibration accuracy, a new primary calibration system was developed to cover a particle size range from 3.6 nm to 5.3 µm (**Paper IV**). Similar size range has been previously covered only by multiple

methods with lower particle concentrations in the µm sizes. The main challenge in the development is in the µm-size range. The setup requires a custom DMA, as commercial instruments are not available for this size range. The DMA dimensions must be large if µm-sized particles are classified using reasonable flow rates. The construction is difficult because the manufacturing tolerances are small compared to the size of the DMA. The electrical calibration requires splitting of the aerosol flow between the instrument and the reference. This must be constructed in a way that particle losses are small and equal for the instrument and reference lines. The operation of all these components must be also verified experimentally.

The following Chapter 2 introduces the theoretical background of the aerosol instrumentation applied in this thesis. Chapter 3 focuses on conventional calibration methods, and includes the calibration of the ELPI+ as this instrument is later used in the charge measurements. Chapter 4 concentrates on particle charge measurement methods, and includes introduction and evaluation of the DMA-ELPI charge measurement method and the BOLAR instrument for studying charge distributions of inhaler-generated particles. In Chapter 5, primary calibration of aerosol instruments is first discussed. Then, the developed calibration system is introduced, evaluated, and applied in an example calibration. The final Chapter 6 contains a summary and outlook of the research topic.

2 Aerosol instrumentation

This chapter introduces the background of the main aerosol instrumentation techniques applied in this thesis. First, the main electrical instrumentation techniques are explained including particle charging and chargers, particle size classification and electrical detection methods. Instruments utilizing these techniques are also introduced, and a brief overview is given to the particle generation methods relevant to this thesis.

2.1 Particle charging and chargers

In diffusion charging, particles acquire electric charges through collisions with free gas-phase ions. Gas-phase ions are generated by ionizing the carrier gas, which is often air. Production of an ion pair in air requires on average 32 eV of energy (Loeb 1955). In nature, sources for this amount of energy include cosmic rays and radiation from the ground in large scale (Tammet 2007). In instruments, e.g. radioactive sources, electric discharges and X-rays can produce this level of energies. The radioactive ion sources include for instance α-active ^{241}Am and ^{210}Po, as well as β-active ^{63}Ni and ^{85}Kr (Flagan 2001). As the transportation of radioactive material is restricted, X-ray sources are used to substitute radioactive ionization in aerosol charging (e.g. Shimada et al. 2002) but the radioactive charging has remained as the standard ionization method in aerosol instruments. Some instruments utilize ionization with an electric discharge, often a corona discharge.

Simplified schematics of a bipolar charger based on the radioactive source and a corona charger are presented in Figure 2.1. Radioactive bipolar chargers are simply aerosol

chambers containing α- or β-active sources. The radiation from the source ionizes the gas in the chamber. The ionization process produces both positive and negative ions, which diffuse onto particles. As both ion polarities are present, radioactive chargers provide bipolar charging. In corona chargers, the charging ions are produced by an electric discharge from a high voltage electrode. The discharge occurs when the electric field around a sharp object, in this case a corona wire or a corona needle, exceeds the gas dielectric strength. The discharge in the electrical breakdown region produces the ions. Due to the electric field, the electrode collects ions having an opposite polarity to the electrode, while the ions with the same polarity drift away from the corona electrode and participate in the charging process. As the charging ions are unipolar, the corona charger provides unipolar particle charging. The ions charge particles mostly by diffusion process but the electric field may also contribute through field charging process. There are various corona charger constructions (Intra and Tippayawong 2011), and from these, a needle type construction is presented in Figure 2.1.

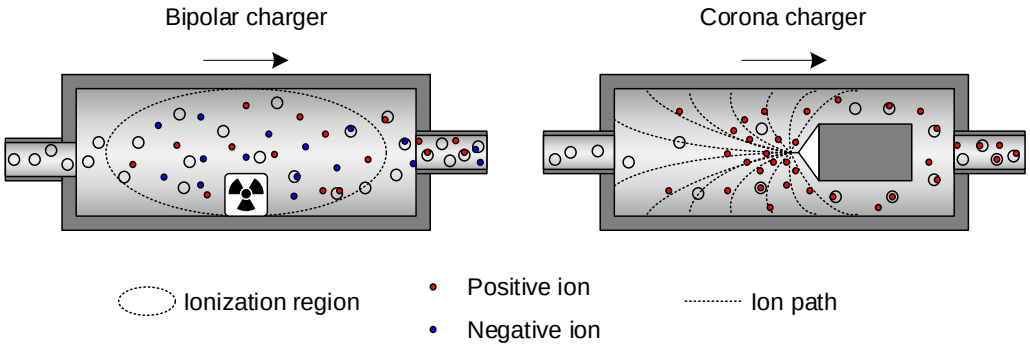

Figure 2.1 Illustration of a radioactive bipolar charger and a unipolar corona charger (needle type with positive polarity). The arrow indicates the flow direction.

Diffusion is the prevailing charging mechanism for nanoparticles. In electrical aerosol instrumentation, a well-known charge distribution is often crucial. The stationary bipolar charge distribution is calculated according to Fuchs (1963) limiting sphere model, which is complex, and has been approximated by Wiedensohler (1988). The approximation is in a form of

$$f(n) = 10^{\sum_{i=0}^{5} a_i(n) \cdot \left(\log \frac{D_p}{nm} \right)^i}, \qquad (1)$$

where f is the fraction of particles, n the number of elementary charges, a_i the approximation coefficient and D_p the particle diameter in nm. The Equation 1 is defined

for stationary case, which is achieved if the concentrations of both polarity ions are equal and the ion concentration is high enough compared to the residence time in the charger. If particles are initially charged or the ion concentration is not significantly higher than the particle concentration, the equation may not predict particle charge accurately (de La Verpilliere et al. 2015).

The unipolar corona charging is a more complicated process to represent mathematically than the bipolar diffusion charging. Theoretical models (e.g. Biskos et al. 2005a, Domat et al. 2014) have been used to describe the operation of the corona charger. These models use the product of the ion concentration and the residence time as an input parameter. Evaluation of this parameter is challenging, which limits the use of these models. Therefore, experimental verification of a corona charger is often required.

The charge distributions of bipolar and corona charger differ significantly as shown in Figure 2.2. The bipolar charger produces low levels of charge. The fraction of uncharged particles is high even at 100 nm diameter and fractions of singly and doubly charged particles are rather low. For instance, the maximum fraction of positively singly charged particles is only 23 % at 100 nm diameter. The unipolar corona charger, analyzed by Kaminski et al. (2012), provides significantly higher charge than the bipolar charger, and the amount of multiply charged particles increases significantly as the particle diameter increases.

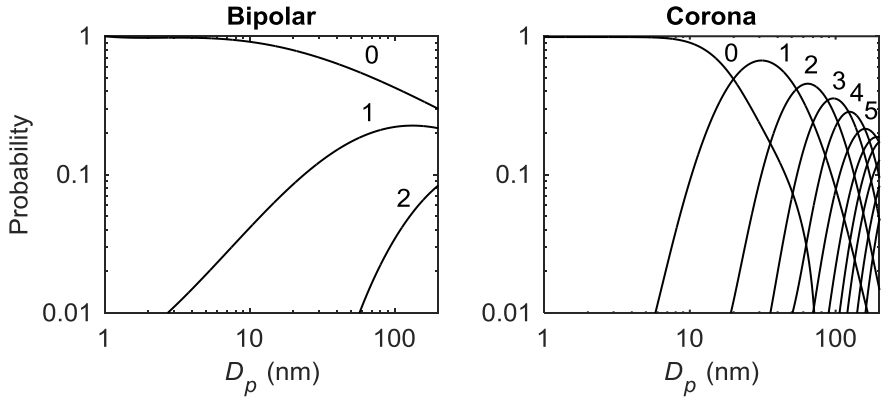

Figure 2.2 Charge distributions of positively charged particles for a bipolar charger according to Wiedensohler (1988) approximation and for a specific corona charger according to Kaminski et al. (2012) model. The lines represent the probability of the corresponding charge given as a number of elementary charges per particle.

A term charging efficiency is used to describe the operation of an aerosol charger. There are several different definitions for the charging efficiency (Marquard et al. 2006), which express the proportion of the charged particles. However, the proportion of the charged particles does not describe the current carried by particles, because the current depends also on the magnitude of the particle charge. Thus, the output of the corona charger is evaluated by measuring the current carried by the particles *I*, which may be expressed with a rather simple equation

$$I = PnNeQ\,, \tag{2}$$

where *P* is the penetration of particles through the charger, *n* the average number of elementary charges per particle, *N* the inlet number concentration, *e* the elementary charge and *Q* the flow rate through the charger (Marjamäki et al. 2000).The *Pn* is dimensionless and particle size dependent value describing charger operation. It is often approximated with a power function

$$Pn = a \cdot D_p^{\,b}\,, \tag{3}$$

where *a* and *b* are fitted parameters for a certain size range. The *b* typically ranges between 1 and 1.5 at 100 nm particle diameter depending on the charger construction to some extent.

The charging state of particles is often expressed through the number of elementary charges per particle *n*. In this thesis, this value may refer to a characteristic non-integer value of a particle distribution (e.g. Equation 2), to a non-integer value used to express charge distributions (e.g. Figure 4.4) or to an exact integer value defined for single particles (e.g. Equation 4).

2.2 Size classification

The following paragraphs introduce principles of the electrical mobility classification and aerodynamic classification in an impactor, which are the principal size classification methods in this thesis.

Electrical mobility analysis classifies charged particles according to their electrical mobility *Z*, which is linked with the particle diameter D_p, through an equation

$$Z = \frac{neC_c}{3\pi\eta_g D_p}, \quad (4)$$

where n is the number of elementary charges per particle, e the elementary charge, C_C the slip correction factor and η_g the viscosity of the carrier gas (Flagan 2001). In particle size analysis, the particle diameter D_p is solved from Equation 4 but this equation allows also the determination of the particle charging state, which is obtained by solving the n from this same equation.

Electrical mobility analysis is possible through using various flow and electrode configurations (Tammet 1970). The following paragraphs introduce the two electrical mobility analyzer constructions, which are used in this thesis.

Integrating (zero-order) analyzer (e.g. Tammet 1970) consist of two electrodes as illustrated in Figure 2.3A. One electrode is at high potential and the other one at low potential, which generates an electric field between the electrodes. This electric field, in combination with the flow, classifies particles according to their electrical mobility and polarity. As such, this device is an electrostatic precipitator (ESP), which only removes charged particles. However, this construction turns into an instrument when electric current is measured from at least one of the electrodes that collect the particles.

Nowadays, the normal electrical classification instrument is the Differential Mobility Analyzer (DMA, Knutson and Whitby 1975), which is an instrument capable of selecting a certain electrical mobility band. The operation principle of a cylindrical DMA is illustrated in Figure 2.3B. DMAs are operated with two input flows and two output flows. The polydisperse input flow contains the particles to be classified. A high voltage electrode generates an electric field in the classification region. This electric field pulls charged particles towards the central electrode through the particle-free sheath flow. Only the particles having the correct electrical mobility can be extracted from the slit in the central electrode. Too high electrical mobility causes particles to collide on the central electrode and too low mobility particles do not drift close enough the slit to be extracted into the monodisperse flow.

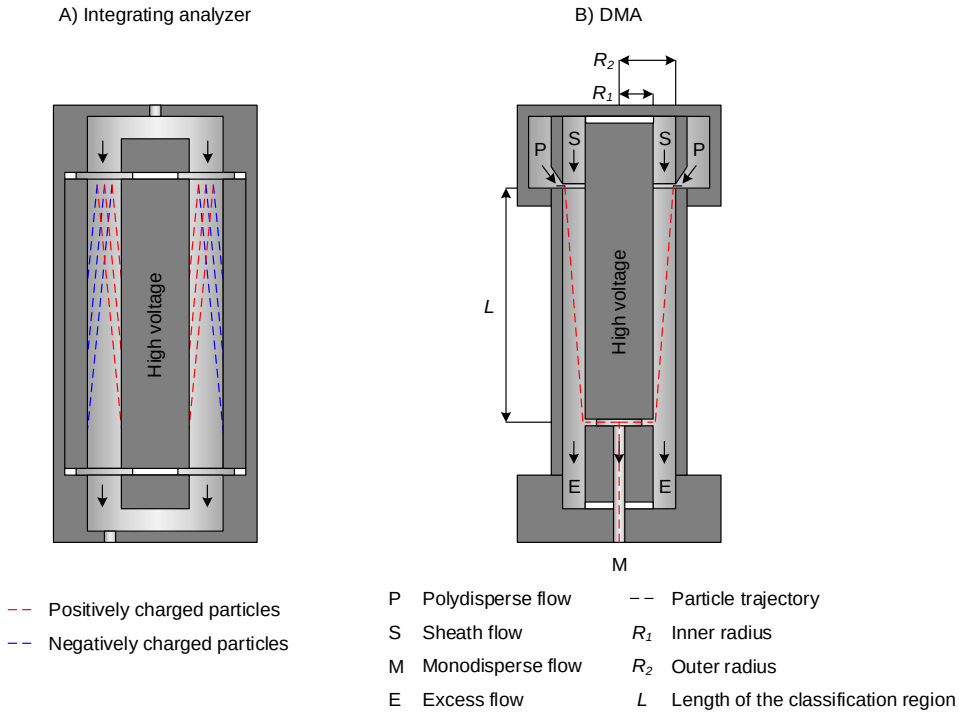

Figure 2.3 Integrating analyzer (A) and DMA (B). The particle trajectories are given for negative high voltage. The particle trajectory in figure (B) is illustrated for particles having an electrical mobility in the DMA pass band.

Ideal transfer functions of an integrating analyzer and a DMA are shown in Figure 2.4. Integrating analyzer (e.g. Tammet 1970) has a distinct critical mobility Z_c. If the particle electrical mobility is higher than this, the analyzer collects all the particles. If the particle mobility is lower than the critical mobility, the analyzer transfer function depends on the particle electrical mobility. The transfer function of the DMA (Knutson and Whitby 1975) differs significantly from the integrating analyzer. The DMA has a specific pass band at a certain electrical mobility. In the ideal case, the width of the transfer function depends on the flow rates. In both analyzer types, the real transfer functions are affected by inconsistent flow rates in the classification region and diffusion, which affects especially small sub-10 nm particles and ions. Often, the real transfer functions resemble the ideal ones but the sharp corners of the transfer functions are rounded.

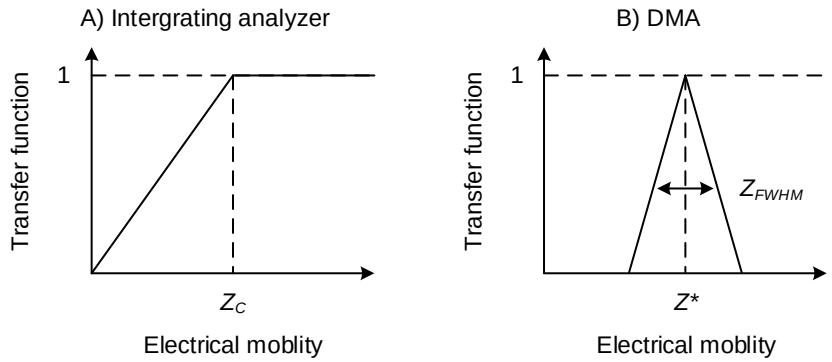

Figure 2.4 Ideal transfer function of an integrating analyzer (A) and a DMA (B). Z_c refers to the critical mobility, Z^* to the central mobility of the pass band and Z_{FWHM} to the width of the DMA transfer function (Full Width Half Maximum). Modified from Tammet (1970) and Knutson and Whitby (1975).

In both analyzers, the measured electrical mobility is a function of dimensions, voltage and flow rates. Often the measurement of the mobility spectrum is achieved by changing the voltage, while the dimensions and flow rates are kept constant.

For a cylindrical DMA, the midpoint of the mobility pass band Z^* is calculated from an equation

$$Z^* = \frac{Q_s + Q_e}{4\pi LV} \ln \frac{R_2}{R_1}, \tag{5}$$

where Q_s is the sheath flow rate, Q_e the excess flow rate, L the length of the classification region, V the classification voltage, R_1 the inner radius of the classification region and R_2 the outer radius (Knutson and Whitby 1975).

Equations 4 and 5 link the instrument parameters to the particle diameter and enables the electrical-mobility-based particle size analysis. The challenging factor is that the number of elementary charges per particle must be known accurately as the measured electrical mobility is directly proportional to this quantity.

The importance of the particle size analysis has led different research groups to develop special DMAs. Winklmayr et al. (1991) developed series of DMAs, which operate in different size ranges. Chen et al. (1998) developed a DMA for small particles from 3 to 50 nm. After this, DMAs have been designed for even smaller particles, clusters and ions (e.g. Rosser and Fernández de la Mora 2005).

Aerodynamic classification measures particle aerodynamic diameter D_a, which can be calculated from equation

$$D_a = D_p \left(\frac{C_c}{C_{c,a}} \right)^{\frac{1}{2}} \left(\frac{\rho_p}{\rho_0} \right)^{\frac{1}{2}}, \quad (6)$$

where C_c is the slip correction factor according to the particle diameter, $C_{c,a}$ the slip correction factor according to the aerodynamic diameter, ρ_p the particle (effective) density, and ρ_0 the unit density of 1000 kg/m^3 (Baron and Willeke 2001).

Impactor is a device, which collects particles according to their aerodynamic diameter (Marple and Olson 2011). The operation of a single jet impactor is shown in Figure 2.5. Particles are accelerated in a nozzle, and the jet from the nozzle hits the collection plate. Large or heavy (high density) particles impact the collection plate due to their large aerodynamic diameter, whereas small or light (low density) particles follow the gas flow and are not collected.

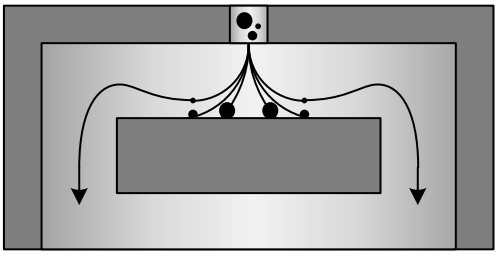

Figure 2.5 Illustration of a single jet impactor stage collecting particles according to their size.

The collection efficiency of a single impactor stage can be represented with a collection efficiency curve (e.g. Marjamäki 2003, Arffman 2016), see Figure 2.6. Ideal impactor has a certain cut diameter D_{50} given as an aerodynamic diameter. Particles larger than this are collected by impaction and particles smaller than this pass the stage. In a real impactor, there is some particle collection below the cut diameter, and above the cut diameter, some of the particles are not collected. As a result, the collection efficiency curve has often an S-shape. The main characteristic of the cut curve is the cut diameter D_{50}, which is the aerodynamic diameter with a 50 % collection efficiency. Around the cut diameter, particles are collected by impaction, but impactor collects particles also by other means than impaction, for instance by diffusion and electrostatic effects (Virtanen et al. 2001). This secondary collection efficiency, now discussed from the diffusion point

of view, occurs only at small particle sizes, as the diffusion of large particles is minimal. Impactor classifies particles according to their aerodynamic diameter but the secondary collection efficiency by diffusion depends principally on the particle diameter, not the aerodynamic diameter. Additionally, if the particle is significantly larger than the cut diameter, it may bounce from the collection plate. Bouncing may also occur around the cut diameter, and various techniques including for instance coating of the collection substrates with adhesive material are used to prevent this (Chang et al. 1999).

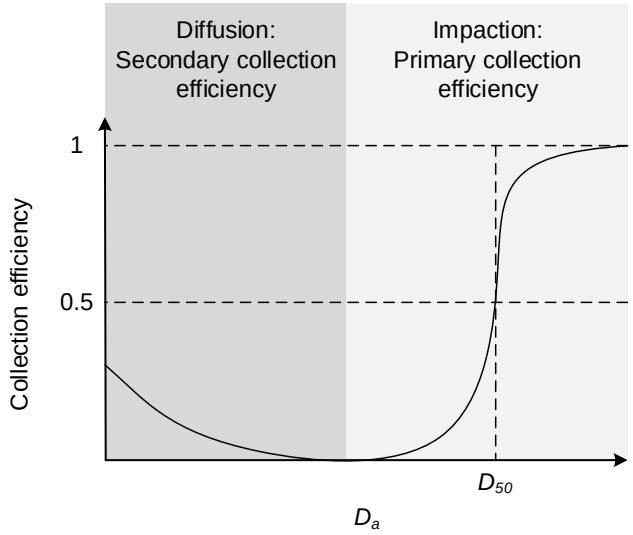

Figure 2.6 Characteristic collection efficiency curve of an individual impactor stage. Impaction depends on the particle aerodynamic diameter D_a, and the D_{50} refers to the stage cut diameter. Secondary collection efficiency due to diffusion depends principally on particle diameter D_p, not on aerodynamic diameter D_a. Modified from Marjamäki (2003) and Arffman (2016).

In a cascade impactor (May 1945), multiple impactor stages with different cut diameters are assembled in series with decreasing cut diameter as shown in Figure 2.7. In an ideal cascade impactor, the first stage collects particles larger than the stage cut diameter. Then, the following stage collects particles larger than its cut diameter. Now, size range collected by the second stage is from its cut diameter to the cut diameter of the first stage. This continues until the last stage. In a real case, the collection efficiency curve of each stage is not sharp as discussed previously. The effect of non-ideal collection characteristics and the effect of previous stages is taken into account in the kernel functions, also illustrated in Figure 2.7. The kernel function *k* for stage *i* is calculated from equation

$$k_i\left(D_a\right) = E_i\left(D_a\right)\prod_{j=i+1}^{N}\left[1-E_j\left(D_a\right)\right], \tag{7}$$

where E is the collection efficiency curve, D_a the aerodynamic diameter, j the index number and N the total number of stages (Marjamäki et al. 2003).

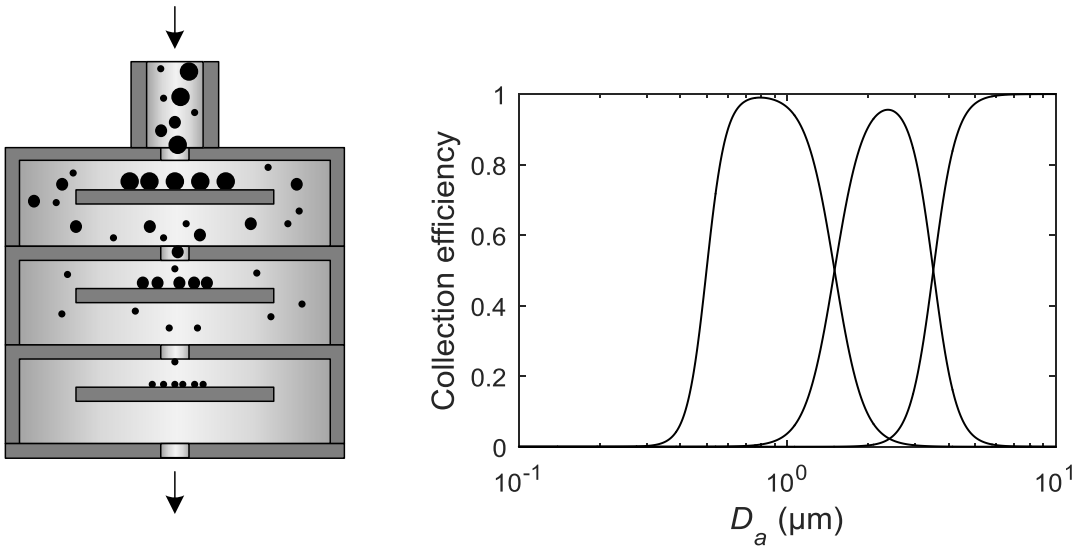

Figure 2.7 Example of a three-stage cascade impactor and its kernel functions. Each line represents the collection efficiency of the particular stage as a function of aerodynamic diameter D_a.

Impactors are widely used instruments, especially in the analysis of µm-sized particles but they are also used to study particles in sub-µm size range. For instance in air quality measurements, the mass-based values, $PM_{2.5}$ and PM_{10}, are often measured using single stage impactors, which remove particles above the corresponding size ranges while the fraction passing the impactor is analyzed. Some extensively used impactors include for instance the Andersen cascade impactor (Andersen 1958), the Berner Low Pressure Impactor (BLPI, Berner et al. 1979), the Micro-Orifice Uniform Deposit Impactor (MOUDI, Marple et al. 1991), and the Electrical Low Pressure Impactor (ELPI, Keskinen et al. 1992, Marjamäki et al. 2000).

2.3 Electrical detection

Electrical detection of particles relies on the conservation of electric charge. A flow of particles, with a net charge, represents an electric current. These particles can be collected using different techniques illustrated in Figure 2.8. A simple electrically isolated conductive plate where particles are collected is one option (Figure 2.8A). It is used for instance for ion detection in mass spectrometers, ion mobility spectrometers and in specific DMAs (e.g. Muccio and Jackson 2009, Flagan 2001, Tammet et al. 2002). Impactors have also been equipped with electrically isolated collection plates, which enable electrical measurement of the collected particles (Tropp et al. 1980) or the calibration of the impactor (Hillamo and Kauppinen 1991).

The impactor construction can be realized in a way where the jet plate and the collection substrate form a Faraday cage (Keskinen et al. 1992), see Figure 2.8B. The operation of such a device is based on the Gauss's law. When a charged particle enters the Faraday cage connected to the ground potential, the Faraday cage shadows the original electric field from the charged particle by moving electric charge from the ground potential. For instance, if one positive elementary charge enters the Faraday cage, one negative elementary charge is taken from the ground potential to shadow the electric field. Highly sensitive ammeter, often named as an electrometer, is used to measure this electric current between the Faraday cage and the ground potential. The advantage of the Faraday cage construction is that electrical conductivity inside the Faraday cage is not needed as the current is generated when the charge enters the Faraday cage.

Impactors collect particles only at certain size range, and particles, which are not collected inside the Faraday cage, do not generate electric current in the case of the stable particle concentration. If all particles need to be collected, a filter can be installed inside the Faraday cage, which is a construction known as a Faraday Cup Aerosol Electrometer (FCAE, Liu and Pui 1974), see Figure 2.8C. If the filtration efficiency is high, the particle losses in the FCAE inlet are low, the flow rate is known accurately, and the particle mean charge is known precisely, the FCAE acts as a precision concentration reference, which links the electric current to the particle concentration.

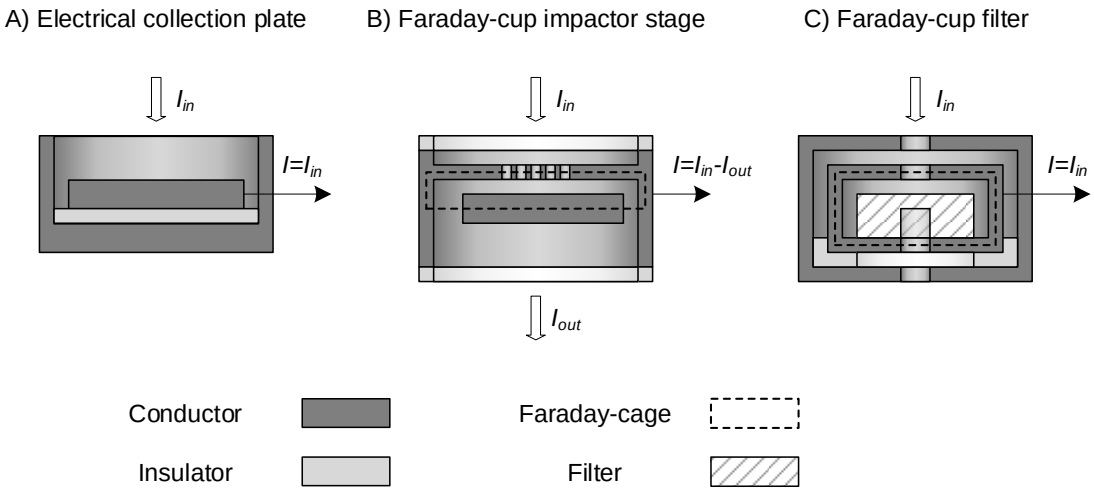

Figure 2.8 Illustration of the collection and measurement of charged particles by detecting the electric current.

In the previously mentioned methods, the electric current is measured from the collection plate or from the Faraday cage using an electrometer. In this case, electrometer (ammeter-type) refers to an electric circuit, which amplifies the small electric current, often in the fA to pA range to easily measurable voltage. Modern electrometers are constructed around monolithic low input bias operational amplifiers. Electrometers utilize a feedback circuit, composed of a high-ohmic (GΩ to TΩ) resistor, forming a resistive feedback circuit (e.g. Aplin 2000), or a capacitor, forming a capacitive feedback circuit (Keithley 2004). In the case of resistive feedback, the output voltage is proportional to the input current and in the case of the capacitive feedback, the output voltage is proportional to input electric charge.

2.4 Electrical aerosol instruments

Electrical aerosol instruments combine the measurement methods described above: particle concentration instruments combine charging and electrical detection, while in the particle size spectrometers, aforementioned techniques are supplemented with particle size classification.

Particle concentration sensors, based on unipolar charging, measure a signal that can be expressed with the *Pn* value (Equations 2 and 3). Response to the number concentration is linear and response to the particle diameter is proportional to $\sim D_p^{1...1.5}$.

Often, electrical particle sensors rely on a corona charger and detection of particles in a FCAE but some sensors utilize non-collecting detection techniques based on change in the average charge of particles. Examples of electrical particle concentration sensors are for instance, the Electrical Aerosol Monitor (Lehtimäki et al. 1983), the Electrical Aerosol Detector (EAD, Johnson et al. 2002) or its refined version the Nanoparticle Surface Area Monitor (NSAM, Fissan et al. 2007), the PPS-M (Rostedt et al. 2014), and the Partector (Fierz et al. 2014). Electrical particle sensors are useful devices in measuring concentration levels. In some cases, their size response can be tuned to provide some size classification capabilities by adjusting the ion trap voltage.

Measurement of the particle size distribution requires particle size classification. In case of the charge-conditioned particles, the size distribution measurement may be realized based on the particle electrical mobility with a DMA and a Condensation Particle Counter (CPC). As the particles in the DMA output are charged, electrical detection with a FCAE is an alternative option for particle detection (e.g. Winklmayr et al. 1991). In both cases, the DMA voltage, and the associated particle size, is either altered in steps as in the Differential Mobility Particle Sizer (DMPS, ten Brink et al. 1983) or in a scanning manner as in the Scanning Mobility Particle Sizer (SMPS, Wang and Flagan 1990), while the detector records particle concentrations producing the size distribution. The electrical detection may also be realized by collecting particles directly onto electrically measured rings in the classification section (e.g. Tammet et al. 2002, Jonson et al. 2004, Biskos et al. 2005b).

Alternatively to electrical classification, diffusion separation onto diffusion screens has been combined with electrical detection of particles (Fierz et al. 2002). This was developed into a handheld particle sensor Disc-Mini (Fierz et al. 2011) consisting only of a single electrically measured diffusion stage and an electrically measured filter stage.

The size classification is possible also in an electrically measured impactor (Troop et al. 1980, Keskinen et al. 1992). The principle of the Electrical Low Pressure Impactor (ELPI) was introduced by Keskinen et al. (1992). The ELPI combines a corona charger and a cascade impactor. First, particles are charged using a unipolar corona charger. Then, particles are led into a cascade impactor. The impactor composes of electrically isolated impactor stages, which form Faraday cages that surround the particles. Particles are collected as in normal impactor, according to their aerodynamic diameter. First stage collects the largest particles and the last stage collects the smallest particles. The charge of the collected particles is detected with a multichannel electrometer, which measures electric current from individual stages.

2.5 Aerosol generation

As there are numerous aerosol generation methods available, the discussion in the following paragraphs is limited only to the main methods used in this thesis. The three main particle generation methods applied are all illustrated in Figure 2.9.

The Vibrating Orifice Aerosol Generator (VOAG, Berglund and Liu 1973) produces particles in the µm size range. The version introduced here is a modification of the original VOAG. Solution containing dissolved particle material is pumped into the device with a syringe pump. The solution enters first into a chamber, which has a small (diameter from a few µm up to a few tens of µm) interchangeable orifice leading into the gas flow line. Droplets are generated when the liquid flows through this small orifice. Highly monodisperse particles are formed when a piezoelectric ceramic produces controlled pressure pulses through changing the volume of the chamber containing the liquid. Dispersion air is fed close to the newly formed droplets, and the mixed droplet-dispersion flow is led through a dispersion orifice, which generates the aerosol. This is supplemented with an additional dilution flow. The initial droplets coming out of the orifice are large, often tens of µm in diameter. The final particle size in the µm size range is achieved when the solvent from the droplets evaporates. The droplet generation method produces often highly charged particles. Particle charge levels are reduced by subjecting them to bipolar ions, which are generated with a radioactive source, in this case by α-radiation from ^{241}Am. One of the VOAG advantages is that the particle size can be derived from the operating parameters: frequency, feed rate, and concentration of the liquid. It is beneficial to monitor the VOAG operation as it works only in the certain envelope, and outside this, particles are not necessarily monodisperse.

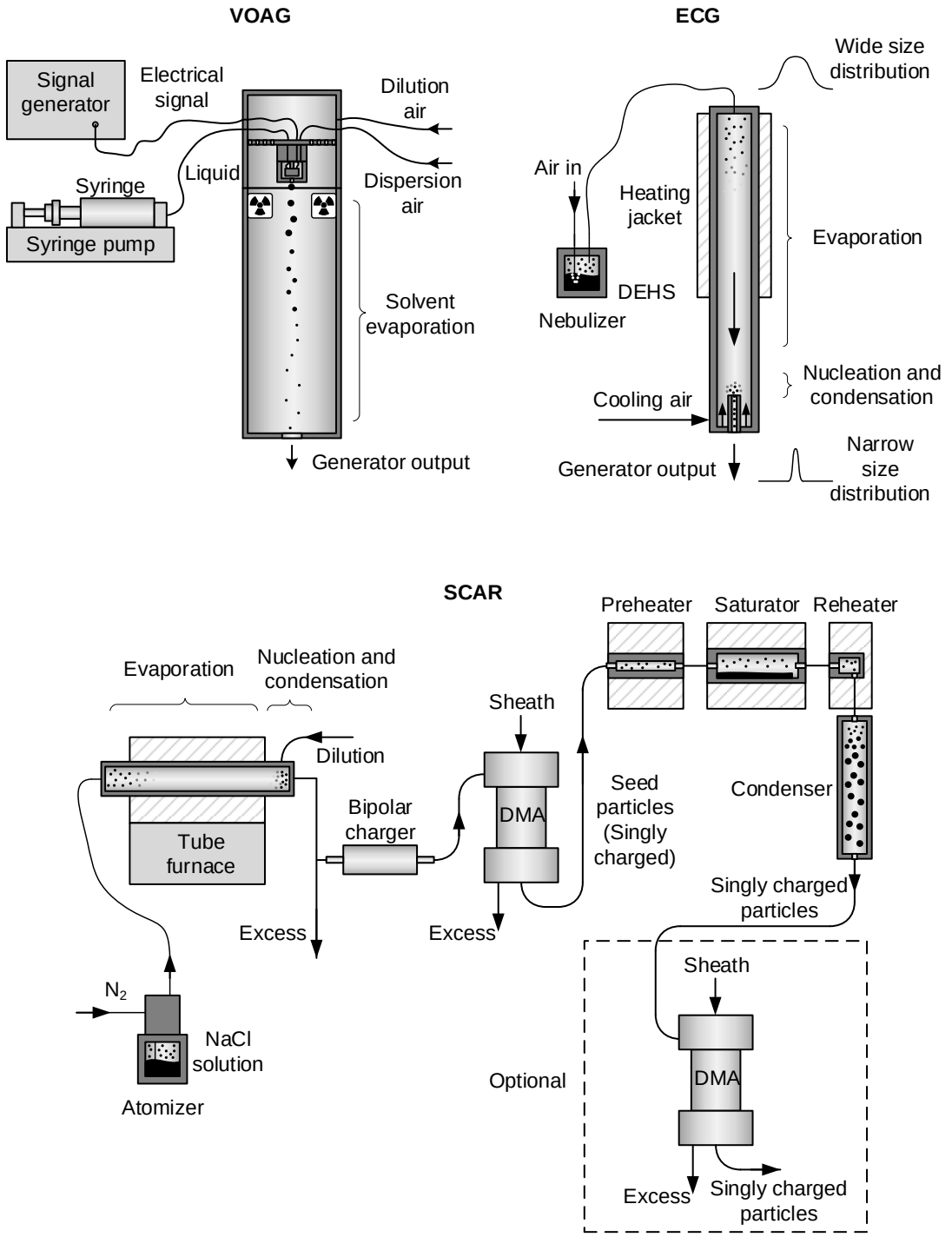

Figure 2.9 General illustration of particle generation setups used in this thesis including the VOAG (modification of the Berglund and Liu 1973 generator), the ECG (modification of the Liu and Lee 1975 generator) and the SCAR (Yli-Ojanperä et al. 2010b).

The Evaporation Condensation Generator (ECG) is a modification of the "An Aerosol Generator of High Stability" (Liu and Lee, 1975). In the modified version Diethylhexyl Sebacate (DEHS) is nebulized into a carrier flow. The aerosol size distribution is wide and particles are large at this point. The flow is led into a heated tube, where particles evaporate. This flow is cooled rapidly with a dilution air, which initiates nucleation. After the particles are generated by nucleation, they grow larger by condensation. The particle size distribution after the nucleation and condensation is narrower than the input distribution, and it is possible to reach smaller particle sizes than with nebulization or atomization.

The Single Charged Aerosol Reference (SCAR) is an aerosol generator introduced first by Yli-Ojanperä et al. (2010b). It shares some of the principles reported earlier by Uin et al. (2009) and by Sinclair and La Mer (1948). As a first stage, NaCl solution is atomized and the formed NaCl particles are led into a furnace, where they are evaporated. The hot NaCl vapor is cooled after the furnace with a nitrogen flow. Rapid cooling initiates nucleation that produces particles with a median diameter of approximately 10 nm. These NaCl particles are charged in a bipolar charger based on β-active ^{85}Kr source. The bipolar charging produces neutral particles or particles acquire a single elementary charge at this size range. Fraction of two elementary charges is minimal for 10 nm particles (Wiedensohler 1988), which is also seen in Figure 2.2 (Chapter 2). The singly charged 10 nm particles of either polarity, positive or negative, are selected with a DMA. The DMA removes neutral particles and particles with other than the selected polarity. Particles from the DMA output, acting as seed particles, are led into a preheater, which increases the flow temperature and prevents nucleation, when the flow enters in the saturator. In the saturator, DEHS is evaporated into the aerosol flow. Then the flow enters the reheater, which is followed by condenser. In the condenser, aerosol cools and the DEHS vapor condenses on all available surfaces including particles. As a result, the seed particles grow into larger sizes, while the original electric charge is conserved. This process generates singly charged particles that are significantly larger than the seed particles. The particle size is adjusted by changing the saturator temperature, which defines the DEHS vapor concentration. When large particles are generated, high DEHS vapor concentrations may lead to homogeneous nucleation, which generates a mode of neutral particles. These particles may be removed with an additional DMA coupled to the output of the SCAR.

3 Calibration of aerosol instruments

This chapter introduces conventional aerosol instrument calibration methods. More specific electrical impactor calibration and charger calibration methods are discussed as they are applied in the calibration of the new instrument, ELPI+ (**Paper I**), which is also included in this chapter.

3.1 Size calibration

Aerosol instrument size calibration refers to comparison of instrument size classification result with a reference size. The reference size is obtained by using a reference instrument or by challenging the instrument with particles of known size.

Spherical traceable size standard particles are readily available. These are typically manufactured from polymers such as polystyrene (PSL). The capability to act as size standards originates from traceable analysis of the produced particles. Although size standard particles enable rather easy calibrations, they have some significant limitations. Calibration at a specific size is often not possible because standard particles are produced only at certain sizes. Another issue is the relatively small particle concentration when particles are atomized or electrosprayed from a low concentration solution used to prevent multiplet particles. Size standard particles are often dispersed in a solution. Non-volatile compounds are often intentionally added to stabilize the particle solution, and these affect the final aerosol particle size. Thus, the uncertainty of the final particle size may be rather high, especially for small aerosol nanoparticles, and depends on the applied aerosolization technique (Mulholland et al. 2001). Size standard particles are

also rather expensive and they have a limited shelf life, which makes it non-desirable to acquire all available sizes.

To produce distinct-sized calibration particles, a source of monodisperse particles is needed. Some particle generators produce highly monodisperse particles, for instance the VOAG (Berglund and Liu 1973, Figure 2.9), the Inkjet Aerosol Generator (IAG, Bottiger et al. 1998, Iida et al. 2014) or the recent modification of the VOAG, the Flow-focusing Monodisperse Aerosol Generator (FMAG, Duan et al. 2016). In the case of the VOAG or FMAG, the particle diameter can be calculated directly from the generator operating parameters.

A polydisperse generator is suitable also for size calibrations if the output distribution is classified into a narrow size range while the classifier acts as a size reference. Several different particle generators are routinely used for generating aerosol distributions, including atomizers, nebulizers, evaporation-condensation generators (Liu and Lee 1975) or high temperature furnaces (Scheibel and Porstendörfer 1983). The normal procedure is to charge condition the generator output aerosol in a bipolar charger and classify particles using a DMA, which acts as a size reference through the definition of the electrical mobility.

Whether the size is defined by the generator or the classifier, it is beneficial and a good practice to ensure that the output size is correct. This is possible by analyzing particles with a calibrated microscope or in the case of the classifier by challenging it with traceable size standard particles. Size classifiers are calibrated by first aerosolizing size standard particles, which are then bipolarly charged and introduced into the classifier (Mulholland and Fernandez 1998). The DMA voltage is scanned over the produced peak while a particle counter is used to detect particles. The standard size is then compared with the calculated diameter of the detected peak.

Calibration of an impactor is an example of a size calibration. The calibration of an impactor refers to the definition of the stage specific collection efficiency curves as a function of particle diameter, which are illustrated in Figure 2.6 in Chapter 2. Impactor collection efficiency curves are often steep, requiring narrow particle size distributions with well-defined particle sizes. In the electrical characterization method (Hillamo and Kauppinen 1991), the collection efficiency for a single impactor stage E is defined with equation

$$E = \frac{I_i}{I_i + I_f}, \tag{8}$$

where I_i is the electric current measured from stage i and I_f the electric current measured from a Faraday cage filter installed after the impactor stage.

In the case of electrical cascade impactors, as the ELPI+, the impactor itself can be used as a reference (Keskinen et al. 1999). The electric current measured from the filter stage in Equation 8 is now replaced with the total electric current measured from succeeding stages. In this case, the collection efficiency is expressed through an equation

$$E_i = \frac{I_i}{\sum_{k=1}^{i} I_k}, \tag{9}$$

where I_k is the current measured from stage k. The numbering begins from the smallest particle size and the case k=1 in Equation 9 refers to the electrical filter stage.

The collection efficiencies are measured for a limited number of particle sizes. A continuous collection efficiency curve is achieved by fitting a suitable function to these obtained values. Often a good fit is achieved with an equation

$$E = \left[1 + \left(\frac{D_{50}}{D_a} \right)^{2s} \right]^{-1}, \tag{10}$$

where D_{50} is the aerodynamic diameter of 50 % collection efficiency, also known as a cut diameter, D_a the aerodynamic diameter and s the fitted steepness value (Dzubay and Hasan 1990, Winklmayr et al. 1990).

Defining an impactor collection efficiency curve requires several measurement points per stage, which is difficult or impossible with standard particles that have certain sizes. Thus, a particle generator or a classifier with an accurate output size is used. However, the size standard particles are useful, because they can be used to check the size calibration at certain points.

3.2 Detection efficiency calibration

Detection efficiencies of common aerosol instruments depend significantly on particle size, and may depend on other factors such as particle concentration. The detection efficiency is defined by calibrating the instrument concentration reading against a concentration reference. A periodic calibration of the detection efficiency is often conducted at the optimal particle size from the instrument point of view to ensure that the instrument response has not changed. In such a case, the requirement for the particle monodispersity is not very high. When new instruments are introduced, more detailed calibrations are needed, including the definition of the detection efficiency as a function of the particle diameter for instance. The latter case requires calibration particles with a precise size, and the particle generation methods discussed earlier are used.

The principal idea of the detection efficiency calibration is to feed the instrument with a known particle concentration. Generators producing certain well-confirmed particle concentrations are rare, only Iida et al. (2014) has described such a calibration setup. The standard procedure is to produce the calibration aerosol with a generator, classify a narrow size range from the generators distribution and split the classified aerosol between the instrument and the reference. Depending on the setup, the reference may be a calibrated precision particle counter (CPC or OPC) or a FCAE. The FCAE has the widest operating size range, minimal particle losses and linear concentration response. However, the FCAE measures the electric current from particles, which can be converted into particle number concentration only if the particle mean charge is well-known.

Calibration of a corona charger is based on the principles of the detection efficiency calibration. Corona chargers are calibrated by measuring how much electric current their output particles generate. This is measured in proportion to the input concentration and as a function of particle diameter. The proportional current can be converted into the *Pn*-value (Equation 2) if the flow rate through the charger is known.

In the characterization of a corona charger, the inlet particle concentration must be known, which is achieved by using a reference instrument in parallel with the charger or by switching the charger off or by-passing it and measuring the electric current from particles as a reference (e.g. Marjamäki et al. 2000). The reference instrument approach takes all the losses in the charger into account, which is a desired property, but requires flow splitting and an accurate reference instrument, which are the challenges in this approach. The charger-off-method does not require a reference instrument but it does

not consider non-electrical losses in the charger, and in addition, the mean charge of the input particles must be accurately known.

Because charger alters the particle electrical state, the effect of initial charge should be minimized when chargers are characterized. The straightforward and common way is to charge the calibration particles bipolarly, which results an equilibrium charge distribution (e.g. Fierz et al. 2011). If this equilibrium level is not sufficient, and completely neutral particles are needed, it is possible to remove all the charged particles with an electrostatic precipitator (e.g. Alonso et al. 2006, Rostedt et al. 2014). While the aerosol is bipolarly charged or charged particles are removed, the electric current generated by particles is small or nonexistent. Additionally, the electric current is not anymore a function of particle number concentration, and thus cannot be used as a reference signal. To both minimize the effect of the initial charge and to enable the electrical reference signal, particle polarity opposite to the corona discharge may be used. The opposite polarity has been found to produce insignificant effect on the charger output (Qi et al. 2009).

3.3 Calibration of the ELPI+

The ELPI+ was developed on the basis of the commercial "Classic" ELPI incorporating significant modifications. The schematics of the ELPI+ is given in Figure 3.1. The first component in the ELPI+ flow line is the needle type unipolar corona charger, which is supplied with a constant electric current produced by a high voltage power supply. Excess ions from the charger are removed by an electric field in the ion trap. Charged particles are then led into the impactor. First, the precut impactor removes the largest particles. Remaining particles are classified in 13 impactor stages, and the final filter stage collects the smallest particles. These 14 stages are electrically isolated from each other and from the ground potential with plastic insulators, and electric currents from these stages are measured with a bipolar multichannel electrometer, which also converts the analog current signals into digital form. With the adjustable valve after the filter, the downstream pressure can be adjusted into the specified value. Pressure sensors measure both the downstream and upstream pressure. Internal flush pump produces particle-free air for electrometer zero-level adjustment. The operation of the instrument is controlled by the internal computer, which also includes data output for an external computer.

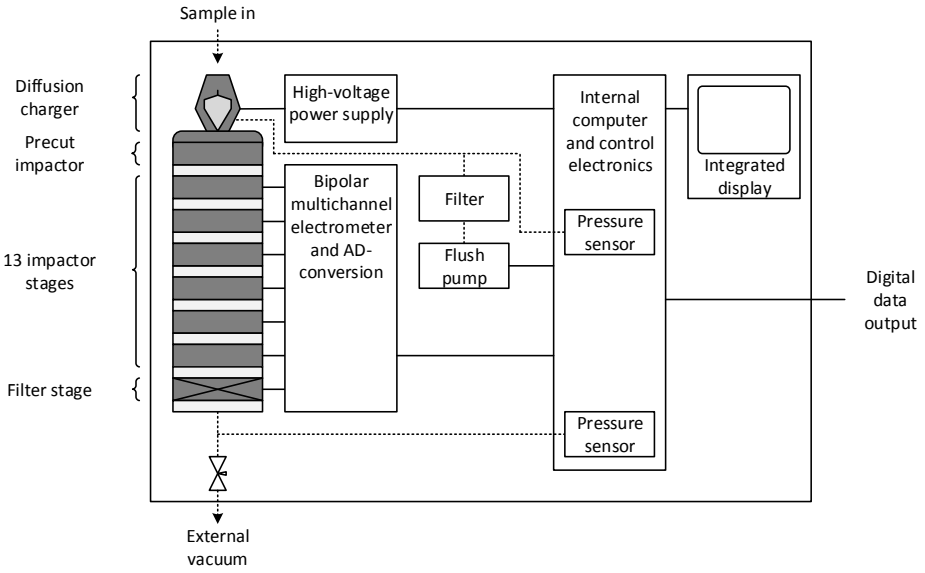

Figure 3.1 Schematics of the ELPI+ (**Paper I**)

The ELPI+ contains some improvements over the original "Classic" ELPI. The charger construction was optimized and the impactor was redesigned to improve the time response, and the number of measured stages was increased from 12 to 14. These two new stages include a new impactor stage with a cut diameter below 20 nm (Yli-Ojanperä et al. 2010a) and a filter stage (Marjamäki et al. 2002). New electrometers provide faster time response and lower electrical noise. Basically all the components in the instrument changed from the previous version, including the charger and the cascade impactor. This change required a complete calibration of the instrument.

The operating size range of the ELPI+ (**Paper I**) is a challenge from the calibration point of view. The smallest calibration particle sizes are in the order of 10 nm, whereas the largest in the order of 10 µm. This size range cannot be covered with a single particle generation and reference method. The ELPI+ calibration requires evaluation of two main components of the instrument, the charger and the impactor. The calibration of the charger is similar to the detection efficiency calibration discussed earlier, and requires a concentration reference. The impactor, on the other hand, requires a size calibration. Because the impactor stage collection efficiency functions are steep, an accurate particle diameter is the significant factor in this calibration.

The operation of the ELPI+ charger was evaluated by measuring its *Pn*-value as a function of the particle diameter. Similar approach was also used in the calibration of the first commercial version of the ELPI (Marjamäki et al. 2000). The *Pn*-value, given in the

Equation 2, is defined by measuring the electric current from particles after the charger, which in this case was measured from all the impactor stages including the filter stage as a total electric current. Furthermore, the inlet number concentration must be known as well as the flow rate through the charger. The corona charger was studied with negative particles, as the charger output is positive. The insignificant effect of the initial charge reported by Qi et al. (2009) was further confirmed in **Paper I** for larger 3.2 µm particles.

The calibration size range of the charger had to be covered with different particle generation techniques as presented in Figure 3.2. In the lowest size range, below 2 µm, the SCAR (Yli-Ojanperä et al. 2010b) was used as a particle generator, while the particle diameter was determined with a DMA (3071, TSI Inc.). The charging efficiency calibration requires a concentration reference, and in this case a calibrated CPC (3776, TSI Inc.) was used for this purpose. As the particles from the SCAR were singly charged, the electric current from the impactor, while charger was switched off, was used as a second reference to ensure that results were reliable. The µm-sized particles were generated with the VOAG, which was observed to produce positively charged particles. A bipolar neutralizer was not sufficient to alter the charge level, and a corona charger with a negative voltage was installed in the flow line to acquire negatively charged particles. The counting efficiency of the CPC decreases in µm sizes. As a result, the APS (3321, TSI Inc.) was selected as a concentration reference for these larger particles. The particle material was liquid DEHS on NaCl seed particles with the SCAR and liquid DEHS with the VOAG.

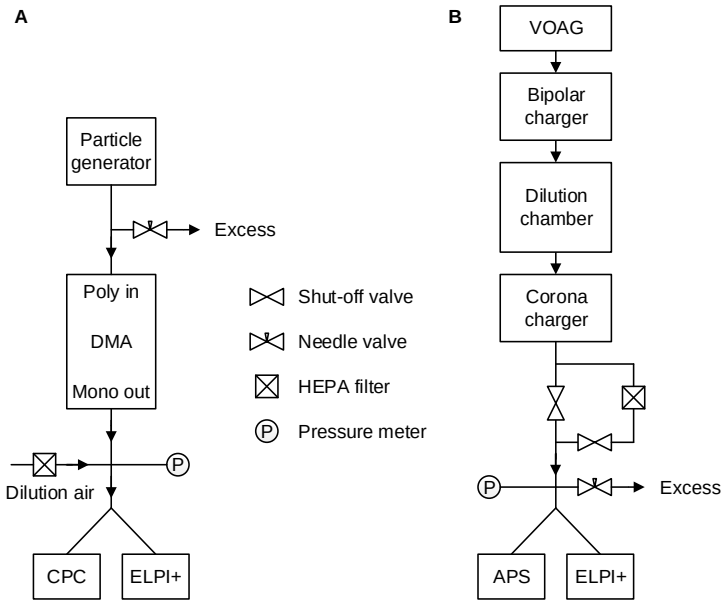

Figure 3.2 Setups used to characterize ELPI+ impactor and charger. The setup A was used in combination with the ECG and the SCAR and setup B with the VOAG (modified from **Paper I**).

The charging efficiency, given as a *Pn*-value is shown in Figure 3.3. The *Pn*-values measured using the APS as a reference did not match the results obtained with the SCAR and the CPC exactly in the overlapping region, and the APS results were reduced by 16 % to overcome this difference.

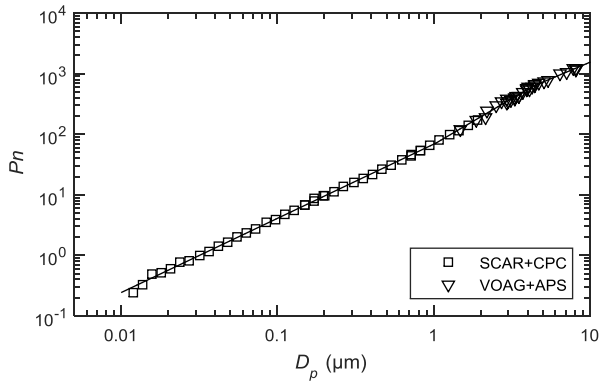

Figure 3.3 ELPI+ charger *Pn* measurement points and fitted power functions (modified from **Paper I**).

The charger *Pn* is approximated for different size ranges with separate equations based on the power form of the Equation 3. The charging efficiency may be calculated from equations

$$Pn = \begin{cases} 68.531 \cdot D_p^{1.225}, D_p < 1.035\mu m \\ 67.833 \cdot D_p^{1.515}, 1.035\mu m \le D_p \le 4.282\mu m \\ 126.83 \cdot D_p^{1.085}, D_p > 4.282\mu m \end{cases}, \quad (11)$$

where D_p is the particle diameter (µm). The charger *Pn* is compared with other similar devices in Table 3.1. In comparison to the previous ELPI model in filter configuration (Marjamäki et al. 2002), the new charger is more efficient. Value of *Pn*=1 is reached at smaller diameter, 31.8 nm for the ELPI+ compared to 40.9 nm for the ELPI. At 100 nm particle diameter, the ELPI+ charger provides 25 % higher *Pn* than the ELPI charger. The ELPI+ charger is highly efficient as most of the other commercial chargers have lower charging efficiencies, including all the ones selected for the comparison. Highly efficient charger provides more electric current from the same particle concentration than low efficiency charger. This enables measurement of lower particle concentrations in the case of equal noise factors.

Table 3.1 Comparison of charger *Pn*-values.

	D_p (nm) at *Pn*=1	*Pn* at 100 nm
ELPI+ (**Paper I**)	31.8	4.08
ELPI (Marjamäki et al. 2000)	67.0	2.10
ELPI with filter (Marjamäki et al. 2002)	40.9	3.26
PPS-M (Rostedt et al. 2014)	38.3	2.74
Disc-Mini (Fierz et al. 2011)	41.8	2.67
EAD (Jung and Kittelson 2005)	34.8	3.30

The ELPI+ impactor was calibrated using the size axis calibration methods, which were rather similar with the charger calibration, with a few exceptions. The main focus was on the particle diameter, and the reference concentration was not needed as the measurement based on Equation 9 (Keskinen et al. 1999). Impactor classifies particles according to their aerodynamic diameter, which is calculated from the physical or mobility

diameter and from the particle effective density using Equation 6. Thus, the particle density must be precisely known in impactor calibrations. This issue was solved by using liquid DEHS with a density of 920 kg/m^3 as particle material. The impactor stage with the smallest cut diameter was measured using particles generated with the ECG as the density of the SCAR-generated particles is unknown in this size range, between 10 and 20 nm, due to the seed particles. The ECG was also used between 0.5 and 1 µm with correction algorithm by Kauppinen and Hillamo (1989).

The ELPI+ impactor collection efficiencies, calculated using Equation 9, are presented in Figure 3.4. The DMA was used as the size reference below 1 µm particle diameters, while the VOAG worked itself as a reference in the µm size range. Figure 3.4 includes fitted collection efficiency curves according to Equation 10.

Different particle generation methods were used in parallel in calibration of certain stages to ensure that the particle generation method does not affect calibration results. The ECG and SCAR produce equal results for Stage 3, which is also the case of the ECG with correction algorithm and the SCAR for Stage 9. The collection efficiency of Stage 10 was measured using the corrected ECG and with the VOAG, and results from these methods also fit well on the same collection efficiency curve.

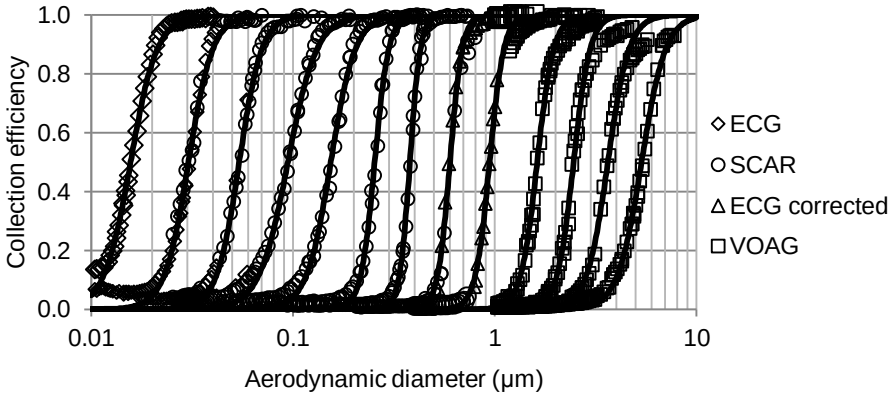

Figure 3.4 Collection efficiency of the ELPI+ reference impactor stages 2-14 (Stage 2 is the leftmost and Stage 14 is the rightmost) as a function of particle aerodynamic diameter including measurement points and fitted collection efficiency curves. The particle generation method is given in the legend. (modified from **Paper I**)

Impactors exhibit particle collection at sizes smaller than the impactor cut diameter due to diffusion and electrostatic effects, including space charge and image charge (Virtanen et al. 2001). This secondary collection efficiency is visible in Figure 3.4 in the case of the Stage 3 for instance. The secondary collection efficiencies were defined from the

impactor calibration measurements conducted at low concentrations. In such a case, the dominant mechanisms are the diffusion and the image charge deposition. This secondary collection efficiency E_{sec} was parametrized using a power relation

$$E_{\mathrm{sec}} = aD_p^{\,b} + c\,, \tag{11}$$

where a, b and c are stage specific fitted parameters and D_p the mobility diameter. These fitting parameters are collected in Table 3.2 along with the impactor cut diameters D_{50} and steepness values s.

Table 3.2 ELPI+ reference impactor parameters.

	Primary collection efficiency		Secondary collection efficiency		
Stage	D_{50} (µm)	s	a	b	c
1 (filter)	-	-	-	-	-
2	0.0157	3.32	-	-	-
3	0.0304	3.65	$9.80\cdot10^{-8}$	-2.73	0.05085
4	0.0541	3.89	$3.63\cdot10^{-8}$	-3.06	0.03083
5	0.0943	3.05	$1.58\cdot10^{-6}$	-2.26	0.02342
6	0.154	3.62	$4.83\cdot10^{-6}$	-2.06	0.02183
7	0.254	6.30	$1.02\cdot10^{-5}$	-1.90	0.02097
8	0.380	8.43	$6.22\cdot10^{-5}$	-1.49	0.01158
9	0.600	7.16	$4.03\cdot10^{-5}$	-1.56	0.00804
10	0.943	6.21	$7.31\cdot10^{-5}$	-1.40	0.00671
11	1.62	5.32	$1.01\cdot10^{-4}$	-1.31	0.00475
12	2.46	5.33	$8.22\cdot10^{-5}$	-1.35	0.00288
13	3.64	4.14	$1.09\cdot10^{-4}$	-1.31	0.00129
14	5.34	3.66	$9.07\cdot10^{-5}$	-1.36	0.00186

The impactor parameters given in Table 3.2 are comparable with the previous version of the ELPI (Marjamäki 2003). The cut diameters and the steepness values are rather similar. The secondary collection efficiencies cannot be compared from the parameters

as the fitting equations are different. According to comparison directly from calibration results, the secondary collection efficiencies are a bit higher in the ELPI+ compared to ELPI. More detailed comparison is given in **Paper I**. The difference may originate from the reduced internal volume of the stages, which improves the time response.

The charger *Pn*-values and the impactor parameters in Table 3.2 are the main results of the calibration. The instrument cannot be used in accurate measurements without these values. The measured cut diameters define the size measurement of the ELPI+, and the charger *Pn* is used to convert the measured current values into particle concentration.

4 Particle charge measurement

Particle charge measurements have not been applied as extensively as size or concentration measurements in aerosol research although they have long traditions. Perhaps the best known particle charge measurement is the oil drop experiment Robert Millikan and Harvey Fletcher conducted to determine the elementary charge (Millikan 1913). The widely used electrical classification method was also developed originally for charge measurement applications (Hewitt 1957).

4.1 Background

Currently, several different particle charge measurement methods are available. In this case, charge measurement methods are divided into four categories depending on how much information they provide. The most primitive particle charge measurement is the net charge from the entire aerosol, which is rather easily measured with a FCAE (Kulvanich and Stewart 1987). The measurement of net charge as a function of particle size requires somewhat more complicated setup including size classification and charge measurement. This is typically achieved with an impactor and an electrical detection of the collected particles (Keskinen et al. 1992, Hoe et al. 2009).

Measurement of bipolar charge requires particle classification according to electrical polarity. This is possible for instance by using electrical collection tubes (similar to the integrating analyzer in Figure 2.3A), where the electric field is used to guide particles onto measurement electrodes according to their polarity (e.g. O'Leary et al. 2008). This does not yet provide any information on particle size. To measure the bipolar charge distribution as a function of particle size, the electric separation must be accompanied with some type of size classification. There are several ways to do this. One rather simple

option is to use a DMPS or an SMPS equipped with a bipolar voltage supply and measure particles with and without the bipolar charger (Maricq 2004). This method can extract the charge information only in cases where the size distribution is simple and charge levels are low. Cases that are more complex require electrical classification using a DMA followed by a simultaneous particle size classification. In µm sizes, the size classification is possible with an Optical Particle Counter (OPC) (e.g. Emets et al. 1991, Vishnyakov et al. 2016). In the size range between 1 and 300 nm another DMA equipped with a bipolar charger, setup known as Tandem-DMA, is the typical charge measurement method (Kim et al. 2005, Maricq 2005). The previously introduced methods utilize typical aerosol instruments, but there is also an instrument developed especially for particle charge measurements. The Electrical Single Particle Aerodynamic Relaxation Time analyzer (E-SPART, Mazumder et al. 1991), which utilizes both electric and acoustic fields combined with a Laser-Doppler measurement, measures both the size and the charge of individual particles.

The existing size classifying charge measurement methods have some limitations. The methods relying on optical detection cannot measure particles significantly smaller than the wavelength of the light, the Tandem-DMA is slow, and the single DMA cannot be used for larger particles that may have complex charge distributions. Thus, a single bipolar charge measurement method capable of operating in a size range from nanometers up to a micrometer at a reasonable measurement speed would be beneficial. From the application point of view, inhalers produce a large amount of particles during short bursts, and there has not been any instrument available to measure the bipolar charging state of inhaler-generated particles. The instrumentation presented in **Paper II** provides means of measuring particle charge in a size range from approximately 30 nm up to 1 µm and the instrument introduced in **Paper III** allows analysis of bipolar charge of inhaler-generated particles in µm size range.

4.2 DMA-ELPI

As described earlier, there has not been a charge measurement method available for a particle size range from nanometers up to micrometers. The DMA-ELPI charge measurement method (**Paper II**) was developed partly to overcome this issue. The size range is possible, because the ELPI, used as the detection instrument, operates from nanometers to micrometers. This range is wide compared to other instruments measuring particle size distributions. Note that, here the ELPI refers to the general operating principle of the instrument including all the variations, and the instrument used in the measurements was the ELPI+.

The operating principle of the DMA-ELPI charge measurement is shown in Figure 4.1. The DMA, operated without the normal bipolar charger, is used to select a certain electrical mobility, which depends on the DMA dimensions, flow configuration and voltage. The electrical mobility of particles is a function of size and charge as Equation 4 shows. Particles in the DMA outlet flow have the same electrical mobility, but the flow may contain particles of different sizes and charging states. The DMA outlet is connected to an ELPI, which is operated charger switched off not to alter the particle charging state. The ELPI classifies particles according to their aerodynamic diameter and measures electric current associated with certain size particles.

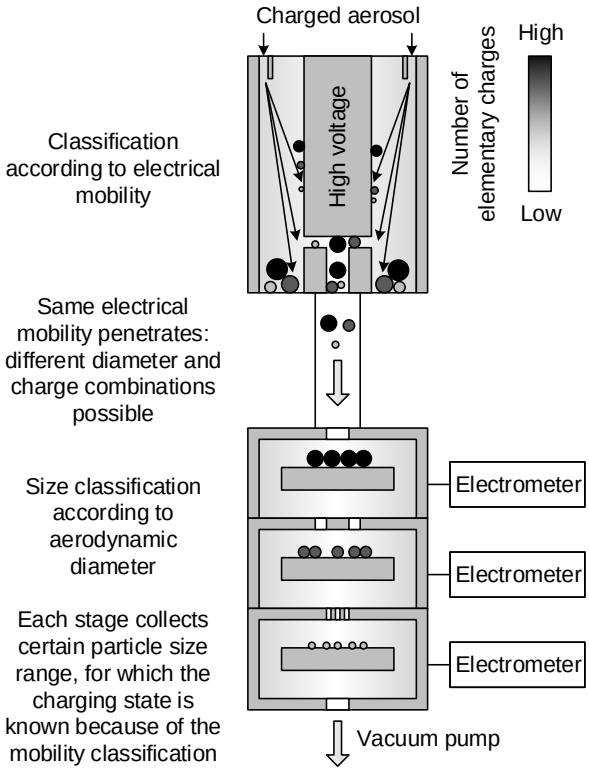

Figure 4.1 Operation principle of the DMA-ELPI charge measurement method (**Paper II**).

The calculation is easiest to explain from the reverse direction compared to the aerosol flow. The ELPI provides electric current from individual stages and these stages collect certain sized particles according to their aerodynamic diameter D_a. First, the aerodynamic diameter of the stage D_a is converted into mobility diameter D_p by using the particle effective density (Equation 6). Then, the particle mean electrical mobility Z^* is calculated based on the DMA operating parameters according to Equation 5. Now, the particle electrical mobility and size is known, which allows the calculation of the particle

charge from Equation 4. Finally, when the particle charge is known, the ELPI stage current can be converted into particle number concentration at the stage specific size and charge. This method provides the concentration of particles as a function of the particle size at certain charging states. The mapping of the charging states of the particles is conducted by varying the DMA classification parameters, especially the voltage. Bipolar measurements are possible by operating the DMA with both polarities.

The previous description was a simplification of the mathematical solution. In **Paper II**, the charge distributions were calculated through solving a group of equations. For a single measurement point, i.e. DMA voltage value, the mathematical solution is determined with a group of equations

$$\begin{aligned} n_1 \cdot a_{1,1} \cdot x_1 + \cdots + n_K \cdot a_{K,1} \cdot x_K &= I_1 \\ \vdots &= \vdots \\ n_1 \cdot a_{1,14} \cdot x_1 + \cdots + n_K \cdot a_{K,14} \cdot x_K &= I_{14} \end{aligned}, \tag{12}$$

where *I* is the current measured by the corresponding ELPI stage, *n* is the number of elementary charges per particle, *a* is the collection efficiency for the selected particle size and *x* is the particle concentration term. In the group of equations, each row represents a single impactor stage where different sized particles generate the detected electric current. The particle sizes were selected from the size range where electric current was detected. Selection of particle sizes is described in more detail in **Paper II**. The *a* values are taken from the ELPI+ kernel functions, which are calculated according to the impactor specific cut diameters and steepness values taken from **Paper I**. The values of *n* are calculated from the DMA parameters for the selected particle sizes (Equations 4 and 5) and they represent the average number of elementary charges per particles penetrating the DMA at the selected particle sizes.

The group of equations may be solved with conventional methods, and in **Paper II** the Tikhonov regularization method (e.g. Hansen 1998) was applied. The particle number concentration for a certain size N_k is calculated from the concentration term with equation

$$N_k = \frac{x_k}{eQ_{DMA}}, \tag{13}$$

where *e* is the elementary charge and Q_{DMA} the sample flow rate through the DMA. The procedure described above was conducted for a single DMA voltage, and the final

charge distribution is determined by applying the procedure for all the DMA voltages, i.e. measurement points.

The tested DMA-ELPI charge measurement consisted of an ELPI+ and a 280 mm long Vienna-type DMA operated with a 2 l/min sample flow in combination with a 20 l/min sheath and excess flows. A separate DMA bypass loop was added to match the flow rates of the ELPI+ and the DMA.

The developed DMA-ELPI charge measurement method was tested in laboratory conditions with particles having different charge levels. Because the particle effective density is required in the calculation, all the test measurement were conducted with particles having a well-known density as the particles composed of liquid DEHS. The capability to measure low particle charge levels was studied by producing singly charged particles with the SCAR at 50, 100 and 200 nm particle sizes. The results are presented in Figure 4.2. At the 50 nm mean particle size, singly charged particles are mostly detected to contain one elementary charge but the calculation produces also small amounts of other charges as an artefact. At 100 and 200 nm particle sizes, singly charged particles are detected to contain one elementary charge and fraction of other charges is small, less than 5 %.

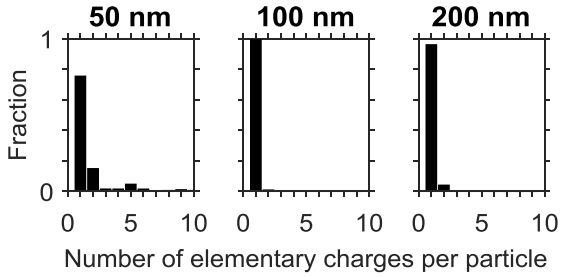

Figure 4.2 Singly charged particles analyzed with the DMA-ELPI method. (modified from **Paper II**)

The higher charge levels were studied by producing narrow size distributions with Geometric Standard Deviations (GSD) between 1.06 and 1.15 and particle sizes from 50 nm to 500 nm with the SCAR and by charging these with a separate ELPI+ charger. The results of this test are presented in Figure 4.3. The peaks are at higher charge levels than the charger *Pn*-values. This is a positive result as the *Pn*-value contains the penetration term. As a result, the average number of elementary charges per particle, *n*, should always be larger than the *Pn*.

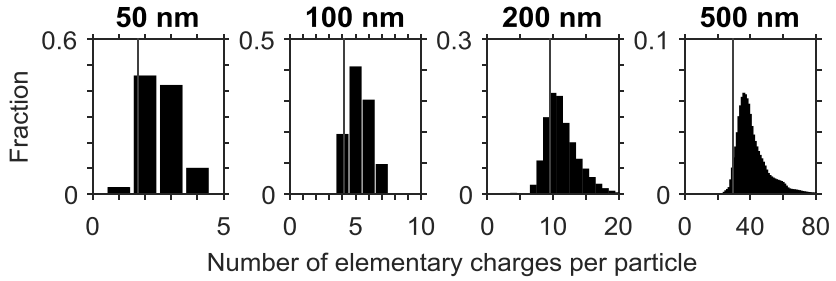

Figure 4.3 Particles charged with the ELPI+ corona charger analyzed with the DMA-ELPI method. The line represents the *Pn*-value of the corresponding particle diameter. (modified from **Paper II**)

Another comparison was conducted using wide size distributions, GSDs between 2 and 2.4. These were produced by atomizing DEHS solutions at three different concentrations. The size ranges spanned from 30 nm to approximately 1 µm. Particles were charged with the same ELPI+ charger as in the case of the narrow size distributions. The high charge of large particles allowed the use of the same flow settings in all the measurements. As seen from Figure 4.4, the charge distributions from the calculation resemble the charger *Pn*-curve in the case of the all three size distributions.

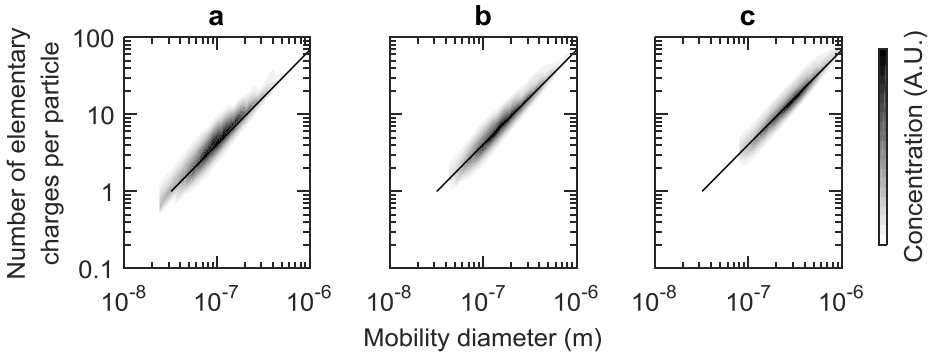

Figure 4.4 DMA-ELPI charge analysis from wide size distributions. The concentration is given for particle number. The line represents the ELPI+ charger *Pn*-curve (modified from **Paper II**)

As Figures 4.2-4.4 suggest, the DMA-ELPI charge measurement can be used to analyze charge distributions in a wide size range. The smallest measured particles were 30 nm and the largest were approximately 800 nm in diameter. The method should be capable of even wider size range than this from the instrument point of view. In the discussion and conclusions of **Paper II**, the size range is estimated to range from 30 nm up to 1 µm. The size range could be perhaps extended from this, as the smallest cut diameter of the ELPI+ impactor is approximately 16 nm, and the precut impactor limits the upper

diameter to approximately 10 µm. However, such a size range would require evaluation of particle losses in the DMA and in the tubing connecting the instruments. The upper size limit for conventional DMAs is approximately 1 µm for singly charged particles, and sizes above this can be detected only if particles are multiply charged.

The DMA-ELPI measurement method involves classification of particles according to their electrical mobility and then according to their size. The size classification could be accomplished also by instruments other than the ELPI. Such instruments include electrical mobility spectrometers that detect particles electrically in real-time, for instance the Engine Exhaust Particle Sizer (EEPS, TSI Inc.) or the Differential Mobility Spectrometer (DMS500, Cambustion Ltd.). The calculation of the charge distribution would be challenging with these instruments because the particles are recharged and the size distribution is measured through the electrical mobility. When the ELPI is used, the calculation is relatively simple and the recharging of the particles after the DMA is not required. The ELPI charger could be used to increase the particle detection efficiency but it would complicate the calculation.

4.3 BOLAR

When aerosols are generated from liquids or solids using mechanical methods, particles may acquire high electric charge. Such particle generation methods are applied for instance in inhalers. As the particle charge affects the deposition into airways (Balachandran et al. 1997), the evaluation of inhalable particle charge is beneficial. ELPI has been applied in such research (e.g. Kwok and Chan 2008), but it is only capable of measuring the size classified net charge. The bipolar charge of inhaler produced aerosols has been largely unknown.

The BOLAR was especially developed to measure this bipolar charge. The requirements for instrument operation arise from the properties of the inhaler-generated aerosols. The size range is in the micrometers, and as the particles are generated in a rapid event, a fast real-time measurement is needed. The BOLAR instrument introduced in **Paper III** uses a parallel impactor configuration to analyze bipolar charge-size distributions. The instrument is designed to operate within the same size range with the inhaler-generated particles, i.e. in the µm size range. The schematic of the instrument is given in Figure 4.5.

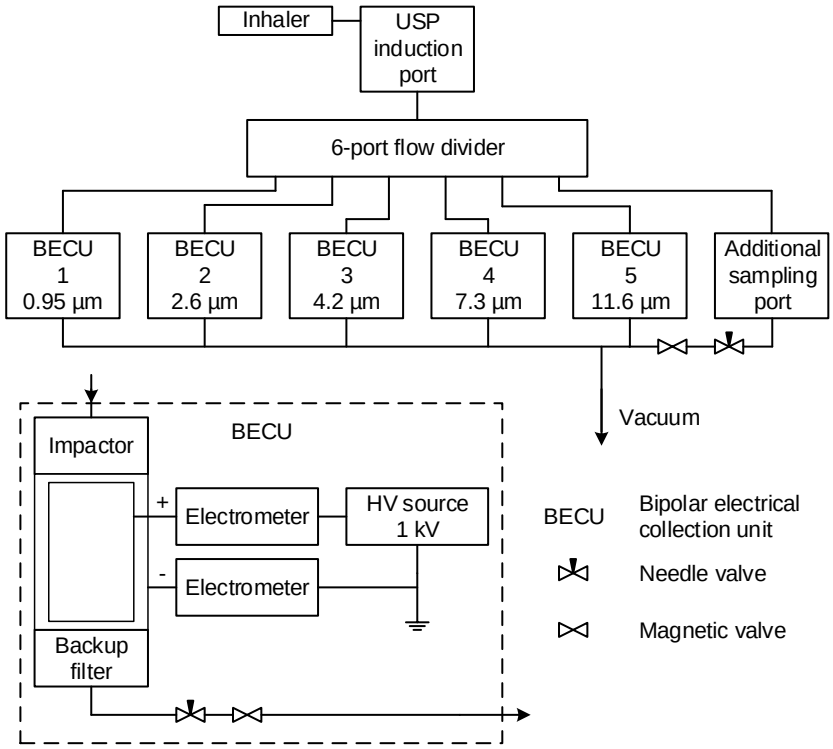

Figure 4.5 Construction of the BOLAR (above) including a more detailed schematic of the BECU (below) (adapted from **Paper III**). The cut diameters of the impactors are given for the corresponding BECUs.

Particles enter the instrument through the United States Pharmacopeia (USP) induction port, which leads particles into a 6-port flow splitter. One of the ports is an additional sampling port and five are used in the actual measurement. Each of these five ports is connected to a Bipolar Electrical Collection Unit (BECU), which contains an impactor, that is followed by an Electrostatic Precipitator (ESP), similar to the integrating analyzer introduced in Chapter 2. Both ESP electrodes are connected to electrometers, which enables the measurement of the collected particles. A backup filter after the ESP collects all of the penetrated particles. The ESP construction enables the bipolar measurement whereas the size classification is achieved with the impactors. The differences between, the bipolar electrical collection units are only in the impactors. Parallel units are equipped with impactors of different cut diameters D_{50}. Each impactor defines the upper limit of the aerodynamic diameter, according to the cut diameter, and only particles smaller than the D_{50} value are measured in the collection tubes.

The operation principle of the BOLAR is illustrated in Figure 4.6. During normal operation, a particle distribution enters the instrument and the flow is splitted between the BECUs.

Now all the BECU inlet size distributions are equal. Then, the flow is introduced into the impactors, which collect particles larger than their specific cut diameter. The penetrated fractions enter the ESPs. The inner electrode is kept at positive high-voltage and the outer electrode is at ground potential, which generates an electric field. Because of the electric field, negative particles drift onto the inner electrode and positive particles onto the outer electrode. The two electrometers connected to inner and outer tubes measure the charge carried by the particles. If neutral particles are present, these penetrate the ESP and the backup filter collects them. Charge-to-mass ratio requires information on particle mass. This is measured by dissolving the particles from the collection tubes with a suitable solvent of known volume and analyzing the material concentration from the solution.

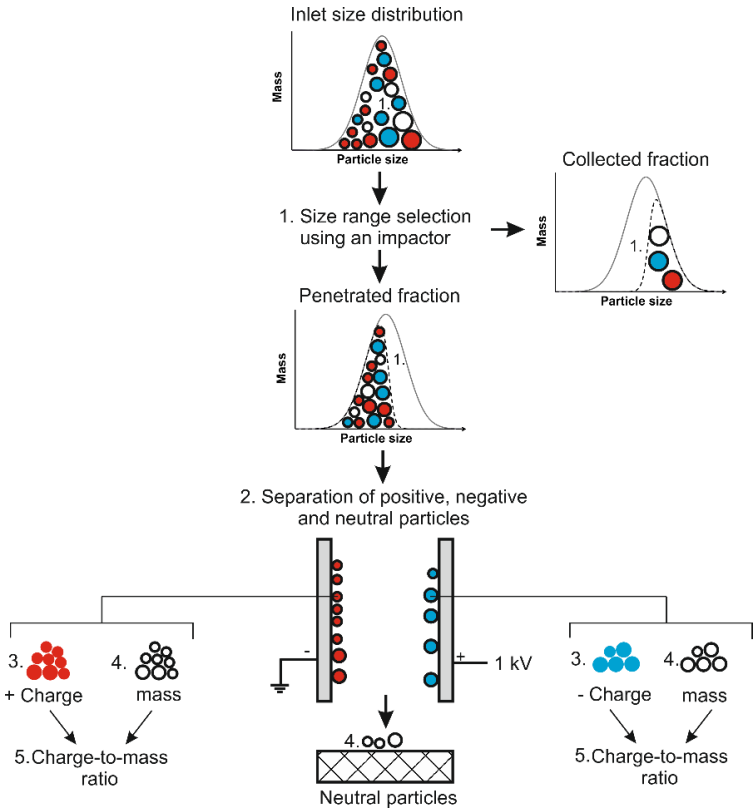

Figure 4.6 Operation principle of the BOLAR. (**Paper III**)

Because of the parallel configuration, the calculation differs from typical cascade impactors. Each stage *n* measures particles smaller than the impactor cut diameter $D_{50,n}$. To acquire results as a function of a certain particle size range $\Delta D_{n,i}$, where *i* refers to particle polarity, the value of the previous stage is subtracted from the result of the

corresponding stage. Thus, the total charge of particles for the specific size range *q* is calculated for stages 1…5 with equation

$$q(\Delta D_{n,i}) = \begin{cases} q_{n,i} \quad for\ n = 1 \\ q_{n,i} - q_{n-1,i} \quad for\ n = 2...5 \end{cases}, \tag{14}$$

and the charge-to-mass ratio *q/m* with an equation

$$\frac{q}{m}(\Delta D_{n,i}) = \begin{cases} \dfrac{q_{n,i}}{m_{n,i,electrode}} \quad for\ n = 1 \\ \dfrac{q_{n,i} - q_{n-1,i}}{m_{n,i,electrode} - m_{n-1,i,electrode}} \quad for\ n = 2...5 \end{cases}. \tag{15}$$

The particle masses *m* are measured by extracting the particles from the positive and negative electrodes as described earlier.

The BOLAR was calibrated using conventional methods, described in more detail in Chapter 3 and in **Paper III**. The particle sizes up to 1.5 µm were generated with the SCAR and larger particles with the VOAG. In the SCAR calibration, a DMA (3071, TSI Inc.) acted as the size reference. In the VOAG measurements, the particle diameter was calculated from the generator operating parameters, and the APS was used to monitor the operation. The measurements were conducted using DEHS as a particle material, either evaporated and condensed on the small seed particles in the case of the SCAR or dissolved in 2-propanol in the case of the VOAG.

The calibration was conducted using the electrical method of Equation 8 (Hillamo and Kauppinen 1991), which requires charged particles. The measurements with the SCAR were straightforward as it generates singly charged particles. The VOAG-generated particles were highly charged during the droplet generation process. The charge was reduced to minimize electrical losses by using a separate corona charger with an opposite polarity to the generated particles, as in the case of the ELPI+, or by using an induction ring (Reischl et al. 1977).

The BOLAR uses parallel impactor configuration, which requires flow splitting before the impactors. The quality of the flow splitting is a significant factor in the µm size range, because such a large particles are prone to inertial losses. The 6-port flow splitter of the BOLAR was studied with charged particles generated using the VOAG and measured with 6 FCAEs connected to the flow splitter outlet ports. The capability to split the particle

flow was studied by calculating the fraction of the FCAE current from the average current of all 6 FCAEs. The relative distribution of particles is presented in Figure 4.7 as a function of the particle aerodynamic diameter. The flow splitter performs well, the maximum deviation is less than 10 % from the average, up to a 12 µm particle diameter. Above this, deviations increase, which is not surprising as the flow splitter acts as an impactor, with a cut diameter of 12.33 µm at 60 l/min flow rate.

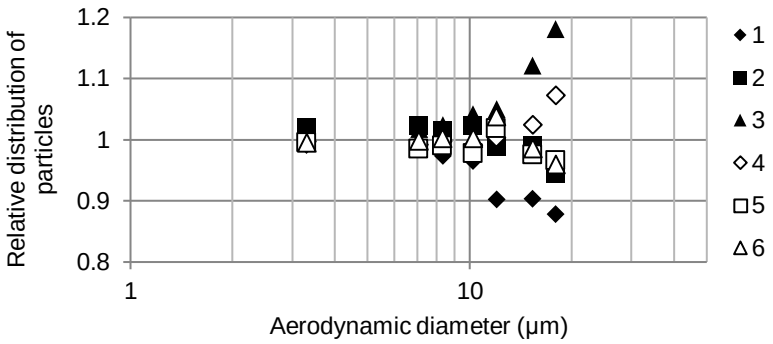

Figure 4.7 Relative distribution of particles between the flow splitter outlets, given in the legend, at 60 l/min inlet flow rate (modified from **Paper III**).

The collection efficiencies of the impactors were measured in a similar way with the flow splitter operation. Now the particle size range of the VOAG was supplemented with the SCAR, which was used to produce particles from 0.7 to 1.2 µm. The reference concentration was measured electrically with Faraday cup filters installed after the impactors. The collection efficiencies of the BOLAR impactors are presented in Figure 4.8 including the fit functions according to Equation 10.

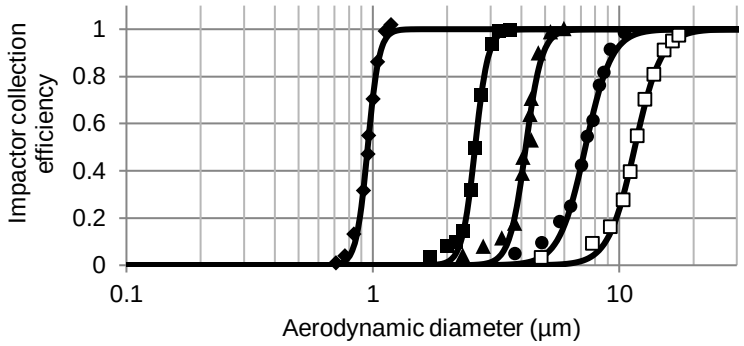

Figure 4.8 Collection efficiencies of the BOLAR impactors including measurement points and fit functions. (modified from **Paper III**)

The impactor cut diameters and curve steepness values are collected in Table 4.1. All the stages have normal or steep cut curves as the steepness values are over 4 for all impactors. As a comparison, the steepness values of the ELPI+ impactor stages ranged from 3 to 8 (Table 3.2). The flow splitter cut diameter was 12.33 µm, which is close to the cut diameter of the largest impactor. Both the close cut diameters and the low steepness value 1.72 indicate that the flow splitter affects the particle distribution of the stages with the largest cut diameters. However, it is possible to compensate this effect in the calculation.

Table 4.1 Cut diameters D_{50} and curve steepness values s for BOLAR impactors operating at 10 l/min flow rate and the flow splitter at 60 l/min. (**Paper III**)

Impactor	D_{50} (µm)	s
1	0.95	9.39
2	2.60	8.22
3	4.17	6.64
4	7.29	4.06
5	11.57	4.02
Flow splitter	12.33	1.72

The real application of the BOLAR was studied by using it to measure charge distributions from Dry Powder Inhalers (DPI) loaded with lactose. A single actuation of a DPI is presented in Figure 4.9A as a time series. The impactor stage with the smallest cut diameter produces the smallest current and the stage with the largest cut diameter produces the largest current. This is an expected result, as the impactors are parallel.

The integration over the measurement period produces the total electric charge per channel. When these charges are subtracted between the parallel BECUs using the Equation 14, the size fractioned charge of particle can be presented, see Figure 4.9B. When the particle material is extracted from the collection tubes, the mass of the material can be measured, as shown in Figure 4.9C, and the charge to mass ratio can be calculated according to Equation 15, which is presented in Figure 4.9D. In this case, the amount of material in Stage 1 was below the limit of detection, and this stage is excluded from the figure.

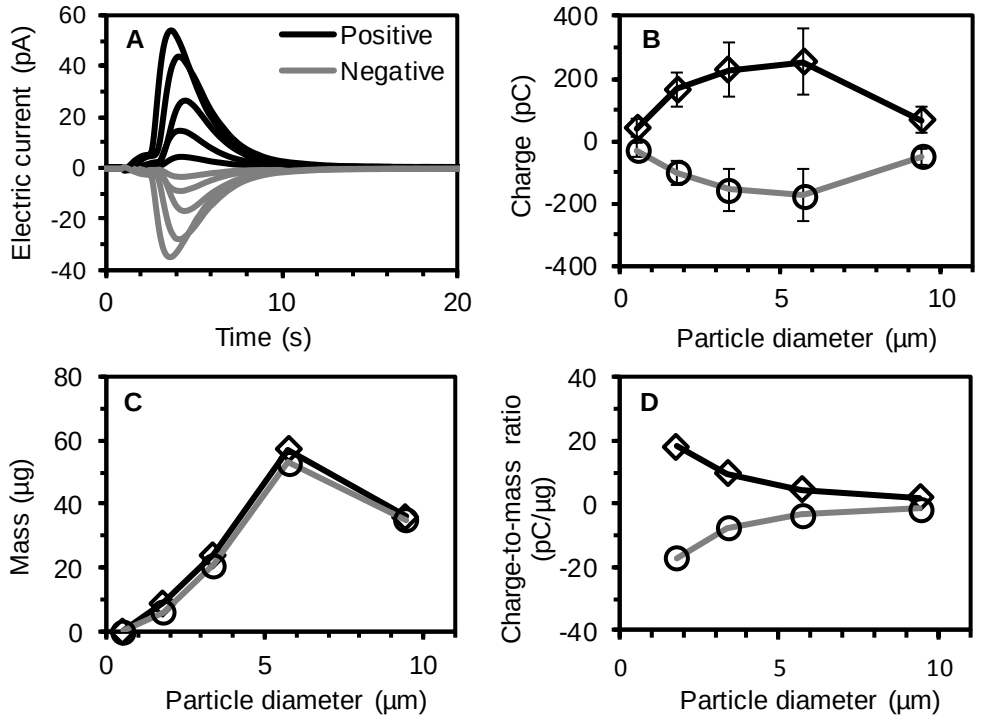

Figure 4.9 Inhaler measurements with BOLAR. The subfigure A) shows the electric currents from the collection tubes as a function of time for a single DPI actuation, B) the average charge per DPI actuation including standard deviation, C) the particle mass from the collection tubes, and D) the average charge-to-mass ratios. (adapted from **Paper III**)

The average charge per particle is high. By using the mass and charge measurement results and the density of lactose, 1.5 g/cm^3, the average number of elementary charges per particle is 500 for positively charged 1.8 µm particles. This value is considerably higher than for instance the value of 165 produced by the ELPI+ corona charger (**Paper I**) for the same particle size. The interesting result is that although significant particle charge levels are detected for both positive and negative channels, the net charge is

approximately zero. Thus, the analysis based on typical net charge measurement would not express the real electrical state of the aerosol.

4.4 Comparison of charge measurement methods

Different charge measurement methods with bipolar capability are compared in Table 4.2 including the developed DMA-ELPI (**Paper II**) and BOLAR (**Paper III**). The significant factors are the measurement size range, duration of the measurement, particle concentration range and specific requirements for particle material. The definition of the particle concentration is complex in charge measurements. CPCs and OPCs count particles and measure the number concentration, whereas electrical instruments such as the ELPI or the BOLAR measure charge carried by particles. As a result, the lowest detectable number concentration varies in the case of the electrical detection as a function of particle charge. Thus, the suitable concentration is given only as an approximate value.

A DMA-CPC operated with and without the bipolar charger is suitable only for simple charge distributions due to the comparison between the two measurements. At large particle sizes, particles can acquire different number of elementary charges resulting in a complex charge distribution. Thus, the single DMA is best suited for measuring small particles with a diameter approximately 50 nm or less. The particle concentration must be high enough to acquire distinct particle distributions during both charge and size measurement. Hence, a single DMA is not suitable for low particle concentrations. Measurement of one polarity requires two DMA voltage scans, one with the charger for size distribution and another one without the charger for charge distribution. As a result, the measurement lasts from approximately 2 to 20 min for a single polarity and from 3 to 30 min for both polarities.

The Tandem-DMA can resolve more complex charge distributions through two-dimensional (charge-size) measurement than the single DMA. The DMA size classification requires a multiple charge correction, which produces noise at large particle sizes. In addition, after the first DMA, all particles are charged, and the bipolar charging must be efficient enough to provide equilibrium charge distribution for the DMA responsible for size measurement. Hence, the maximum measurable particle size is approximately 300 nm. A single measurement requires scanning of voltages of two

DMAs, and as a result, a single measurement point lasts from half an hour up to an hour and half, if both polarities are measured.

Table 4.2 Size classifying bipolar charge measurement methods. The concentration range depends on the particle charge in the electrical methods and is given as an approximate value. The duration of the measurement is given for a bipolar measurement.

	Size range	Duration	Concentration range	Special requirement
DMA-CPC	1…50 nm	3…30 min	Med-High	No
Tandem-DMA	1…300 nm	0.5…1.5 h	Med-High	No
DMA-OPC	0.3…10 µm [a] 0.15…1.5 µm [b]	2…20 min	Low-Med	Index of refraction
E-SPART [c]	0.4…20 µm	<1 s	Low	No
DMA-ELPI **(Paper II)**	30…800 nm [d] 16 nm…10 µm [a, e]	2…20 min	Med-High	Effective density
BOLAR **(Paper III)**	1…15 µm	~1 s	Med-High	No

[a] Particles larger than ~1 µm can be measured only if they are multiply charged
[b] Vishnyakov et al. (2016)
[c] Mazumder et al. (1991)
[d] Tested size range
[e] Potential size range based on ELPI+ specifications

The DMA-OPC is suitable for larger particles. The lower size range is limited by the OPC detection capability. Normally, OPC detection efficiency is low below 300 nm. Some OPCs can reach slightly smaller sizes, such as the 150 nm used by Vishnyakov et al. (2016), but still the lowest detectable particle size is large compared to other DMA methods. The measurement requires only a single DMA scan, which lasts from 2 to 20 min in total for both polarities. The method is suitable for low to medium particle concentrations because of the OPCs individual particle counting capability. The OPC measures the particle optical diameter, and as a result, the particle index of refraction must be known to obtain correct results.

The E-SPART has a size range from 0.4 µm up to 20 µm according to Mazumder et al. (1991). Measurement is fast and lasts less than 1 s. Both polarities are measured simultaneously. As the measurement is based on individual particles, the maximum

concentration is extremely low. The maximum particle measurement rate is 100 1/s, which is equivalent to a concentration of 6 1/cm^3 at 1 l/min flow rate.

The DMA-ELPI method developed in **Paper II** was tested in the size range from 30 to 800 nm. Most likely, the size range could be increased from this. As stated earlier, the ELPI+ impactor has a minimum cut diameter of 16 nm and the maximum of approximately 10 µm, which could set the size limits of the charge measurement, if the large particles only penetrate the DMA. The duration of the measurement is similar to the DMA-OPC, as both are based on the DMA voltage scan, which takes from 1 to 10 min for a single polarity and from 2 to 20 min for both polarities. Electrical particle measurement from the impactor stages cannot be used for the lowest particle concentrations, but is well suited for medium to high concentrations. Because the impactor measures the particle aerodynamic diameter, the particle effective density must be known. If the particle material is a known liquid, the literature density value represents effective density well. If the particle material is not known or particles are solid, the density must be measured. This is possible with a small modification, adding a bipolar charger in front of the DMA (Maricq and Xu 2004).

The BOLAR (**Paper III**) was designed for the same particle size range that inhalers produce, between 1 and 15 µm. The time resolution is in the order of 1 s for the electrical measurement, which is fast compared to the DMA scanning and is required for inhaler studies. Both polarities are measured simultaneously, similar to the E-SPART. As with the DMA-ELPI, the electrical measurement cannot be used to detect low concentrations, but on the other hand, it is capable of measuring high concentrations. Additionally, the entire output of the inhaler can be analyzed, which is not possible with for instance with the E-SPART, which detects individual particles.

None of the available charge measurement techniques is superior, and the new methods, DMA-ELPI and BOLAR, developed in **Papers II** and **III** supplement the existing ones. The DMA-ELPI was designed to work as a universal charge measurement method for faster measurement and wider size range than the Tandem-DMA while the BOLAR was designed for special application, inhaler studies.

5 Primary calibration of detection efficiency

This chapter focuses on the most precise aerosol instrument calibration methods, i.e. on primary calibration. First, the challenge of the detection efficiency calibration is discussed. Later, experience from earlier instrument calibration work is refined by introducing a new electrical wide size range calibration setup.

5.1 Calibration methods

Calibration of the instrument detection efficiency is often conducted as a function of the particle size or as a function of the particle concentration. In both cases, the particle input concentration must be known. As already discussed in Chapter 3, there are two principal methods to determine the inlet concentration. If the particle generator output is precisely known, and the losses are minimal, the generator can be used as a number concentration reference (Iida et al. 2014). The other option is to measure the inlet concentration using a reference instrument. The FCAE has been selected to act as a primary concentration standard in CPC calibrations (ISO 27891:2015). As a consequence, the particle concentration is traceable to SI primary units through the electric current charged particles carry and through the flow rate.

As the particle charge affects the calibration uncertainty directly, large effort has been put towards producing singly charged particles for the FCAE. Producing singly charged sub-30 nm particles is relatively straightforward: particle generator, bipolar charging and DMA classification is sufficient. The problem arises at larger particle sizes when the amount of multiply charged particles increases and the DMA outlet may contain a

combination of different sizes and charge levels. This effect can be corrected (ISO 27891:2015) to some extent, but, for more accurate calibrations elimination of multiple charged particles is desired. Removal of charged particles and weak bipolar charging of the remaining aerosol is one option (Gupta and McMurry 1989). On the other hand, if particle size range is limited with an impactor stage after the DMA classification, the large multiple charged particles can be removed rather effectively (Romay-Novas and Pui 1988). Feeding the DMA with a narrow particle size distribution is another option (Fletcher et al. 2009). If calibration particles are generated by growing small singly charged seed particles with condensation in La Mer type generator (Sinclair and La Mer 1948), it is possible to create large µm-sized calibration particles that are singly charged (Uin et al. 2009, Yli-Ojanperä et al. 2010b, Yli-Ojanperä et al. 2012).

5.2 Electrical wide size range calibration system

The complexity of multiple different particle generation and concentration reference methods, especially in **Paper I** and also in **Paper III**, raised a question: is it possible to simplify the calibration procedure into a single particle generation and concentration reference setup, and is there a possibility to improve the calibration accuracy?

The IAG (Iida et al. 2014) would produce the maximum accuracy, but the size range is limited only to large particles and the output particle concentration is low. Thus, this method cannot be used as a basis for the wide size range calibration system. The second option is a FCAE-based system. If the particle charge is accurately known, especially in the case of the singly charged particles, the FCAE works as a reliable internationally recognized concentration reference (Högström et al. 2014, ISO 27891:2015). The SCAR (Yli-Ojanperä et al. 2010b) used in **Papers I-III** is based on the generation of singly charged particles, while the FCAE acts as a concentration reference. This setup could be used to generate larger particles than 1 µm (Yli-Ojanperä et al. 2012) or larger than 1.9 µm (**Paper I**) with some modifications. The saturator-condenser construction needs to withstand higher temperatures, up to 300 °C, which are needed to evaporate enough DEHS for large µm-sized particles. As discussed below, a large sized DMA is needed to classify these large singly charged particles. These issues have been previously solved. Uin et al. (2009) generated µm-sized particles with a rather similar particle generator and classified these large particles with a large DMA (Uin et al. 2011). What has not been previously demonstrated, is the confirmation that equal concentrations reach the

instrument under calibration and the reference, and µm-sized DMA-classified particles have not been applied in actual instrument calibration.

The schematics of the **Paper IV** calibration setup is presented in Figure 5.1. The seed particle generation, bipolar charging with an ^{85}Kr β-source and selection of 10 nm singly charged particles in a DMA is the same as in the SCAR (Yli-Ojanperä et al. 2010b), except that the primary particle material was changed from sodium chloride to silver to reduce corrosion effects. The saturator and condenser were manufactured from stainless steel, which can easily withstand 300 °C temperatures. The saturator saturates the flow with DEHS vapor, which is impregnated as liquid into a ceramic wick installed inside the saturator.

If large particles are generated, high DEHS vapor concentration leads to homogeneous nucleation, which produces neutral particles, and the FCAE cannot detect these. The DMA after the condenser removes the unwanted homogenously nucleated neutral particles. The second function of the DMA is to act as the size reference through known dimensions, classification voltage and flow rates. The third function of the DMA is to produce variation in the particle concentration by removing all particles periodically, during which the electrometer zero-level is measured. In the calibration setup, the DMA is selected according to the size range. A commercial Nano-DMA (3085, TSI Inc., Chen et al. 1998) was used for the smallest size range and a Vienna-type DMA (Winklmayr et al. 1991) for the intermediate range. For the largest µm-sized particles a new large-sized DMA, named as the Tampere Long DMA, was designed and manufactured.

The Tampere Long DMA was constructed based on the design principles of the traditional cylindrical DMAs. The challenge in the design and construction is how to ensure that the distance between the inner and outer tube is equal over the entire classification zone. This requires that the tubes are parallel, circular, and that the construction is highly concentric. To fulfill these requirements, highly circular aluminum roller and cylinder tubes were selected and effort was put to ensure that these tubes are concentric in the DMA construction. The classification zone inner diameter is 72 mm, outer diameter 80 mm and length 1.7 m, which define the particle size in combination with the flow rates and the classification voltage. With a sheath flow of 10 l/min, the mobility diameter is 5.3 µm at a classification voltage of 9000 V. Gravity affects particles in this size range but the effect is compensated using a method presented by Uin et al. (2011).

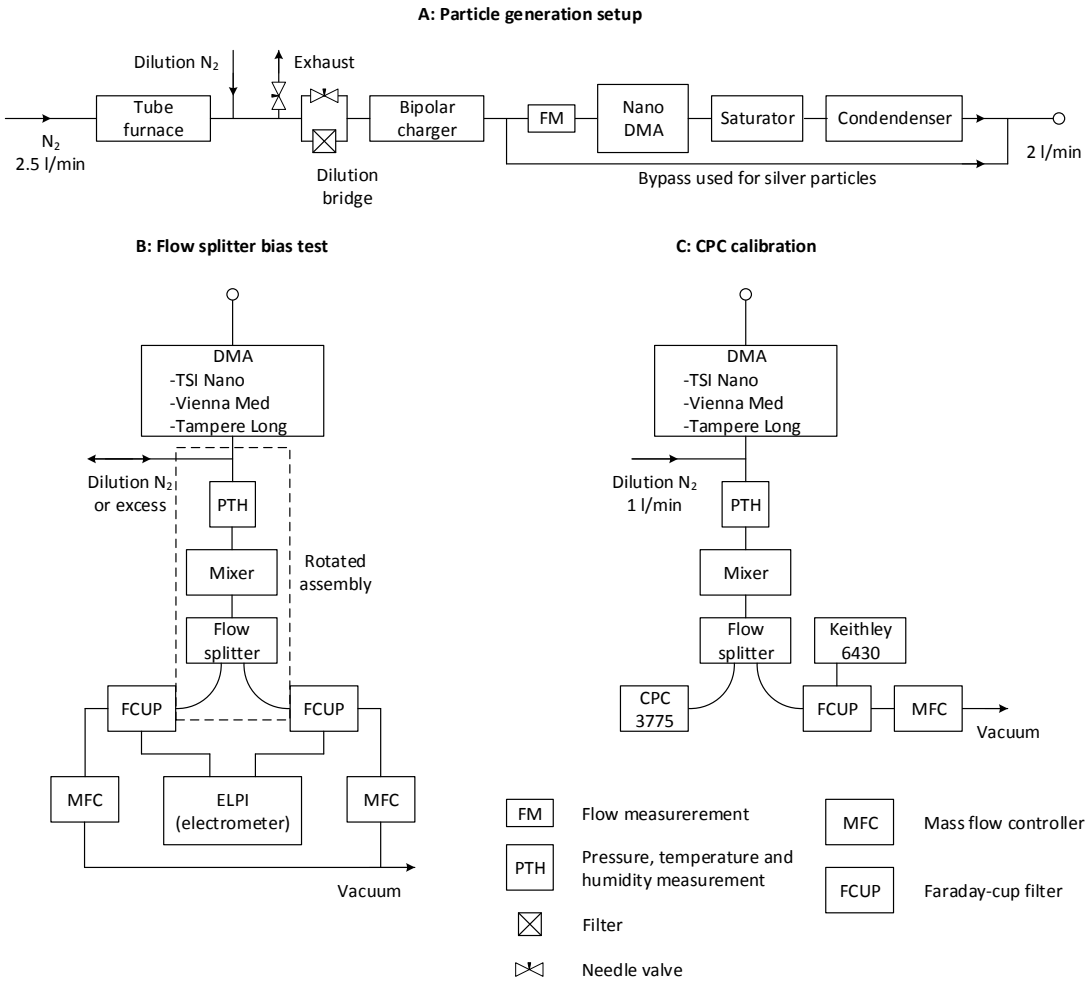

Figure 5.1 The electrical primary calibration setup (modified from **Paper IV**). Subfigure A shows the particle generation setup, subfigure B the configuration used in the flow splitter bias test and subfigure C the setup used in the CPC calibration.

In the calibration setup, pressure, temperature and humidity measurement (PTU303, Vaisala Oyj) is located between the DMA and the mixer. The mixer is required for producing constant concentration throughout the entire flow channel. After the mixer, the flow is led into a commercial flow splitter (3708, TSI Inc.), which splits the aerosol flow between the instrument and the reference.

The FCAE acts as a concentration reference, and the reference concentration is defined through the electric current and flow rate. The main advantage of the FCAE is the minimal dependency on the particle size compared to other number concentration instruments such as CPCs or OPCs. However, the rather high noise and zero-level drifting require a rather long measurement time and the zero-level compensation without particles. The used FCAE consists of a Faraday cup filter and a commercial electrometer (6430, Keithley Instruments LLC). The flow information is provided by a mass flow controller (MC-2SLPM-D/5M, Alicat Scientific Inc.).

Characterization of a DMA transfer function in the µm size range is challenging due to the lack of reference instruments. The size standard particles are one option, but when these were tested, the final concentration after the DMA was low. As a result, the characterization of the transfer function was conducted at smaller particle size. Approximately 400 nm singly charged highly monodisperse particles were generated with the developed setup and classified with a DMA (3071, TSI Inc.) operated at 6 l/min sheath and 0.3 l/min sample flow with a balanced sheath and excess.

The transfer function of the Tampere Long DMA is presented in Figure 5.2 for 20 l/min and 10 l/min sheath flows with 2 l/min sample flow measured using a closed sheath flow loop configuration (Jokinen and Mäkelä 1997). At the 20 l/min sheath flow rate, the acquired transfer function deviates slightly from the ideal triangular shape shown in Figure 2.4 (Knutson and Whitby 1975) at lower electrical mobilities, i.e. larger particle sizes. However, the transfer function is still rather narrow. The full width half maximum resolution is 7.95, while the ideal value from the flow configuration would be 10. When the sheath to sample ratio is decreased the transfer function broadens as predicted by the basic DMA theory (Knutson and Whitby 1975).

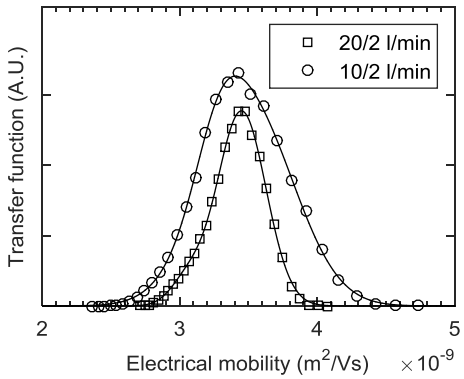

Figure 5.2 Transfer function of the Tampere Long DMA at two different sheath flow rates. (modified from **Paper IV**)

The electrical calibration method relies on the flow splitting between the instrument and the FCAE. The quality of this flow splitting is critical as it generates a bias, which is directly affecting the calibration result. The most important factor is the equal particle concentration throughout the entire flow. This is achieved by mixing the flow. Small particles suffer from diffusion deposition, especially sub-10 nm particles. The diffusional effects are eliminated by using equal-length tubing and equal flow rates. Another factor is the electrical effects, which are relevant because of charged calibration particles. For instance, accumulated charge in the tubing generates electric fields, which increase the losses of the charged particles. This factor is minimized with the use of conductive tubing. The largest particles, in µm sizes, suffer from inertial losses. These are minimized by using tubing with equal bending radius, by using equal flow rates, and by keeping the flow velocities low. While the electrical calibration setup is used from a few nm particle sizes up to µm sizes, all these factors have to be considered.

In the developed calibration setup (**Paper IV**), the equal concentration throughout the flow is achieved using a static mixer, which mixes the flow in prior to the flow splitting. A large diameter static mixer (FMX8412S, Omega Engineering Ltd.) was selected to minimize large particle losses. The diffusion and electrical effects were minimized using the techniques introduced in the previous paragraph. The flow rate of the FCAE was adjusted with a MFC to match the instrument flow rate.

In a careful calibration work, the effects of flow splitting are not only minimized, but also tested. Previously, the performance of the BOLAR flow splitter was studied in **Paper III**, and a rather similar approach is taken for this calibration setup. The advantage of the electrical setup is, that studying these effects is easy using two identical Faraday cup

filters, the normal reference Faraday cup (1) and an additional Faraday cup (2) installed in the place of the instrument under calibration. The interesting factor is the bias of the flow splitting (Yli-Ojanperä et al. 2012, ISO 27891:2015), which is calculated from the detection efficiencies. The detection efficiency of Faraday cup 2 η is defined with equation

$$\eta = \frac{I_2 Q_1}{I_1 Q_2}, \tag{16}$$

where I is the electric current from the Faraday cup and Q the flow rate through the Faraday cup, while the numbers refer to the corresponding Faraday cups. The detection efficiency was measured in normal configuration, named *a*, and in configuration *b* where the entire mixer-splitter-tubing assembly was rotated so that the outlets were switched. The bias β is then defined (Yli-Ojanperä et al. 2012, ISO 27891:2015) with an equation

$$\beta = \sqrt{\frac{\eta_a}{\eta_b}}. \tag{17}$$

The bias of the flow splitting was tested at the full calibration size range and as a function of the flow rate using large particles. These both are presented in Figure 5.3 with associated uncertainties for which the calculation is presented in **Paper IV**. High quality flow splitting, bias less than ±1 %, was obtained for the entire size range from 3.6 nm up to 5.3 µm at 1.5 l/min flow rate (per FCAE). The most challenging situation, the largest particle size of 5.3 µm, was studied in more detail. The flow splitting operates rather well between 1 and 2 l/min flow rates (per FCAE). The maximum bias is 2.1 % at this flow range. Below this, some bias is observed as a bias value of -5.0 % is measured at 0.75 l/min flow rate.

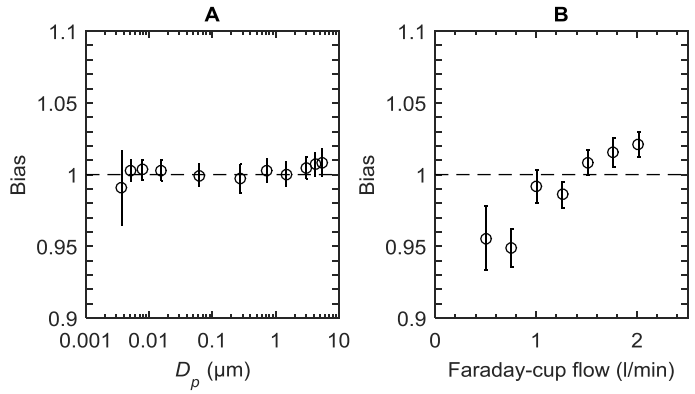

Figure 5.3 Calibration setup bias including expanded uncertainties (k=2) for the CPC calibration size range (A) and as a function of the Faraday cup flow rate (B). (**Paper IV**)

The potential of the developed calibration system was studied with a calibration of a CPC (3775, TSI Inc.). The CPC detection efficiency was studied from 3.6 nm up to 5.3 µm. This required three different DMAs, a Nano-DMA (3085, TSI Inc.), a Vienna-type DMA with a 280 mm long classification section, and the developed Tampere Long DMA. The detection efficiency of the CPC varies significantly in the studied size range as Figure 5.4 presents. The calculation of the uncertainties is presented in **Paper IV**.

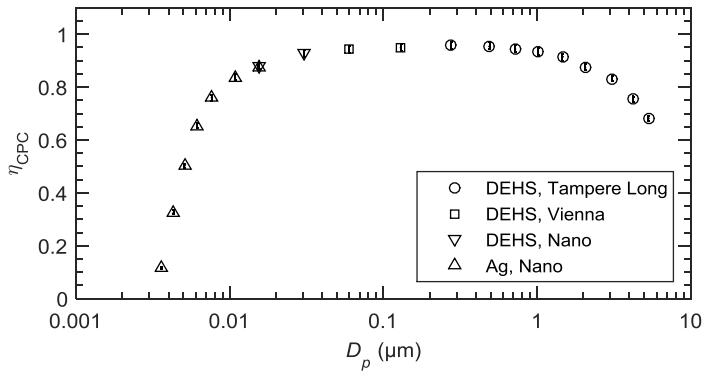

Figure 5.4 Detection efficiency of the CPC 3775 η_{CPC} as a function of particle mobility diameter D_p including expanded uncertainties (k=2). The main particle material and the DMA type is given in the legend. (**Paper IV**)

The cut diameter of the CPC 3775, measured using silver particles, is at 5.1 nm, and above this, the detection efficiency increases until the maximum value of 0.957 is reached at 275 nm particle diameter. Then, the detection efficiency begins to decrease, and at the maximum calibration particle diameter of 5.3 µm, the detection efficiency is

0.68. The decline of the detection efficiency at µm sizes probably results from inertial or gravitational losses inside the CPC. Calibration size of 15 nm was measured with both silver and DEHS, and dependency on the particle material was not observed as the results are within the uncertainty limits.

The expanded calibration uncertainties (coverage factor k=2), calculation given in **Paper IV**, are less than 4 % over the entire size range and less than 1.5 % between 6 nm and 5.3 µm. The highest uncertainty factor in this size range is the flow measurement with an uncertainty of 1.1 % followed by the bias evaluation. As a comparison, the SCAR was previously used in a CPC calibration, and the uncertainties ranged from 1.1 % to 2.6 %, while the size range was smaller than now (Yli-Ojanperä et al. 2012). During the same Yli-Ojanperä et al. (2012) measurements, the calibration system of the National Institute of Advanced Science and Technology of Japan (AIST) achieved uncertainties between 0.8 and 1.1 %. Only Iida et al. (2014) from AIST reports significantly lower uncertainties of 0.6 % from 0.4 to 10 µm particle sizes but this value is given for particle generation efficiency, not for particle concentration, which is often larger as it is affected by the uncertainty of the flow rate. Fletcher et al. (2009) report an uncertainty of 2.4 % for FCAE based system at the optimum case and the Federal Institute of Metrology of Switzerland (METAS) offers number concentration calibrations with uncertainties less than 10 % from 50 nm to 5 µm with PSL particles and less than 5 % with combustion generated particles between 10 and 200 nm (METAS 2018).

The concentration uncertainty of the developed system is lower than offered by METAS but higher than what AIST can achieve. The uncertainty could be improved by investing into a more precise flow measurement and by re-evaluating the flow splitter bias with lower uncertainties. After these steps, the uncertainty level of less than 1 % would be most likely achievable.

5.3 Comparison of calibration methods

Calibrating aerosol instruments in a wide size range is challenging. In **Papers I** and **III** new aerosol instruments (ELPI+ and BOLAR) were calibrated using different particle generation methods to cover the size range in **Paper I** from approximately 10 nm up to 10 µm and in **Paper III** from 700 nm up to 17 µm. Originally, the SCAR was applied up to 1 µm with a conventional DMA (Yli-Ojanperä et al. 2012), and in **Paper I** using low,

out of specifications flow rate, 1.9 µm calibration size was reached. This was supplemented with the VOAG in the µm size range.

The operation of the VOAG between 1 and 3 µm is troublesome as the generator is prone to clogging. Furthermore, finding an accurate concentration reference for the VOAG is a challenge. During the measurements of **Paper I**, it was noticed that a SCAR and DMA based particle generation method, producing singly charged calibration particles, would be highly beneficial. It would make the calibration work easier and provide a reliable number concentration reference through using a FCAE, which is, with a calibrated electrometer and flow meter, an SI-traceable concentration reference.

In **Paper IV**, the new calibration setup was introduced including the Tampere Long DMA, the new particle growth unit withstanding high temperatures, and the flow mixing and splitting for µm-sized particles, all along with appropriate test measurements. As particles in the µm sizes are prone to inertial losses, the splitting of the aerosol between the instrument and the reference was studied carefully using simultaneous dual FCAE measurements with identical Faraday cup filters. Capability to conduct such a dual measurement is a significant advantage allowing the setup to be configured for different type of instruments. The electrical calibration setup was furthermore used to calibrate a CPC from 3.6 nm up to 5.3 µm with a high accuracy and SI-traceability through calibrated current and flow measurements.

Similar wide-range calibration setups have not been available. Other institutes combine different particle generation and reference methods to reach the same size range, see Figure 5.5. For instance, the Swiss Federal Institute of Metrology (METAS) combines small soot particles classified with a DMA and larger PSL particles to reach similar size range (METAS 2018). This requires two different concentration references, a FCAE with the DMA and an optical particle counter with the PSL. The National Institute of Advanced Industrial Science and Technology of Japan (AIST) combines PSL particles classified with a DMA and detected with an FCAE reference with an IAG (Iida et al. 2014) to reach a wide particle size range (AIST 2018).

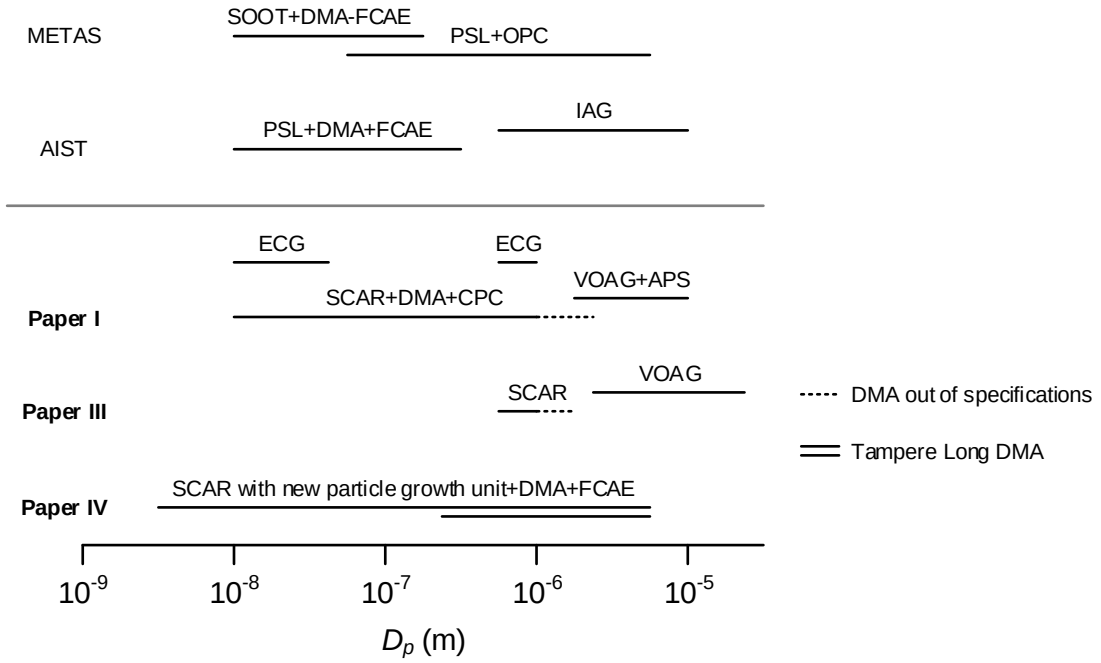

Figure 5.5 Applied particle generation and classification methods in calibration measurements (**Papers I, III, and IV**) and available calibration services with monodisperse particles at two selected National Metrological Institutes: METAS (2018) and AIST (2018).

The comparison of different concentration reference instruments and calibration setups is presented in Table 5.1. The CPC and OPC are typical concentration reference instruments. The advantage of both instruments is the high sensitivity due to measurement based on single particle counting, which on the other hand results non-linear response at high concentrations. Typically, OPCs are constructed with relatively simple flow lines, and as a result, particle losses are low. In the CPCs, the flow configuration is more complex resulting in larger particle losses than in the OPCs. The operating size range, with a constant and high detection efficiency, of both instruments is actually rather narrow. OPCs can typically detect only large particles with high accuracy. In the accurate single flow CPCs, all the small particles do not necessarily grow to the detectable size, while the large µm-sized particles suffer from losses inside the instrument. As a result, the constant high detection efficiency range is rather narrow, for instance in Figure 5.4 from approximately 30 nm to 1 µm. As a result, a CPC as such without a thorough size calibration cannot operate as a concentration reference in a wide size range.

Table 5.1 Particle concentration reference instruments and generators. The size range is defined for high and approximately constant detection efficiency. The number concentration is estimated for 1 l/min instrument flow rate and equal flow rate for reference if the flow is splitted. The lowest calibration concentration with the FCAE is estimated to be 200 1/cm^3 as in **Paper IV**.

Instrument/setup	Size range	Concentration (1/cm^3)
CPC	30 nm…1 µm	~10…~10 000
OPC	0.3…15 µm [a]	<1…~100
IAG [b]	0.4…10 µm	1…50
DMA+FCAE	~1 nm…~50 nm	200…~100 000
PSL+DMA+FCAE	50…300 nm [c]	200…~17 000 [d]
SCAR+FCAE [c]	<10 nm…1.0 µm	200…>21 000 (36 nm… 460 nm) [e]
Paper IV	3.6 nm…5.3 µm	200…>18 000 (10 nm…3 µm) 200…>1 700 (3.6 nm…5.3 µm)

[a] Chen et al. (2011)
[b] Iida et al. (2014)
[c] Yli-Ojanperä et al. (2012)
[d] Fletcher et al. (2009)
[e] Yli-Ojanperä et al. (2010b)

Because particle counters have only limited capabilities, various calibration setups based on alternative detection methods have been developed. The comparison of the developed calibration system (**Paper IV**) to other existing calibration methods presented in Table 5.1 reveals that the size range of the developed system is exceptionally wide for a single setup and for a single concentration reference. The Faraday cup filter has a minimal size dependency, and the high linearity and accuracy are obtained with the electric current measurement. The major limitation is the sensitivity, in this case the capability to detect low concentrations, which is limited compared to particle counting instruments. Of course, the sensitivity can be increased by using a longer measurement time, which increases the signal to noise ratio, but the level of single particle counting is not achievable.

6 Summary

Electrical aerosol instrumentation techniques were developed for particle charge measurement and instrument calibration applications. A commercial instrument was calibrated thoroughly and two new charge measurement methods were developed, one for general aerosol research and one for inhaler-generated particles. In addition, a new primary calibration system was designed, constructed, evaluated, and applied in an example calibration.

The commercial instrument, ELPI+, was calibrated using traditional techniques in a wide particle size range from approximately 10 nm to 10 µm in **Paper I**. The calibration included determination of the charger *Pn*-value and the impactor cut diameters and the secondary collection efficiencies. The *Pn*-value was high, i.e. the charger was efficient, compared to other commercial chargers. The impactor cut diameters and the steepness values were approximately the same as in the previous ELPI model. Without the calibration presented in **Paper I**, the ELPI+ could not be used as an accurate aerosol instrument in scientific or industrial applications.

The DMA-ELPI particle charge measurement method was introduced and developed, and is reported in **Paper II**. It utilizes the calibrated ELPI+ as a detecting instrument. The developed method was characterized with particles of known charge levels in the size range from 30 to 800 nm. The operating size range of this method is already wide, compared to other available methods, and based on the specifications of the used instruments, the size range could be perhaps extended in the future. The main result of **Paper II** is the introduction of the charge measurement method, which allows measurements in a wider size range than any single existing technique, and has a reasonable minute-scale measurement duration.

As the particle charge is a significant factor in pulmonary drug delivery, a new instrument, BOLAR, was developed for measuring the bipolar charge levels from inhaler-generated particles in **Paper III**. BOLAR utilizes parallel impactors, which are followed by electrically measured particle collection tubes. This construction enables fast measurement of the inhaler-generated particles. The main components of the BOLAR were calibrated in laboratory conditions, and the instrument was used to analyze bipolar charge from particles generated with an inhaler. Previously, there were no instruments capable of conducting such a bipolar charge measurements directly from inhalers.

The instrument calibration with traditional methods in **Papers I** and **III** required significant effort. The SCAR used in **Papers I-III** offered a basis for a new calibration system, which was developed in **Paper IV**. The aim was to reach larger particle sizes than with the SCAR. A new particle growth unit producing larger particles was constructed. The larger particles also required designing and constructing of a new large DMA named as Tampere Long DMA. The electrical calibration is based on the reference measurement with an FCAE, which requires careful flow splitting. A new flow mixing and splitting system was constructed. Operation of all these components was analyzed, and the setup was used in an example calibration of a CPC in the size range from 3.6 nm to 5.3 µm. Such a wide calibration size range has not been reported previously for a single setup. Calibration uncertainties below 1.5 % were obtained between 6 nm and 5.3 µm. The achieved uncertainty level is low, as only one metrological institute has reported better uncertainties for such a size range (Yli-Ojanperä et al. 2012, Iida et al. 2014). The largest uncertainty factor in the developed system was the flow measurement, and it could be improved by investing into a flow meter with greater accuracy. This modification would allow reaching even lower total uncertainties than now reported. As a conclusion, **Paper IV** proves that a single calibration setup and singly charged particles can be used in instrument calibration from nanometers up to micrometers with low uncertainties.

6.1 Outlook

Both the ELPI+ and the BOLAR are commercial instruments and the results from **Papers I** and **III** are used by the manufacturer as reference values. The ELPI+ is now used by the research community and industry in various applications including for instance engine emissions, air quality, occupational hygiene and pharmaceutical research. The BOLAR is currently used in inhaler related research. The data-analysis method of the

ELPI+ has been improved with a new high-resolution inversion algorithm (Saari et al. 2018), which utilizes the charger and impactor parameters defined in **Paper I**.

The DMA-ELPI charge measurement was introduced in **Paper II** as a first stage solution and could be improved in the future. For instance, with small effort, the total measurement time could be reduced by minimizing the residence time in the tubing and optimizing the DMA scan times as suggested in **Paper II**. The stepped DMA scan always requires a certain stabilization period that could be removed with a continuous voltage scan similar to the SMPS. The calculation could be improved by utilizing some steps from the recent ELPI high-resolution inversion method (Saari et al. 2018). To utilize the full potential of the DMA-ELPI, the effective density measurement with the aid of a bipolar charger could be integrated with the current setup. This could be realized for instance with an X-ray charger switched on during the density measurement and off during the charge measurement; a configuration suitable for field conditions.

The general trend in the calibration measurements is to achieve lower calibration uncertainties and reach new calibration ranges. As discussed in **Paper IV**, lower uncertainties would be achievable through more accurate flow measurement in the introduced calibration system. Another improvement could be a more accurate calibration of the DMA-based size classification with multiple reference sizes. The effect of gravity was taken into account with a correction calculation, but it would be beneficial to ensure that it provides correct results especially at the largest particle sizes. Yet another improvement could be related to the particle growth unit, which could be integrated with the seed particle classification to minimize the particle losses and maximize the output concentration, in a similar way as with the original SCAR. Perhaps some changes in the construction could be made to even increase the maximum particle size and to decrease the homogenous nucleation. Even without any modifications, the principle of the introduced calibration setup might be taken into use by national metrological institutes as a new primary standard for particle number concentration in a wide size range. The introduced system would increase the available calibration size and concentration ranges from the present level, and it would simplify the calibration procedure by defining the particle concentration through the electric current also in the µm size range.

References

AIST (2018). Calibration Services & Reference Materials. Available on (Cited 23.1.2018): https://unit.aist.go.jp/mcml/rg-pm/en/services.html

Ali M. (2010). Pulmonary Drug Delivery, in Handbook of Non-Invasive Drug Delivery Systems, First Edition, Kulkarni V.S. (ed.), Willian Andrew Publishing, Boston, 209-246.

Alonso M., Martin M.I., and Alguacil F.J. (2006). The Measurement of Charging Efficiencies and Losses of Aerosol Nanoparticles in a Corona Charger. Journal of Electrostatics, 64, 203-214.

Andersen A. (1958). New Sampler for Collection, Sizing, and Enumeration of Viable Airborne Particles. Journal of Bacteriology, 76, 471-484.

Aplin K.L. (2000). Instrumentation for Atmospheric Ion Measurements (PhD. thesis). Department of Meteorology, The University of Reading, 274 p.

Arffman A. (2016). Numerical and Experimental Study on Inertial Impactors (D.Sc. thesis). Publication 1372, Tampere University of Technology.

Athanassiou E.K., Grass R.N., and Stark W.J. (2010). Chemical Aerosol Engineering as a Novel Tool for Material Science: From Oxides to Salt and Metal Nanoparticles. Aerosol Science and Technology, 44, 161-172.

Badyda A.J., Grellier J., and Dąbrowiecki P. (2016). Ambient PM2.5 Exposure and Mortality Due to Lung Cancer and Cardiopulmonary Diseases in Polish Cities. In: Pokorski M. (eds) Respiratory Treatment and Prevention. Advances in Experimental Medicine and Biology, vol 944. Springer, Cham

Balachandran W., Machowski W., Gaura E., and Hudson C. (1997). Control of Drug Aerosol in Human Airways Using Electrostatic Forces. Journal of Electrostatistics, 40-41, 579-584.

Baron P.A. (1986). Calibration and Use of the Aerodynamic Particle Sizer (APS 3300). Aerosol Science and Technology, 5, 55-67.

Baron P.A., and Willeke K. (2001). Aerosol Fundamentals, in Aerosol Measurement: Principles, Techniques, and Applications, Second Edition, Baron P.A., and Willeke K. (eds.), John Wiley and Sons, New York, 537-567.

Beelen R., et al. (2014). Effects of Long-Term Exposure to Air Pollution on Natural-Cause Mortality: an Analysis of 22 European Cohorts within the Multicentre ESCAPE Project. Lancet, 383, 785-795.

Berglund R. N., and Liu B. Y. H. (1973). Generation of Monodisperse Aerosol Standards. Environmental Science and Technology, 7, 147-153.

Berner A., Lürzer Ch., Pohl F., Preining P., and Wagner P. (1979). The Size Sistribution of the Urban Aerosol in Vienna. Science of the Total Environment, 13, 245-261.

Biskos G., Reavell K., and Collings N. (2005a). Unipolar Diffusion Charging of Aerosol Particles in the Transition Regime. Journal of Aerosol Science, 36, 247-265.

Biskos G., Reavell K., and Collings N. (2005b). Description and Theoretical Analysis of a Differential Mobility Spectrometer. Aerosol Science and Technology, 39, 527-541.

Bottiger J.R., Deluca P.J., Stuebing E.W., and Vanreenen D.R. (1998). An Ink Jet Aerosol Generator, Journal of Aerosol Science, 29 Suppl. 1, pp. S965-S966.

Boucher O., Randall D., Artaxo P., Bretherton C., Feingold G., Forster P., Kerminen V.-M., Kondo Y., Liao H., Lohmann U., Rasch P., Satheesh S.K., Sherwood S., Stevens B., and Zhang X.Y. (2013). Clouds and Aerosols. In: Climate Change 2013: The Physical Science Basis. Contribution of Working Group I to the Fifth Assessment Report of the Intergovernmental Panel on Climate Change, Stocker, T.F., Qin D., Plattner G.-K., Tignor M., Allen S.K., Boschung J., Nauels A., Xia Y., Bex V., and Midgley P.M. (eds.). Cambridge University Press, Cambridge and New York.

ten Brink H.M., Plomp A., Spoelstra H., van de Vate J.F. (1983). A High-Resolution Electrical Mobility Aerosol Spectrometer (MAS). Journal of Aerosol Science, 14, 589-597.

Chang M., Kim S., and Sioutas C. (1999). Experimental Studies on Particle Impaction and Bounce: Effects of Substrate Design and Material. Atmospheric Environment, 33, 2313-2322.

Chen D.-R., Pui D.Y.H., Hummes D., Fissan H., Quant F.R., and Sem G.J. (1998). Design and Evaluation of a Nanometer Aerosol Differential Mobility Analyzer (Nano-DMA). Journal of Aerosol Science, 29, 497-509.

Chen B.T., Fletcher R.A., and Cheng Y.-S. (2011). Calibration of Aerosol Instruments, in Aerosol Measurement: Principles, Techniques, and Applications, Third Edition, Kulkarni P., Baron P.A., and Willeke K. (eds.), John Wiley and Sons, Hoboken, 449-478.

Dockery D.W., Pope III C.A., Xu X., Spengler J.D., Ware J.H., Fay M.E., Ferris B.G., and Speizer F.E. (1993). An Association Between Air Pollution and Mortality in Six U.S. Cities. The New England Journal of Medicine, 329, 1753-1759.

Domat M., Kruis F.E., and Fernandez-Dias J.M. (2014). Determination of the relevant charging parameters for the modeling of unipolar chargers. Journal of Aerosol Science, 71, 16-28.

Duan H., Romay F.J., Li C., Naqwi A., Deng W., and Liu B.Y.H. (2016). Generation of Monodisperse Aerosols by Combining Aerodynamic Flow-Focusing and Mechanical Perturbation. Aerosol Science and Technology, 50, 17-25.

Dzubay T.G., and Hasan H. (1990). Fitting Multimodal Lognormal Size Distributions to Cascade Impactor Data. Aerosol Science and Technology, 13, 144-150.

Emets E.P., Kascheev V.A., and Poluektov P.P. (1991). Simultaneous Measurement of Aerosol Particle Charge and Size Distributions. Journal of Aerosol Science, 22, 389-394.

European Comission (2008). Directive 2008/50/EC of the European Parliament and of the Council of 21 May 2008 on Ambient Air Quality and Cleaner Air for Europe. Available on (Cited 11.5.2018): http://data.europa.eu/eli/dir/2008/50/2015-09-18

European Comission (2011). European Comission Regulation 582/2011. Available on (Cited 28.06.2017): http://data.europa.eu/eli/reg/2011/582/oj

Fierz M., Scherrer L., and Burtscher H. (2002). Real-Time Measurement of Aerosol Size Distributions with an Electrical Diffusion Battery. Journal of Aerosol Science, 33, 1049-1060.

Fierz M., Houle C., Steigmeir P., and Burtscher H. (2011). Design, Calibration, and Field Performance of a Miniature Diffusion Size Classifier. Aerosol Science and Technology, 45, 1-10.

Fierz M., Meier D., Steigmeier P., and Butscher H. (2014). Aerosol Measurement by Induced Currents. Aerosol Science and Technology, 48, 350-357.

Fissan H., Neumann S., Trampe A., Pui D.Y.H., and Shin W.G. (2007). Rationale and Principle of an Instrument Measuring Lung Deposited Nanoparticle Surface Area. Journal of Nanoparticle Research, 9, 53-59.

Flagan R.C. (2001). Electrical Techniques, in Aerosol Measurement: Principles, Techniques, and Applications, Second Edition, Baron P.A., and Willeke K. (eds.), John Wiley and Sons, New York, 537-567.

Fletcher R.A., Mullholland G.W., Winchester M.R., King R.L., and Klinedinst D.B. (2009). Calibration of a Condensation Particle Counter Using a NIST Traceable Method. Aerosol Science and Technology, 43, 425-441.

Fuchs, N. A. (1963). On the Stationary Charge Distribution on Aerosol Particles in a Bipolar Ionic Atmosphere. Geofis. Pura e Applica, 56, 185-193.

Gupta A., and McMurry P.H. (1989). A Device for Generating Singly Charged Particles in the 0.1-1.0-µm Diameter Range. Aerosol Science and Technology, 10, 451-462.

Hansen P.C. (1998). Rank-Deficient and Discrete Ill-Posed Problems: Numerical Aspects of Linear Inversion. Society of Industrial and Applied Mathematics, Philadelphia.

Hering S.V, Lewis G.S., Spielman S.R., Eiguren-Fernandez A., Kreisberg N.M., Kuang C., and Attoui M. (2017). Detection Near 1-nm with a Laminar-Flow, Water-Based Condensation Particle Counter. Aerosol Science and Technology, 51, 354-362.

Hewitt G.W. (1957). The Charging of Small Particles for Electrostatic Precipitation. Transactions of the American Institute of Electrical Engineers, 76, 300-306.

Hillamo R., and Kauppinen E. (1991). On the Performance of the Berner Low Pressure Impactor. Aerosol Science and Technology, 14, 33-47.

Hoe S., Young P.M., Chan H.-K., and Traini D. (2009). Introduction of the Electrical Next Generation Impactor (eNGI) and Investigation of its Capabilites for the Study of Pressurized Metered Dose Inhalers. Phamaceutical Research, 26, 431-437.

Högström R., Quincey P., Sarantaridis D., Lüönd F., Nowak A., Riccobono F., Tuch T., Sakurai H., Owen M., Heinonen M., Keskinen J., and Yli-Ojanperä J. (2014). First

Comprehensive Inter-Comparison of Aerosol Electrometers for Particle Sizes up to 200 nm and Concentration Range 1000 cm−3 to 17 000 cm−3. Metrologia, 51, 293-303.

Iida K., Sakurai H., Saito K., and Ehara K. (2014). Inkjet Aerosol Generator as Monodisperse Particle Number Standard. Aerosol Science and Technology, 789-802.

Intra P., and Tippayawong N. (2011). An Overview of Unipolar Charger Developments for Nanoparticle Charging. Aerosol and Air Quality Research, 11, 187-209.

ISO 27891:2015. Aerosol Particle Number Concentration – Calibration of Condensation Particle Counters.

Johson T., Kaufman S., and Medved A. (2002). Response of an Electrical Aerosol Detector Based on a Corona Jet Charger. Proceedings of the 6th ETH-Conference on Nanoparticle Measurement, Zürich, Switzerland.

Johnson T., Caldow R., Pöcher A., Mirme A., and Kittelson D. (2004). A New Electrical Mobility Particle Sizer Spectrometer for Engine Exhaust Particle Measurements. SAE Technical Paper, 2004-01-1341.

Jokinen V., and Mäkelä J. (1997). Closed-Loop Arrangement with Critical Orifice for DMA Sheath/Excess Flow System. Journal of Aerosol Science, 28, 643-648.

Jung H., and Kittelson D.B. (2005). Characterization of Aerosol Surface Instrumetns in Transition Regime. Aerosol Science and Technology, 39, 902-911.

Kaminski H., Kuhlbusch T., Fissan H., Ravi L., Horn H.-G., Han H.-S., Caldow R., and Asbach C. (2012). Mathematical Description of Experimentally Determined Charge Distributions of a Unipolar Diffusion Charger. Aerosol Science and Technology, 46, 708-716.

Kangasluoma J., Ahonen L., Attoui M., Vuollekoski H., Kulmala M., and Petäjä T. (2015). Sub-3 nm Particle Detection with Commercial TSI 3772 and Airmodus A20 Fine Condensation Particle Counters. Aerosol Science and Technology, 49, 674-681.

Kauppinen E.I., and Hillamo R.E. (1989). Modification of the University of Washington Mark 5 In-Stack Impactor. Journal of Aerosol Science, 20, 813-827.

Keithley (2004). Low Level Measurements Handbook. 6th edition, Keithley Instruments Inc., Cleveland.

Keskinen J., Pietarinen K., and Lehtimäki M. (1992). Electrical Low Pressure Impactor. Journal of Aerosol Science, 23, 353-360.

Keskinen J., Marjamäki M., Virtanen A., Mäkelä T., and Hillamo R. (1999). Electrical Calibration Method for Cascade Impactors. Journal of Aerosol Science, 30, 111-116.

Kim S.H., Woo K.S., Liu B.Y.H., and Zachariah M.R. (2005). Method of Measuring Charge Distribution of Nanosized Aerosols. Journal of Colloid and Interface Science, 282, 46-57.

Knutson E. O., and Whitby K. T. (1975). Aerosol Classification by Electric Mobility: Apparatus, Theory, and Applications. Journal of Aerosol Science, 8, 443-451.

Kulvanich P., and Stewart J. (1987). An Evaluation of the Air Stream Faraday Cage in the Electrostatic Charge Measurement of Interactive Drug System. International Journal of Pharmaceutics, 36, 243-252.

Kwok P.C.L., and Chan H.-K. (2008). Effect of Relative Humidity on the Electrostatic Charge Properties of Dry Powder Inhaler Aersosols. Pharmaceutical Research, 25, 277-288.

Lehtimäki M. (1983). Modified Electrical Aerosol Detector, in Aerosols in the Mining and Industrial Work Environments, Vol. 3, Marple, V.A. and Liu B.Y.H. (eds.), Ann Arbor Science Publishers, Ann Arbor, 1135-1143.

Liu B.Y.H., and Pui D.Y.H. (1974). A Submicron Aerosol Standard and the Primary, Absolute Calibration of the Condensation Nuclei Counter. Joural of Colloid and Interface Science, 47, 155-171.

Liu B.Y.H., and Lee K.W. (1975). An Aerosol Generator of High Stability. Americal Industrial Hygiene Association Journal, 36, 861-865.

Loeb L.B. (1955). Basic Processes of Gaseous Electronics. 1st edition, University of California Press, Berkeley and Los Angeles,

Maricq M.M. (2004). Size and Charge of Soot Particles in Rich Premixed Ethylene Flames. Combustion and Flame,137, 340-350.

Maricq M.M, and Xu N. (2004). The effective density and fractal dimension of soot particles from premixed flames and motor vehicle exhaust. Journal of Aerosol Science, 35, 1251-1274.

Maricq M.M. (2005). The Dynamics of Electrically Charged Sootparticles in a Premixed Ethylene Fame. Combustion and Flame, 141, 406-416.

Marjamäki M., Keskinen J., Chen D-R., and Pui, D.Y.H. (2000). Performance Evaluation of Electrical Low Pressure Impactor (ELPI). Journal of Aerosol Science, 31, 249-261.

Marjamäki M., Ntziachristos L., Virtanen A., Ristimäki J., Keskinen J., Moisio M., Palonen M., and Lappi M. (2002). Electrical Filter Stage for ELPI, SAE Technical Paper Series, 2002-02-055.

Marjamäki M. (2003). Electrical Low Pressure Impactor: Modifications and Particle Collection Charasteristics (D.Sc. thesis). Publication 449, Tampere University of Technology.

Marple V.A., Rubow K.L., and Behm S. (1991). A Microorifice Uniform Deposit Impactor (MOUDI): Description, Calibration, and Use. Aerosol Science and Technology, 14, 434-446.

Marple V.A., and Olson B.A. (2011). Sampling and Measurement Using Inertial, Gravitational, Centrifugal, and Thermal Techniques, in Aerosol Measurement: Principles, Techniques, and Applications, Third Edition, Kulkarni P., Baron P.A., and Willeke K. (eds.), John Wiley and Sons, Hoboken, 449-478.

Marquard A., Meyer J., and Kasper G. (2006). Characterization of Unipolar Electrical Aerosol Chargers—Part I A Review of Charger Performance Criteria. Journal of Aerosol Science, 37, 1052-1068.

May K.R. (1945). The Cascade Impactor: An Instrument for Sampling Coarse Aerosols. Journal of Scientific Instruments, 22, 187-195

Mazumder M.K., Ware R.E., Yokoyama T., Rubin B.J., Kamp D. (1991). Measurement of Particle Size and Electrostatic Charge Distributions on Toners Using E-SPART Analyzer. IEEE Transactions on Industry Applications, 27, 611-619.

METAS (2018) Messmöglichkeiten für Partikel in Aerosolen. Available on (Cited 23.1.2018): https://www.metas.ch/metas/de/home/fabe/partikel-und-aerosole.html

Miller K.A., Siscovick D.S.,Sheppard L., Shepherd K., Sullivan J.H., Anderson G.L., and Kaufman J.D. (2007). Long-Term Exposure to Air Pollution and Increase of Cardivascular Events in Women. The New England Journal of Medicine, 356, 447-458.

Millikan R.A. (1913). On the Elementary Electrical Charge and the Avogadro Constant. Physical Review, 2, 109-143.

Muccio Z., and Jackson G.P. (2009). Isotope Ratio Mass Spectrometry. Analyst, 134, 213-222.

Mulholland G.W., and Fernandez M. (1998). Accurate Size Measurement of Monosize Calibration Spheres by Differential Mobility Analysis. AIP Conference Proceedings, 449, 819-823.

Mulholland G.W., Chen D.-R., and Pui D.Y.H. (2001). Comparison of Size distribution of Polystyrene Spheres Produced by Pneumatic and Electrospray Nebulization. AIP Conference Proceedings, 550, 322-326.

O'Leary M., Balachandran W., Rogueda P., and Chambers F. (2008). The Bipolar Nature of Charge Resident on Supposedly Unipolar Aerosols. Journal of Physics: Conference Series 142, 012022, 1-4.

Pope C.A. III, Burnet R.T., Thun M.J., Calle E.E., Krewski D., Ito K., and Thurston G.D. (2002). Lung Cancer, Cardiopulmonary Mortality, and Long-Term Exposure to Fine Particulate Air Pollution. JAMA, 287, 1132-1141.

Qi C., Asbach C., Shin W.G., Fissan H., and Pui D.Y.H. (2009). The Effect of Particle Pre-Existing Charge on Unipolar Charging and Its Implication on Electrical Aerosol Measurements. Aerosol Science and Technology, 43, 232-240.

Reischl G., John W., and Heigwer W. (1977). Uniform Electrical Charging of Monodisperse Aerosols. Journal of Aerosol Science, 8, 55-65.

Romay-Novas, F., and Pui, D.Y.H. (1988). Generation of Monodisperse Aerosols in the 0.1–1.0-μm Diameter Range Using a Mobility Classification–Inertial Impaction Technique. Aerosol Science and Technology, 9, 123-131.

Rosser S., and Fernández de la Mora J. (2005). Vienna-Type DMA of High Resolution and High Flow Rate. Aerosol Science and Technology, 39, 1191-1200.

Rostedt A., Arffman A., Janka K., Yli-Ojanperä J., and Keskinen J. (2014). Characterization and Response Model of the PPS-M Aerosol Sensor, Aerosol Science and Technology, 48, 1022-1030.

Saari S., Arffman A., Harra J., Rönkkö T., and Keskinen J. (2018). Performance evaluation of the HR-ELPI+ inversion. Aerosol Science and Technology, DOI:10.1080/02786826.2018.1500679.

Scheibel H.G., and Porstendörfer J. (1983). Generation of Monodisperse Ag- and NaCl-Aerosols with Particle Diameters between 2 and 300 nm. Journal of Aerosol Science, 14, 113-126.

Shimada M., Han B., Okuyama K., and Otani Y. (2002). Bipolar Charging of Aerosol Nanoparticles by a Soft X-Ray Photoionizer. Journal of Chemical Engineering of Japan, 35, pp. 786-793.

Sinclair D., and La Mer V.K. (1948). Light Scattering as a Measure of Particle Size in Aerosols. Chemical Reviews, 44, 245-267.

Stockfelt L., Andersson E.M., Molnár P., Gidhagen L., Segersson D., Rosengren A., Barregard L., and Sallsten G. (2017). Long-Term Effects of Total and Source-Specific Particulate Air Pollution on Incident Cardiovascular Disease in Gothenburg, Sweden. Environmental Research, 158, 61-71.

Tammet H.F. (1970). Transactions on Air Ionization and Electroaerosols, Vol. II: The Aspiration Method for the Determination of Atmospheric-Ion Spectra. Israel Program for Scientific Translations, Jerusalem.

Tammet H., Mirme A., and Tamm E. (2002). Electrical Aerosol Spectrometer of Tartu University, Atmospheric Research, 62, 315-324.

Tammet H. (2007). Atmospheric electricity, Vol II: Air Ions, in CRC Handbook of Chemistry and Physics, 88th Edition, Lide D.R. (ed.), CRC Press, Boca Raton, (14-33)-(14-35).

Tropp R.J., Kuhn P.J., and Brock J.R. (1980). A New Method for Measuring the Particle Size Distribution of Aerosols. Review of Scientific Instruments, 51, 516-520.

Uin J., Tamm E., and Mirme A. (2009). Electrically Produced Standard Aerosols in a Wide Size Range. Aerosol Science and Technology, 43, 847-853.

Uin J., Tamm E., and Mirme A. (2011). Very Long DMA for the Generation of the Calibration Aerosols in Particle Diameter Range up to 10 µm by Electrical Separation. Aerosol and Air Quality Research, 11, 531-538.

Vanhanen J., Mikkilä J., Lehtipalo K., Sipilä M., Manninen H.E., Siivola E., Petäjä T., and Kulmala M. (2011). Particle Size Magnifier for Nano-CN Detection. Aerosol Science and Technology, 45, 533-542.

de La Verpilliere J.L., Swanson J., and Boies A.M. (2015). Unsteady Bipolar Diffusion Charging in Aerosol Neutralisers: A Non-Dimensional Approach to Predict Charge Distribution Equilibrium Behaviour. Journal of Aerosol Science, 86, 55-68.

Virtanen A., Marjamäki M., Ristimäki J., and Keskinen J. (2001). Fine Particle Losses in Electrical Low-pressure Impactor. Journal of Aerosol Science, 32, 389-401.

Vishnyakov V.I., Kiro S.A., Oprya M.V., and Ennan A.A. (2016). Charge Distribution of Welding Fume Particles After Charging by Corona Ionizer. Journal of Aerosol Science, 94, 9-21.

Wang S.C., and Flagan R.C. (1990). Scanning Electrical Mobility Spectrometer. Aerosol Science and Technology, 13, 230-240.

Wiedensohler A. (1988). An Approximation of the Bipolar Charge Distribution for Particles in the Submicron Size Range. Journal of Aerosol Science, 19, 387-389.

Winklmayr W., Wang H-C., and John, W. (1990). Adaptation of the Twomey Algorithm to the Inversion of Cascade Impactor Data. Aerosol Science and Technology, 13, 322-331.

Winklmayr W., Reischl G.P., Lindner A.O., and Berner A. (1991). A New Electromobility Spectrometer for the Measurement of Aerosol Size Distributions in the Size Range from 1 to 1000 nm. Journal of Aerosol Science, 22, 289-296.

Yli-Ojanperä J., Kannosto J., Marjamäki M., and Keskinen J. (2010a). Improving the Nanoparticle Resolution of the ELPI. Aerosol and Air Quality Research, 10, 360-366.

Yli-Ojanperä J., Mäkelä J.M., Marjamäki M., Rostedt A., and Keskinen J. (2010b). Towards Traceable Particle Number Concentration Standard: Single Charged Aerosol Reference (SCAR). Journal of Aerosol Science, 41, 719-728.

Yli-Ojanperä J., Sakurai H., Iida K., Mäkelä J., Ehara K., and Keskinen J. (2012). Comparison of Three Particle Number Concentration Calibration Standards Through Calibration of a Single CPC in a Wide Particle Size Range. Aerosol Science and Technology, 46, 1163-1173.

ORIGINAL PAPERS

Paper I

Järvinen A., Aitomaa M., Rostedt A., Keskinen J., and Yli-Ojanperä J. (2014). Calibration of the New Electrical Low Pressure Impactor (ELPI+), Journal of Aerosol Science, 69, 150-159.

Journal of Aerosol Science 69 (2014) 150–159

Contents lists available at ScienceDirect

Journal of Aerosol Science

journal homepage: www.elsevier.com/locate/jaerosci

Calibration of the new electrical low pressure impactor (ELPI+)

A. Järvinen*, M. Aitomaa, A. Rostedt, J. Keskinen, J. Yli-Ojanperä

Tampere University of Technology, Department of Physics, Aerosol Physics Laboratory, P.O. Box 692, FI-33101 Tampere, Finland

ARTICLE INFO

Article history:
Received 12 September 2013
Received in revised form
2 December 2013
Accepted 9 December 2013
Available online 18 December 2013

Keywords:
Electrical Low Pressure Impactor
ELPI+
Impactor
Charger

ABSTRACT

A renewed Electrical Low Pressure Impactor (ELPI+) was introduced by Dekati Ltd. in late 2010. This study presents the collection efficiencies of the ELPI+ cascade impactor stages and the back-up filter as well as the charging efficiency of the corona charger in the size range of 0.01–10 μm. According to the measurements the impactor cut diameters are within ±10% to the predecessor except the upmost stage for which the difference was found to be −18%. The secondary collection of nanoparticles was found to be similar to the predecessor for stages with the largest cut diameters but higher for the stages with the smallest cut diameters. The charging efficiency is higher for the new charger compared to the old one by 54% at 20 nm particle size. This study also presents the first use of the Single Charged Aerosol Reference (SCAR) for impactor and charger calibrations.

1. Introduction

Cascade impactors are widely applied for aerosol particle measurements. Numerous impactors have been designed, manufactured, and applied for aerosol studies (Marple, 2004). The Electrical Low Pressure Impactor (ELPI) enabled real-time detection of particles by combining electrical detection of charged particles with a 12-stage low pressure cascade impactor (Keskinen et al., 1992; Marjamäki et al., 2000). The ELPI has been manufactured and distributed by Dekati Ltd. since 1995. It has become a widely used instrument for air quality (Gouriou et al., 2004), combustion aerosol (Yi et al., 2008; Coudray et al., 2009) and engine exhaust measurements (Shi et al., 1999; Maricq et al., 2000; Zervas et al., 2005). It has also been applied to pharmaceutical inhaler development (Glower & Chan, 2004), as well as to atmospheric aerosol research (Held et al., 2008; Virtanen et al., 2010).

Along with time, the measuring particle size range of the ELPI has been extended towards smaller nanoparticles. Marjamäki et al. (2002) introduced a filter stage in order to detect particles smaller than 30 nm, which was the cut diameter of the lowest impactor stage at that time. In addition, an extra stage with a design cut diameter of 17 nm was developed by Yli-Ojanperä et al. (2010a). The extra stage was demonstrated to improve the nanoparticle resolution of the ELPI, but it has not been commercially available. Owing to the fixed dimensions of the impactor assembly, two uppermost stages had to be removed in order to make use of both the filter stage and the extra stage at the same time.

In 2010 Dekati Ltd. introduced a new instrument version called ELPI+, in which the impactor assembly was realized so that all the designed stages, including the 17 nm extra stage, can be used simultaneously. This increased the total number of stages to 15, including 14 impactor stages (contains one precut stage, not measured electrically) plus a filter stage. This allows real-time measurements of particle size distributions in wide particle size range from 6 nm to 10 μm according to manufacturer with 14 particle size fractions. The appearance is changed moderately from the previous model, including modification of the impactor stages. The new instrument can also be used as stand-alone, thus PC connection is not required

* Corresponding author. Tel.: +358 40 198 1024.
E-mail address: anssi.jarvinen@tut.fi (A. Järvinen).

0021-8502/$ - see front matter © 2013 Elsevier Ltd. All rights reserved.
http://dx.doi.org/10.1016/j.jaerosci.2013.12.006

but can be used. The electrometers have been redesigned and a sampling rate of 10 Hz can now be achieved. The unipolar corona charger is completely new. The most significant modification to the previous model is the smaller inner volumes of the charger and the impactor. The smaller volumes are motivated by decreased instrument size and mass, improved time response, and by smaller space charge losses at high concentrations.

The calibrations are the subject of this study. Both the charger efficiency and the impactor collection efficiency functions were measured over the operating particle size range of the instrument. The collection efficiency of the new filter stage was measured using nanoparticles. In addition to the cutpoints, all the other impactor stage parameters that are required in order to apply inversion algorithms (e.g. Lemmetty et al., 2005) and to estimate the effective density of the particles (Ahlvik et al., 1998; Maricq et al., 2000; Ristimäki et al., 2002) were evaluated. All of the calibration results and associated uncertainty values, as well as the calibration setups are presented in this paper. All measurements were conducted using monodisperse di-octyl sebacate (DOS) particles generated either with an Evaporation Condensation Generator (ECG), a Vibrating Orifice Aerosol Generator (VOAG) or with the recently introduced Single Charged Aerosol Reference (SCAR, Yli-Ojanperä et al., 2010b).

2. ELPI+ instrument

The particle measurement method of the ELPI+ has been introduced by Keskinen et al. (1992) and is based on unipolar charging of particles, size classification of these particles in cascade impactor and electrical measurement of collected particles. The operating principle and main components of the ELPI+ are presented in Fig. 1.

The aerosol is introduced into a unipolar diffusion charger which is based on needle type corona discharge. The discharge is achieved by positive high voltage of approximately 3.5 kV. In order to achieve stable charging conditions, the discharge current is kept at a constant value of 1 μA. Both discharge current and voltage are monitored by the electronics for diagnostic purposes. In the following stage the remaining ions from the corona discharge are removed from the flow by an ion trap. In the ion trap aerosol flows between two concentric cones with a potential difference of 20 V, resulting in an electric field which removes the ions from the flow.

The size classification occurs in the cascade impactor. The first stage is used as a pre-separator to remove large particles. The following 13 impactor stages are separated from each other by electrical insulators and connected to a multichannel electrometer. The unipolarly charged particles depositing on the stages are detected by measuring electric current from each stage. The last impactor stage is based on design by Yli-Ojanperä et al. (2010a). The final stage is the filter collecting the particles which are too small to be deposited by impaction in the previous stages. The filter stage is connected to the electrometer as the impactor stages. The downstream pressure is measured and can be set to the manufacturer specified value of 40 mbar by adjusting a control valve, situated between the filter stage and the connection to external vacuum. In addition to downstream pressure also the absolute pressure in the charger is measured by the electronics.

The ELPI+ is equipped with a pump which provides filtered particle free air into the charger region when the flush mode is activated. This enables zero check and adjustment of the electrometer zero levels. The electrometers are bipolar allowing particle charge studies when the diffusion charger is switched off. The operation of the instrument is controlled by an internal computer and as already mentioned, the instrument can be used as a stand-alone unit.

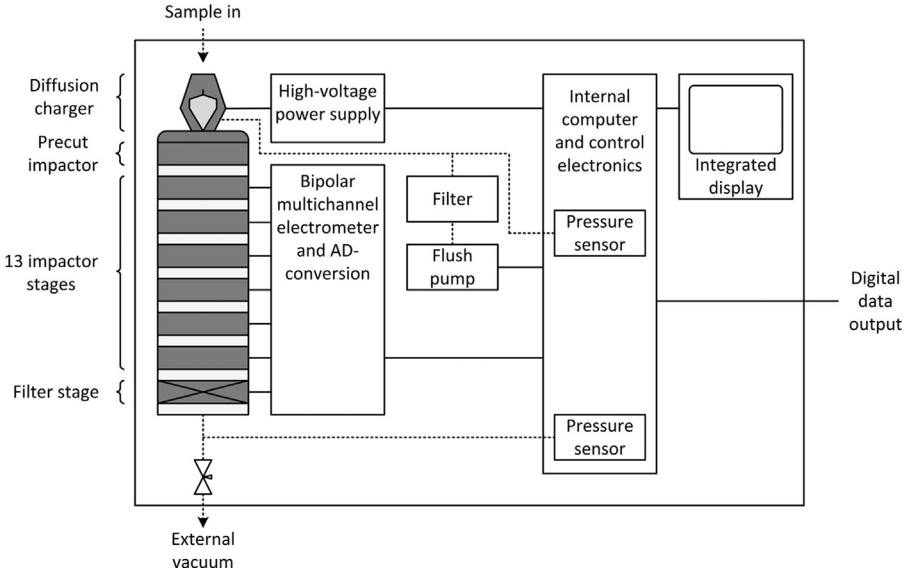

Fig. 1. The schematics of the ELPI+.

3. Impactor and charger calibration

An electrical calibration method for impactors was presented by Hillamo and Kauppinen (1991) and modified by Keskinen et al. (1999) for the cascade impactors. Fraction of the particles collected by each stage is calculated from the measured electric current values. Provided that the input particle size distribution is monodisperse and particles are unipolarly charged, the collection efficiency for stage n, is calculated based on the following equation:

$$E_n = \frac{I_n}{\sum_{i=1}^{n} I_i}, \tag{1}$$

where I_i is the current measured from the stage i ($i=1$ for the filter stage). This equation is used to estimate the secondary collection of fine particles onto the impactor stages as well (Virtanen et al., 2001). The collection efficiency of the filter stage is measured using two identical electrically insulated filters on top of each other. By assuming that the collection efficiencies of both filters are the same, the collection efficiency becomes

$$E_1 = 1 - \frac{I_{F2}}{I_{F1}}, \tag{2}$$

where I_{F1} is the current measured from the first filter stage and I_{F2} is the current measured from the filter stage located last in the flow direction. Based on the experimental collection efficiency curves, cutpoints of the stages and the steepness of the curves are obtained using the following fit function for the calibration data (Dzubay & Hasan, 1990; Winklmayr et al., 1990)

$$E_n = \left[1 + \left(\frac{d_{50}}{d_a}\right)^{2s}\right]^{-1}, \tag{3}$$

where d_a is the aerodynamic particle diameter, d_{50} the cutpoint and s describes the steepness of the collection efficiency curve. In addition to the cutpoints, the corresponding Stokes numbers (Stk_{50}) are calculated as

$$Stk_{50} = \frac{\rho_p U C(d_{50}) d_{50}^2}{9\eta W}, \tag{4}$$

where ρ_p is the particle density, U is the average jet velocity in the impactor nozzle exit calculated according to Hering (1987), η is the dynamic viscosity of gas, W is the jet diameter at the nozzle and $C(d_{50})$ is the slip correction factor at the stage inlet stagnation conditions.

The electric currents measured by the ELPI+ electrometers depend on the performance of the charger. In order to calculate the particle concentration for each impactor stage, the charging efficiency has to be known as a function of particle size. Typically, it is represented as a product of penetration P and the average number of elementary charges per particle n as follows:

$$Pn = \frac{I}{NeQ}. \tag{5}$$

In Eq. (5), I is the measured electric current after the charger which is generated by the flow of charged particles, N is the particle number concentration, e is the elementary charge and Q is the flow rate through the charger (Marjamäki et al., 2000). Concentration N can be measured with a calibrated instrument which is connected in parallel with the charger.

4. Experimental

4.1. Collection efficiency measurements

Monodisperse particles were generated using three different methods. In addition to the conventional means of Evaporation Condensation Generator (ECG) and Vibrating Orifice Aerosol Generator (VOAG), a new method for generating monodisperse particles, namely the SCAR (Yli-Ojanperä et al., 2010b), was also applied. With the SCAR, originally designed to be a concentration reference, it is possible to generate truly monodisperse particles with electrical classification, since only 0.5% of the particles from SCAR outlet have more than one elementary charge at worst case (Högström et al., 2011).

The schematics of the calibration setups are presented in Fig. 2. Setup A was applied to the particles generated using the ECG and the SCAR in the size range of 0.01–1 μm. Both methods were based on the same setup A except the particle generation was different. In the ECG method dioctyl sebacate (DOS) was first nebulized, then evaporated in a heated glass tube and cooled rapidly leading to homogeneous nucleation. The particle size was controlled by regulating the evaporation and cooling temperatures and DOS droplet concentration. The formed particles were charged by a ^{85}Kr aerosol neutralizer.

In the SCAR method 10–12 nm NaCl seed particles were generated in a tube furnace (Yli-Ojanperä et al., 2010b). Particles were charged by a ^{85}Kr-neutralizer and classified using a differential mobility analyzer, DMA (Model 3085, TSI Inc.). These singly charged particles were then introduced to a saturator where DOS is evaporated. When this DOS rich aerosol is cooled,

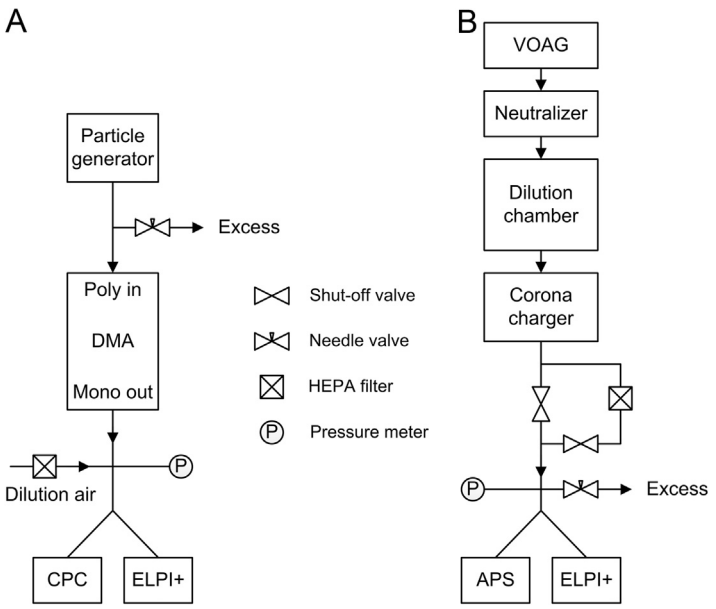

Fig. 2. ELPI+ calibration setup in case of (A) ECG, SCAR and (B) VOAG.

the vapor condenses on the charged seed particles resulting in larger particles, each with a single elementary charge. The size was controlled mainly by regulating the saturator temperature of the SCAR.

The charged aerosol generated either by the ECG or the SCAR method was introduced to a calibrated DMA (Models 3071 and 3085, TSI Inc.) to select monodisperse particles. In case of ECG, the DMA voltage was adjusted to classify particles larger than the peak size of the distribution to reduce the effect of multiple charging. In case of SCAR this was not needed as it produces particles with a single elementary charge. After the DMA aerosol was diluted with HEPA filtered air and divided between a condensation particle counter, CPC (Model 3025, TSI Inc.) and ELPI+. The CPC was only used to monitor the stability of the particle generation. The actual impactor calibration results were achieved solely by using the electrical currents measured by the ELPI+. The instrument inlet pressure was measured and adjusted to standard conditions by controlling the excess flow between the particle generator and the DMA.

The filter stage collection efficiency was measured using two identical filters on top of each other located at the bottom of the impactor assembly. The measurement setup was similar to the one presented in Fig. 2A with some differences. The particles were generated using the SCAR in the range of 10–20 nm. These particles were NaCl seed particles which were classified by the internal DMA of the SCAR allowing the second DMA to be removed.

Larger particles, sized from 1 to 10 μm were generated with a modified VOAG (Fig. 2). The vibrating piezoelectric disc of the VOAG was taken from Model 3050 (TSI Inc.), but otherwise the device comprised of a high pressure syringe pump (Nexus 6000, Chemyx Inc.), orifices with diameters of 10 and 20 μm (Lenox Laser Corp.), a signal generator (E-310B, B&K Precision) and a counter (Model 5314A, Hewlett-Packard Co.). The operation of the signal generator and counter was ensured with an oscilloscope (TDS 224, Tektronix Inc.). The particle material was DOS dissolved in 2-propanol (HPCL grade with reported evaporation residue). The droplets generated by the VOAG were introduced to a radioactive neutralizer consisting of ^{241}Am foil with an activity of 59 MBq to decrease particle losses due to electrostatic effects. After this, the droplets were brought to a dilution chamber where 2-propanol was evaporated resulting particles composing of DOS only. Particles were found to be positively charged even after the neutralization. A corona charger with negative polarity was installed after the dilution chamber to control the charge level of the aerosol for reasons discussed in Section 4.2. The aerosol was directed either straight to the instruments or through HEPA filter to provide a zero level. The inlet pressure was measured and controlled by adjusting the excess flow before the instruments. An Aerodynamic Particle Sizer (APS, Model 3321, TSI Inc.) was used in parallel with the ELPI+ to ensure the monodispersity of the generated particles. The particle diameter in each measurement point was calculated from the VOAG operating parameters according to Berglund and Liu (1973).

All collection efficiency measurements were conducted at the inlet pressure of (1013 ± 2) mbar and in typical laboratory temperature, from 19 to 24 °C. The ELPI+ downstream pressure was measured after the last impactor stage and adjusted to 40 mbar for correct operation. The sample flow rate was measured to be 10.1 lpm (Gilian Gilibrator 2, Sensidyne LP). The DMA flow rates were calibrated against a reference consisting of a combination of a calibrated laminar flow element and a differential pressure sensor (FCO332 DP, Furness Controls Ltd.). The size response of the DMA was confirmed with standard particles (Thermo Fisher Scientific Inc.).

4.2. Charging efficiency measurements

The charging efficiency was determined using monodisperse particles by measuring the total electric current from the impactor which was connected to the charger as in normal use. Particles were generated with SCAR in the size range of 0.01–1.9 μm and with VOAG in the size range of 1.5–10 μm, by using the setups shown in Fig. 2 with minor modifications.

The ELPI+ charger provides positive charge onto the particles. If the particles going into the charger are initially positively charged the output of the charger may be affected especially in the small particle sizes where the charging efficiency is low. To avoid this effect, initially negatively charged particles were used in the calibration.

In order to produce negatively charged particles using the setup A in Fig. 2, the polarities of the internal DMA of the SCAR and the following classifying DMA were changed from negative to positive (negative particle output). To be able to measure particles larger than 1 μm, the inlet and outlet tubing of the classifying DMA were modified. By applying these modifications it was possible to calibrate the ELPI+ charger using singly charged particles with a mobility diameter from 0.01 to 1.9 μm. The DMA output was diluted and connected to a static mixer (Kenics 37-06-110, Chemineer Inc.) followed by a flow splitter (Model 3708, TSI Inc.). From this flow splitter, the aerosol was introduced to the ELPI+ and to a CPC (Model 3776, TSI Inc.). The CPC was used as concentration reference in the calibration. Both the CPC counting efficiency and the size response were calibrated prior to the ELPI+ measurements using the SCAR and a Faraday-cup electrometer as a reference (see, e.g. Yli-Ojanperä et al., 2012). The charging efficiency was measured also by switching the ELPI+ charger on and off. Both methods were found to give equal results but the CPC provided more stable results with less scatter. The actual charging efficiency was calculated using Eq. (5) where the electric current was measured from the impactor by ELPI+ electrometers and the particle number concentration was measured by the CPC.

The VOAG was used in measurement of the charging efficiency from 1.5 to 10 μm for which the setup B shown in Fig. 2 was applied. To achieve reliable results the smallest VOAG particle sizes were selected to overlap with the results measured with the SCAR. In the VOAG measurements, the APS was used as a concentration reference and to ensure that the particle distribution was monodisperse. Residual particles were observed when the VOAG was operated using the solvent only. For this reason, the APS was used as particle size reference from 1.5 to 4 μm. The APS-measured aerodynamic diameter was converted into mobility diameter. In case of the largest particle size range from 2.9 to 10 μm the diameters were calculated according to the parameters used for the VOAG, again this size range had an overlap with the smaller measurement series.

In the VOAG measurements particles were initially neutralized by a radioactive neutralizer. However, the particles were observed to be still positively charged as in case of collection efficiency measurements. Thus, a study was conducted to evaluate the effect of the initial particle charge on the operation of the charger. Particles having a high positive initial charge will have higher charge state at the output than expected which leads to higher electric current and overestimation of the particle concentration. To investigate this, a test was conducted using a constant particle size of 3.2 μm. In this test initial charge was adjusted with an additional corona charger installed between the dilution chamber of the VOAG and the instruments. The measurement was conducted for both ELPI and ELPI+. An APS was used to determine the particle concentration. Together with the electrometer readings, the APS number concentration was used to calculate the elementary charges per particle ratio.

It was found that the initial negative charge on the particles does not have an effect on the efficiency of the charger which can be noticed from Fig. 3. However, an initial charge of more than 100 positive elementary charges will result in an increased charging state and error in particle concentration if it is calculated using the pre-defined *Pn*-value which is approximately 400 for 3.2 μm particles. The two different slopes in Fig. 3 correspond to measurements conducted on two separate days with the same calibration setup. The reason for this difference is unknown but may be related to electrostatic losses in the tubing.

The results of the initial charge test were applied to the measurement of the charging efficiency. To ensure reliable measurements negative corona charger was placed between the VOAG and the measuring instruments, ELPI+ and APS as in

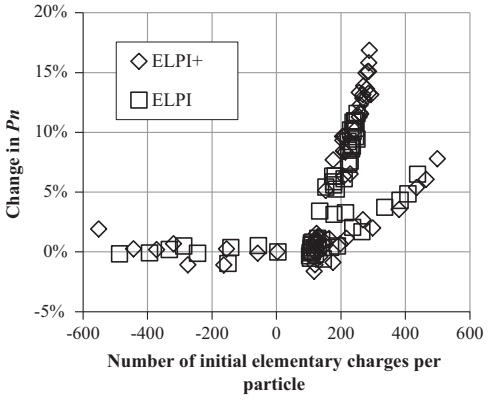

Fig. 3. The effect of particle initial charge on ELPI and ELPI+ charger output. The particle physical diameter was 3.2 μm.

case of the charge test. Particles were given a slightly negative charge which was checked before and after the measurement by switching the ELPI+ charger off.

5. Results

5.1. Impactor

The impactor calibration was conducted using monodisperse particles with well-defined mobility or physical diameter. These diameters were converted into particle aerodynamic diameter which was calculated at the inlet stagnation pressure of each impactor stage. The collection efficiencies of the ELPI impactor stages as a function of aerodynamic diameter are presented in Fig. 4 with *s*-functions fitted according to Eq. (3). The data for the multiple charged ECG generated particles was corrected up to 6 elementary charges using a method described by Kauppinen and Hillamo (1989). The measured data points determined using the SCAR and the corrected data points obtained using the ECG method were in a good agreement for stage 9, which implies that the correction algorithm works rather well. The collection efficiencies of the impactor stages having the smallest cut diameters do not reach zero towards smaller particle sizes. This effect arises from secondary collection of particles by diffusion. For the largest particles (stages 12, 13 and 14) the collection efficiency approaches unity slower than expected. In general, the measurement points having different particle generation methods overlap nicely, implying that the particle diameters are well defined for the different methods.

Cut diameters d_{50} were calculated from the fitted *s*-functions. Cut diameters, the corresponding Stokes numbers and fitted steepness values are listed in Table 1, together with the data of the previous model. However, the measurements in Marjamäki (2003) for previous ELPI were carried out at the ambient pressure of 985.4 mbar. Therefore the calibration data taken from the Marjamäki (2003) was converted to the standard inlet pressure of 1013 mbar with the conversion described by Hering (1987).

Comparison to previous model shows very similar cut sizes and Stokes numbers with the exception of the two upmost stages. Stages 13 and 14 have distinctively smaller cut sizes than the previous model. This implies that the smaller volume of the stages has in fact modified the impaction characteristics of the stages. For stage 7, where a first significant pressure drop occurs, the collection efficiency curve is much steeper. Therefore it appears that the stage works more like an ideal stage. The lowest impactor stage cut diameter 15.7 nm is close to the 16.7 nm value given by Yli-Ojanperä et al. (2010a). The collection efficiency of the new filter stage was found to be 97% for particles in the size range of 10–20 nm. In general the ELPI+ impactor cut diameters and curve steepness values are close to the values of the previous model with the additional information given by the new 15.7 nm impactor stage. In terms of nanoparticles, the new ELPI+ impactor should have better response to inversion algorithms (Lemmetty et al., 2005) and to the measurement of the effective density of the particles (Ristimäki et al., 2002) compared to the previous model because of the new 15.7 nm stage.

The uncertainties of the experimentally determined cut-points were evaluated separately for different particle generation methods. From 0.01 to 1 μm the uncertainty of the particle size is mainly caused by the sizing accuracy of the DMA. Following the uncertainty evaluation presented by Mulholland and Fernandez (1998), the uncertainties of the reported cut-points are 5% with 95% confidence interval. For larger particles the uncertainty of the particle size derives from the uncertainty of the VOAG operating parameters, including liquid concentration, feed rate, frequency, impurity concentration and doublet particles. By taking all these factors into account 2% uncertainties for the cut-points are obtained with 95% confidence interval, which is in good agreement with the values reported by Berglund and Liu (1973).

In order to calculate the true particle concentration and distribution, the secondary collection of particles in the ELPI+ needs to be known. Particle collection in impactor occurs in addition to impaction due to diffusion and electric effects: space charge and image charge. These effects have been analyzed by Virtanen et al. (2001) and Marjamäki et al. (2005). In this

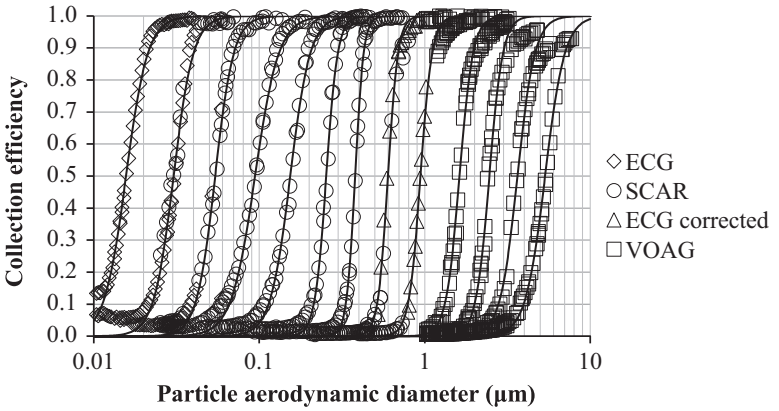

Fig. 4. Measured collection efficiency curves and fitted *s*-functions for stages 2–14. "ECG corrected" refers to results which were achieved by using the multiple charge correction algorithm.

Table 1
Cut diameters d_{50}, corresponding square roots of the Stokes numbers $\sqrt{Stk_{50}}$ and curve steepness values s for the calibrated ELPI+. The values for the previous model calibrated by Marjamäki (2003) are given for comparison.

ELPI+ stage	ELPI+			ELPI stage	ELPI		
	d_{50} (μm)	$\sqrt{Stk_{50}}$	s		d_{50} (μm)	$\sqrt{Stk_{50}}$	s
1 (Filter)	–	–	–	Filter	–	–	–
2	0.0157	0.447	3.32	–	–	–	–
3	0.0304	0.431	3.65	1	0.0289	0.421	3.41
4	0.0541	0.438	3.89	2	0.0541	0.453	4.29
5	0.0943	0.442	3.05	3	0.0905	0.439	2.94
6	0.154	0.449	3.62	4	0.153	0.448	3.10
7	0.254	0.472	6.30	5	0.260	0.477	3.58
8	0.380	0.457	8.43	6	0.380	0.456	9.27
9	0.600	0.443	7.16	7	0.617	0.450	5.87
10	0.943	0.445	6.21	8	0.921	0.445	8.77
11	1.62	0.469	5.32	9	1.59	0.461	4.88
12	2.46	0.466	5.33	10	2.43	0.451	5.59
13	3.64	0.427	4.14	11	3.98	0.465	4.53
14	5.34	0.390	3.66	12	6.53	0.483	4.50
Average		0.444				0.455	

study secondary collection of fine particles was calculated using Eq. (1) considering only total efficiency of secondary collection which occurs due to diffusion and image charge because calibration was performed in low concentration environment. A power function was fitted to the data which resulted parameters listed in Table 2. The applied power function has the form of

$$E_i(D_p) = a_i D_p^{b_i} + c_i, \tag{6}$$

where E is the secondary collection efficiency, i stands for stage number and D_p is the particle mobility diameter in μm. Fitted parameters a, b and c are defined for each stage individually. Parameters were not measured for stages 1 and 2. In case of stage 2, fine particles are being collected by the impaction mechanism and the stage 1 is the filter for which the secondary collection cannot be defined. Figure 5 presents the measured data for the ELPI+ impactor stages 8 and 14. When comparing to the secondary collection data presented by Marjamäki et al. (2005), it can be seen that the secondary collection efficiency is similar to the previous ELPI for stage 14. When the stage number and the cut diameter is decreasing higher values of secondary collection are observed for the ELPI+ than for the ELPI which is visible in the stage 8 data in Fig. 5. This effect may be explained by different construction of the impactor stages between the ELPI+ and ELPI. The differences in the secondary collection should be taken into account when measurement signals are processed into particle concentration values.

5.2. Charger

The charging efficiency of the ELPI+ charger was measured from 0.012 to 8.1 μm using the SCAR and the VOAG and by applying the Eq. (5). By combination of SCAR and a calibrated CPC, high precision results were obtained from 0.012 up to 1.9 μm. For larger particle sizes, the VOAG and the APS as a reference were used. Ranges of these two different methods were selected to overlap slightly. It was found out that charger efficiencies were not identical in the overlapping section. This is attributed to a non-ideal counting efficiency of the APS. The VOAG+APS results were reduced by 16% to match the charging efficiencies obtained with the SCAR. The charger response measurement results are presented in Fig. 6 as a penetration multiplied by the average number of charges Pn as a function of particle mobility diameter.

The overall charging efficiency was found to be higher than for the previous model. This can be explained by the smaller volume of the new charger and differences in the flow patterns through the charger. A power function fitted to the data in Fig. 6 in three particle size ranges was derived as

$$Pn = \begin{cases} 68.531 D_p^{1.225}, & D_p < 1.035\ \mu\text{m} \\ 67.833 D_p^{1.515}, & 1.035\ \mu\text{m} \le D_p \le 4.282\ \mu\text{m} \\ 126.83 D_p^{1.085}, & D_p > 4.282\ \mu\text{m} \end{cases}, \tag{7}$$

where D_p is the particle mobility diameter in μm. The charging efficiency Pn is rather well described by the power functions although there is a noticeable step toward higher charging efficiencies when the particle size is increasing from 1 to 4 μm. In the smaller particle sizes the diffusion charging is the prevailing mechanism and the step may be a result of increased field charging. For particle size larger than 4 μm the charging efficiency slope (in log–log scale) is decreasing which may be due to particle losses in the charger or due to measurement errors. The latter could be caused by a number concentration

Table 2
Fitted power function parameters for the secondary collection efficiency of the ELPI+ stages.

ELPI+stage	a_i	b_i	c_i
3	9.80×10^{-8}	−2.73	0.05085
4	3.63×10^{-8}	−3.06	0.03083
5	1.58×10^{-6}	−2.26	0.02342
6	4.83×10^{-6}	−2.06	0.02183
7	1.02×10^{-5}	−1.90	0.02097
8	6.22×10^{-5}	−1.49	0.01158
9	4.03×10^{-5}	−1.56	0.00804
10	7.31×10^{-5}	−1.40	0.00671
11	1.01×10^{-4}	−1.31	0.00475
12	8.22×10^{-5}	−1.35	0.00288
13	1.09×10^{-4}	−1.31	0.00129
14	9.07×10^{-5}	−1.36	0.00186

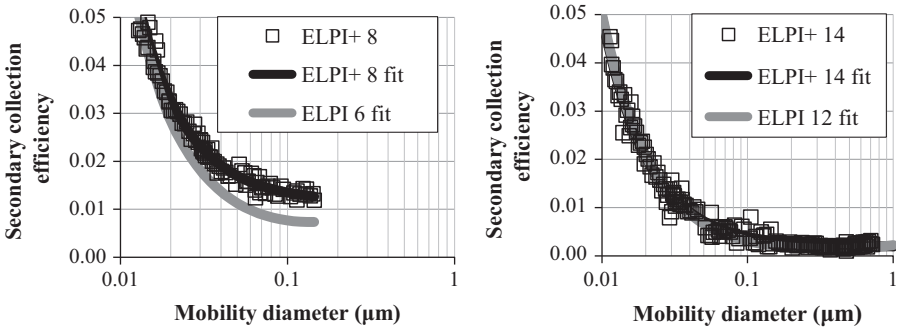

Fig. 5. Secondary collection efficiency of ELPI+ and ELPI impactors for two corresponding stages presented as a function of particle mobility diameter (ELPI fit taken from Marjamäki et al., 2005).

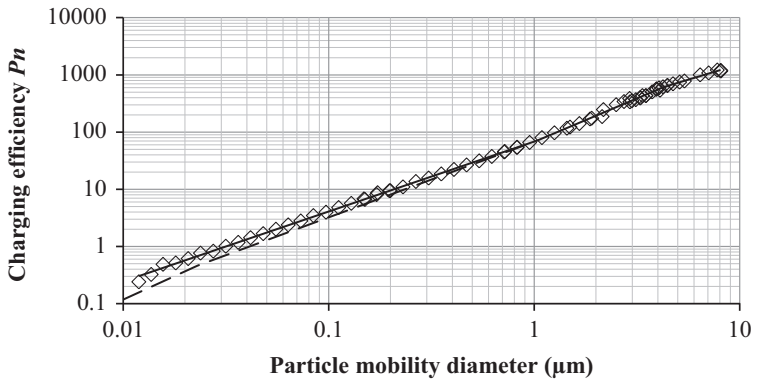

Fig. 6. ELPI+ charger efficiency *Pn*, measurement points and fitted 3-part power function. The ELPI charging efficiency by Marjamäki et al. (2002) is shown as reference (dashed line).

difference between the ELPI+ inlet and the reference inlet. Another source of error is the lack of traceable number concentration reference in this size range.

The uncertainty related to the use of the *Pn* fit-functions presented in Eq. (7) was evaluated in the size range of 0.01–2 μm. For particle sizes larger than 2 μm, no uncertainty evaluation was conducted, because of the lack of reliable number concentration references in this size range. The uncertainty consists of two components. These are the deviation of the values calculated using Eq. (7) from the experimental values and the uncertainty of the experimentally determined *Pn* values. For the deviation part, the uncertainty was estimated to be equal to two times the standard deviation of the relative difference between the experimentally determined and calculated *Pn* values. This resulted in 10.8% uncertainty with 95% confidence interval. The second uncertainty component was derived from Eq. (5) by applying the law of propagation of the uncertainty. Following uncertainty values were used in the calculation: 1% ± 1 fA for the electric current, 3% for the particle concentration, and 1% for the flow measurement. These are all based on the calibrations of the instruments. By combining

the uncertainty components (deviation and accuracy of the experimental *Pn* values) by root of the sum of squares method, size dependent uncertainty values were obtained. For the smallest particle size, the overall uncertainty is 20% (95% confidence interval), which decreases towards larger sizes and levels at 40 nm particle diameter to 12%.

6. Discussion

In this study the new Electrical Low Pressure Impactor ELPI+ was calibrated in laboratory environment. Results were in good agreement with the previous model of the ELPI for most of the impactor stages, but two upmost stages had significantly smaller cut sizes. Also the collection efficiency curve for the 7th stage was much steeper in the ELPI+. The filter stage collection efficiency was tested with nanosized particles and it was found to be approximately 97%. The secondary collection of fine particles was found to be similar to the previous model in case of the stages with the largest cut diameters. The efficiency of secondary collection was found be larger in ELPI+ in comparison to ELPI for stages with smaller cut diameters. The largest detectable particle size of the ELPI+ is a bit lower than for the previous model, but the overall particle size resolution is better since all the designed 14 impactor stages and the filter stage can now be used together in the impactor assembly. For the previous model, the two upmost stages had to be removed for the installation of the later on developed non-commercial nanoparticle stage and the filter stage. The ELPI+ impactor characteristics are close to the predecessor model allowing inversion method (Lemmetty et al., 2005) and density measurement algorithm (Ristimäki et al., 2002) to be applied to the ELPI+ data with only minor modification of the calculation parameters. The included nanoparticle stage allows these methods to be applied to smaller particle sizes with higher precision.

The new ELPI+ charger was found to be more efficient than the previous model and a new fit was derived for the conversion of measured current signal into particle number concentration. However, a study should be made to investigate the effect of particle concentration on the ELPI and ELPI+ charger's efficiency. It was found that particle initial charge has an effect on the charger output which could be studied in more detail.

It was found out that the SCAR and electrical classifying can be applied in calibrations from 10 nm up to 1.9 μm particle size allowing straightforward and accurate measurements. Above this size calibration was found to be a challenge because lack of a reliable references and possible non-uniform distribution of the particles between the instrument being calibrated and the reference. The reference issue might be solved by constructing a longer DMA cylinder in the future which would allow the SCAR to be used for even larger particle sizes.

Acknowledgments

The authors would like to acknowledge Dekati Ltd. for providing instruments to the study. This work was funded by CLEEN Ltd., the Cluster for Energy and Environment through the Measurement, Monitoring and Environmental Assessment (MMEA) research program.

References

Ahlvik, P., Ntziachristos, L., Keskinen, J., & Virtanen, A. (1998). Real Time Measurements of Diesel Particle Size Distributions with an Electrical Low Pressure Impactor. SAE Technical Paper Series 980410.

Berglund, R.N., & Liu, B.Y. H. (1973). Generation of monodisperse aerosol standards. *Environmental Science and Technology*, *7*, 147–153.

Coudray, N., Dieterien, A., Roth, E., & Trouvé, G. (2009). Density measurement of fine aerosol fractions from wood combustion sources using ELPI distributions and image processing techniques. *Fuel*, *88*, 947–954.

Dzubay, T.G., & Hasan, H. (1990). Fitting multimodal lognormal size distributions to cascade impactor data. *Aerosol Science and Technology*, *13*, 144–150.

Glower, W., & Chan, H.-K. (2004). Electrostatic charge characterization of pharmaceutical aerosols using electrical low-pressure impaction (ELPI). *Journal of Aerosol Science*, *36*(6), 755–764.

Gouriou, F., Morin, J-P., & Weill, M.-E. (2004). On-road measurements of particle number concentrations and size distributions in urban and tunnel environments. *Atmospheric Environment*, *38*, 2831–2840.

Held, A., Zerrath, A., McKeon, A., Fehrenbach, T., Niessner, R., Plass-Dülmer, C., Kaminski, U., Berresheim, H., & Pöschl, U. (2008). Aerosol size distributions measured in urban, rural and high-alpine air with an electrical low pressure impactor (ELPI). *Atmospheric Environment*, *42*, 8502–8512.

Hering, S.V. (1987). Calibration of the QCM impactor for stratospheric sampling. *Aerosol Science and Technology*, *7*, 257–274.

Hillamo, R.E., & Kauppinen, E.I. (1991). On the performance of the Berner low pressure impactor. *Aerosol Science and Technology*, *14*, 33–47.

Högström, R., Yli-Ojanperä, J., Rostedt, A., Iisakka, I., Mäkelä, J.M., Heinonen, M., & Keskinen, J. (2011). Validating the Single Charged Aerosol Reference (SCAR) as a traceable particle number concentration standard for 10 nm to 500 nm aerosol particles. *Metrologia*, *48*, 1–11.

Kauppinen, E.I., & Hillamo, R.E. (1989). Modification of the University of Washington Mark 5 in-stack impactor. *Journal of Aerosol Science*, *20*, 813–827.

Keskinen, J., Marjamäki, M., Virtanen, A., Mäkelä, T., & Hillamo, R. (1999). Electrical calibration method for cascade impactors. *Journal of Aerosol Science*, *30*, 111–116.

Keskinen, J., Pietarinen, K., & Lehtimäki, M. (1992). Electrical low pressure impactor. *Journal of Aerosol Science*, *23*, 353–360.

Lemmetty, M., Marjamäki, M., & Keskinen, J. (2005). The ELPI response and data reduction II: properties of kernels and data inversion. *Aerosol Science and Technology*, *39*, 583–595.

Maricq, M.M., Podsiadlik, D.H., & Chase, R.E. (2000). Size distributions of motor vehicle exhaust PM: a comparison between ELPI and SMPS measurements. *Aerosol Science and Technology*, *33*, 239–260.

Marjamäki, M. (2003). Electrical low pressure impactor: modifications and particle collection characteristics (Ph.D. dissertation). Tampere University of Technology, Tampere, Publication 449.

Marjamäki, M., Keskinen, J., Chen, D-R., & Pui, D.Y. H. (2000). Performance evaluation of the electrical low-pressure impactor (ELPI). *Journal of Aerosol Science*, *31*, 249–261.

Marjamäki, M., Lemmetty, M., & Keskinen, J. (2005). ELPI response and data reduction I: response functions. *Aerosol Science and Technology*, *39*, 575–582.

Marjamäki, M., Ntziachristos, L., Virtanen, A., Ristimäki, J., Keskinen, J., Moisio, M., Palonen, M., & Lappi, M. (2002). Electrical Filter Stage for the ELPI. SAE Technical Paper Series, 2002-01-0055.
Marple, V.A. (2004). History of impactors—the first 110 years. *Aerosol Science and Technology*, *38*, 247–292.
Mulholland, G., & Fernandez, M. (1998). Accurate size measurement of monosize calibration spheres by differential mobility analysis. *AIP Conference Proceedings*, *449*, 819–823.
Ristimäki, J., Virtanen, A., Marjamäki, M., Rostedt, A., & Keskinen, J. (2002). On-line measurement of size distribution and effective density of submicron aerosol particles. *Journal of Aerosol Science*, *33*, 1541–1557.
Shi, J.P., Harrison, R.M., & Brear, F. (1999). Particle size distribution from a modern heavy duty diesel engine. *The Science of the Total Environment*, *235*, 305–317.
Virtanen, A., Joutsensaari, J., Koop, T., Kannosto, J., Yli-Pirilä, P., Leskinen, J., Mäkelä, J.M., Holopainen, J.K., Pöschl, U., Kulmala, M., Worsnop, D.R., & Laaksonen, A. (2010). An amorphous solid state of biogenic secondary organic aerosol particles. *Nature*, *476*, 824–827.
Virtanen, A., Marjamäki, M., Ristimäki, J., & Keskinen, J. (2001). Fine particle losses in electrical low-pressure impactor. *Journal of Aerosol Science*, *32*, 389–401.
Winklmayr, W., Wang, H-C., & John, W. (1990). Adaptation of the Twomey Algorithm to the inversion of cascade impactor data. *Aerosol Science and Technology*, *13*, 322–331.
Yi, H., Hao, J., Duon, L., Tang, X., Ning, P., & Li, X. (2008). Fine particle and trace element emissions from an anthracite coal-fired power plant equipped with a bag-house in China. *Fuel*, *87*, 2050–2057.
Yli-Ojanperä, J., Kannosto, J., Marjamäki, M., & Keskinen, J. (2010a). Improving the nanoparticle resolution of the ELPI. *Aerosol and Air Quality Research*, *10*, 360–366.
Yli-Ojanperä, J., Mäkelä, J.M., Marjamäki, M., Rostedt, A., & Keskinen, J. (2010b). Towards traceable particle number concentration standard: Single Charged Aerosol Reference (SCAR). *Journal of Aerosol Science*, *41*, 719–728.
Yli-Ojanperä, J., Sakurai, H., Iida, K., Mäkelä, J.M., Ehara, K., & Keskinen, J. (2012). Comparison of three particle number concentration calibration standards through calibration of a single CPC in a wide particle size range. *Aerosol Science and Technology*, *46*, 1163–1173.
Zervas, E., Dorlhène, P., Forti, L., Perrin, C., Momique, J.C., Monier, R., Ing, H., & Lopez, B. (2005). Interlaboratory test of exhaust PM using ELPI. *Aerosol Science and Technology*, *39*, 333–346.

Paper II

Järvinen A., Heikkilä P., Keskinen J., and Yli-Ojanperä J. (2017). Particle Charge-size Distribution Measurement Using a Differential Mobility Analyzer and an Electrical Low Pressure Impactor, Aerosol Science and Technology, 51, 20-29.

AEROSOL SCIENCE AND TECHNOLOGY
2017, VOL. 51, NO. 1, 20–29
http://dx.doi.org/10.1080/02786826.2016.1256469

Taylor & Francis
Taylor & Francis Group

Particle charge-size distribution measurement using a differential mobility analyzer and an electrical low pressure impactor

A. Järvinen, P. Heikkilä, J. Keskinen, and J. Yli-Ojanperä

Aerosol Physics Laboratory, Department of Physics, Tampere University of Technology, Tampere, Finland

ABSTRACT

We introduce a particle charge-size distribution measurement method using a differential mobility analyzer and an electrical low pressure impactor in tandem configuration. The main advantage of this type of measurement is that it is suitable for a wide range of particle sizes, from approximately 30 nm up to a micrometer, and for high charge levels, which have been problematic for previously used methods. The developed charge measurement method requires information on the particle effective density, and the accuracy of the measurement is dependent on how well the particle effective density is known or estimated. We introduce the measurement and calculation procedures and test these in laboratory conditions. The developed method has been tested using narrow and wide particle size distributions of a known density and well-defined particle charging states. The particles have been produced by the Singly Charged Aerosol Reference (SCAR) and an atomizer and charged with the previously well-characterized unipolar diffusion chargers used in the Nanoparticle Surface Area Monitor (NSAM) and in the Electrical Low Pressure Impactor (ELPI+). The acquired charge-size distributions are in good agreement with the reference values in terms of the median charge levels and widths of the charge distributions.

ARTICLE HISTORY
Received 9 June 2016
Accepted 22 September 2016

EDITOR
Jing Wang

Introduction

As listed below, the electrical charge level of particles (charging state) is important information in many applications of aerosol technology. The size and concentration measurement of nanoparticles relies heavily on particle charging to a known level. Diffusion charging is commonly used to produce controlled charge levels (Intra and Tippayawong 2011), and it is used in combination with electrical detection in instruments measuring particle concentration, for instance the Nanoparticle Surface Area Monitor (NSAM; Fissan et al. 2007), the Partector (Fierz et al. 2014), and the PPS-M (Rostedt et al. 2014). The operation principles of various particle sizing instruments, including the Scanning Mobility Particle Sizer (SMPS; Wang and Flagan 1990), Electrical Low Pressure Impactor (ELPI; Keskinen et al. 1992; Marjamäki et al. 2000), and Engine Exhaust Particle Sizer (EEPS; Johnson et al. 2004), require that particles are charged to a known level. Electrostatic precipitation is widely used in industry and power generation to reduce harmful particle emissions. The collection efficiency of these precipitators depends on the charging efficiency and the final charging state of the particles (Zhuang et al. 2000). In aerosol medicine, the charge level affects the lung deposition because of image and space charge effects (Balachandran et al. 1997). In engine exhaust aerosol measurements, the charge level gives information on the particle formation conditions (Maricq 2006; Lähde et al. 2009), and in outdoor aerosol studies, elevated electric charge levels have been found for particles originating from engine exhaust (Hirsikko et al. 2007; Tiitta et al. 2007; Lee et al. 2012; Jayaratne et al. 2014). While bipolar charge levels in normal conditions can be rather accurately predicted theoretically (Fuchs 1963; Wiedensohler 1988), unipolar charging levels and high temperature bipolar charging levels must be experimentally measured.

Particle charge levels can be experimentally studied by various methods. An aerosol electrometer can be used to measure the net charge of the particle size distribution (Kulvanich and Stewart 1987; Murtomaa and Laine 2000). The ELPI can be used to measure the net charge-size distributions by bypassing the charger or by simply turning off the internal unipolar diffusion charger and the ion trap (Kwok and Chan 2008; Kuuluvainen et al.

CONTACT A. Järvinen anssi.jarvinen@tut.fi Aerosol Physics Laboratory, Department of Physics, Tampere University of Technology, P.O. Box 692, Tampere FI 33101, Finland; J. Keskinen jorma.keskinen@tut.fi Aerosol Physics Laboratory, Department of Physics, Tampere University of Technology, P.O. Box 692, Tampere FI 33101, Finland.
Supplemental data for this article can be accessed on the publisher's website.

2015; Simon et al. 2015). Another method is to conduct electrical mobility based measurement in which, particles are led to an electric field resulting in a constant drift velocity according to their electrical mobility. The electrical mobility is dependent on the particle size and charging state. In the case of a narrow size distribution of known diameter, direct measurement by differential mobility analyzer (DMA) followed by a particle counter may be used to analyze particle charge levels (Hewitt 1957). More advanced techniques combine electrical mobility analysis and particle size measurement. Mobility analyzers accompanied with an optical particle size and concentration measurement have been applied to measure the charging state of larger particles (Emets et al. 1991; Forsyth et al. 1998; Vishnyakov et al. 2016). In the case of nanoparticles, a straightforward solution is to measure the particle size distribution by an SMPS and then bypass the neutralizer to study the original charge of the particles (Maricq 2004). The latest and the most accurate methods are based on two DMAs used in tandem configuration (Kim et al. 2005; Maricq 2005). In the tandem configuration, the particles are classified in the first DMA according to their electrical mobility, which is determined by their initial charging state and size. After the first DMA, the particles are brought to a known charging state in a bipolar diffusion charger and classified by the second DMA, which is followed by a detection instrument, a condensation particle counter (CPC) or an aerosol electrometer. The tandem-DMA measurement provides accurate three-dimensional (concentration as a function of size and charge) information, but the method has some limitations. Tandem-DMA measurement requires a long measurement time, and as a result, the aerosol source must be stable over a long period of time. In addition, the charge level must be well defined before the second DMA, which can be difficult to achieve if the particles were initially highly charged (de La Verpilliere et al. 2015). Thus, the tandem DMA method is most suitable for nanosized particles from 1 to 100 nm, for which the initial particle charge levels can be expected to be relatively low. It is notable that the tandem DMA method with a CPC is the only applicable charge measurement technique for studying the nanoparticle charge in low number concentration environments. For particle sizes larger than 1 μm, the charge-size distributions can be measured for instance with a bipolar charge analyzer (BOLAR; Yli-Ojanperä et al. 2014).

In this study, we introduce a charge measurement method intended to be used mainly in the sub-micrometer size range. The favorable measurement application is highly charged particles of a known density. We introduce the charge measurement method and present the calculation routine for the determination of charge-size distributions. The performance of the developed method is verified experimentally by using particles of a known size and two different charge conditions: singly charged and charging state resulting from the unipolar diffusion chargers. The charger designs are those used in the Nanoparticle Surface Area Monitor (NSAM) and in the Electrical Low Pressure Impactor (ELPI+). We also test the developed method using wide size distributions subjected to unipolar diffusion charging.

Charge measurement concept

Concept of operation

The new charge-size distribution measurement concept is illustrated in Figure 1. The concept combines electrical mobility selection with aerodynamic size classification accompanied with electrical detection of the collected particles. The first step is conducted with a DMA and the second step is conducted with an ELPI. Let us consider what happens when a polydispersed aerosol size distribution with an unknown electric charge (bipolar or unipolar) enters the DMA, which is operated at a constant voltage difference between electrodes. In this case, the output of the DMA consists of particles with nearly the same electrical mobility. The output particles may have *1, 2, …, n* number of elementary charges. Each different number of elementary charges corresponds to a different particle size (mobility diameter) and, consequently, to a different aerodynamic diameter. The DMA is followed by the ELPI. The ELPI charger is switched off because, in this way, the detected current is not affected by the charging efficiency. The particles with a different number of elementary charges represent different aerodynamic diameters and are distributed to different impactor stages and thereby detected as an electric current with separate electrometers. If the density of the particles is known, it is straightforward to calculate to which impactor stages the penetrated particles with a different number of elementary charges are distributed at any given DMA voltage setting. This enables the determination of the particle number concentrations at each impactor stage based on the measured electric currents. In other words, a measurement at one DMA voltage results in pairs of a number of elementary charges n and corresponding number concentrations N, one pair for each particle size. By conducting the described measurement routine at different DMA operating voltages, the number of elementary charges and corresponding number concentrations measured by the impactor stages change while the particle sizes collected by the individual impactor stages remain the same.

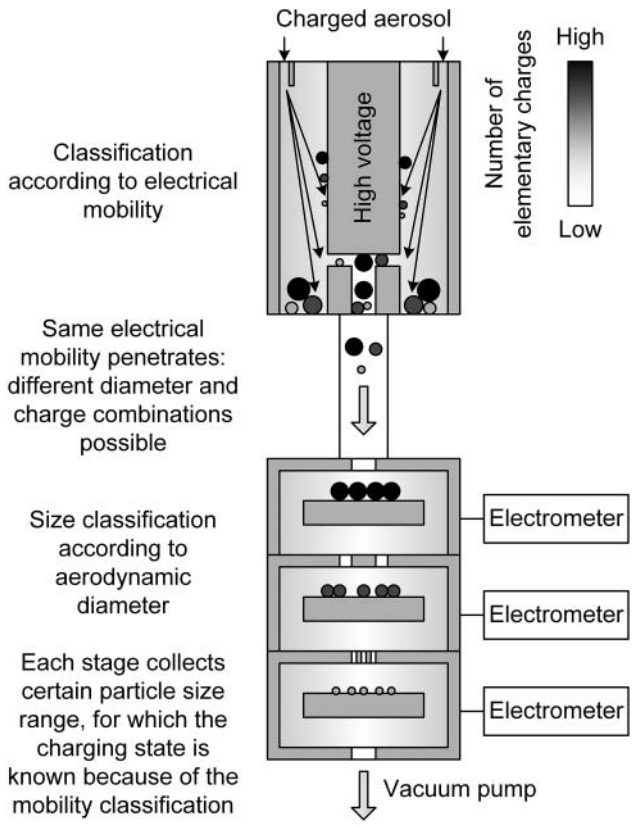

Figure 1. The principle of the DMA-ELPI charge measurement system.

As a result, number concentrations as a function of the number of elementary charges are obtained for the particle sizes collected at different impactor stages. By combining the obtained information, the initial charge-size distribution of the inlet aerosol can be calculated from the results. A thorough description of the calculation procedure will be given in the section "Calculation of charge-size distribution."

Measurement procedure

As mentioned earlier, the measurement setup consists of a DMA and of an ELPI, which are connected in tandem configuration. During one charge-size distribution measurement, the classification voltage of the DMA is changed in a stepwise manner, beginning from low values and proceeding towards larger values. Each stepwise voltage change is followed by a stabilization period, during which the ELPI electrometer signals stabilize.

The stabilization period is followed by a measurement period, during which the electric current signals are recorded and an average current value for each stage is calculated. As a result, the electric current values and also number concentrations are obtained as a function of the DMA voltage separately for each impactor stage. In Figure 2a an example of the charge-size measurement procedure is shown. In this example raw electrometer signals from two impactor stages and the DMA voltage are recorded as a function of time.

Calculation of charge-size distribution

For one measurement point, the DMA defines the particle electrical mobility and the ELPI defines the current distribution as a function of particle aerodynamic diameter, which compose the basis of the calculation. The collection efficiency function parameters for the ELPI+, which is used in this case, are given in Järvinen et al. (2014), except the stage cut diameters and pressures, which are impactor specific and are taken from the manufacturer calibration datasheet. In the first stage, the impaction collection efficiency functions of the ELPI+ are converted from aerodynamic to mobility diameter by assuming an appropriate constant density for the particles. Next, the diffusion part of the collection efficiency functions, not dependent on particle density, are added and the kernel (response) functions are formed. The values of the kernel functions are calculated at certain particle sizes, which is explained later. This results in response terms $a_{k,m}$ for each impactor stage m and particle size k. The particle charging state, the number of elementary charges per particle n_k, is calculated from the DMA parameters for the particle size of index k based on basic DMA equations, given in the online supplemental information (SI). It is now possible to represent the electric currents measured by the ELPI stages by a simple group of equations

$$\begin{aligned} n_1 \cdot a_{1,1} \cdot x_1 + \cdots + n_K \cdot a_{K,1} \cdot x_K &= I_1 \\ \vdots \qquad\qquad\qquad\qquad\quad &= \vdots \\ n_1 \cdot a_{1,14} \cdot x_1 + \cdots + n_K \cdot a_{K,14} \cdot x_K &= I_{14} \end{aligned} \qquad [1]$$

where I_m is the electric current measured by stage m and x_k is the particle concentration (electric current) term for particle size k. The K is the number of particle size bins used in the calculation. This group of equations forms an inversion problem that can be solved by conventional methods. In this case, the Tikhonov regularization method (Hansen 1998) was used. Constant values of 14 and 1 were used for the number of size bins and the Tikhonov regularization parameter, respectively. Finally, the particle number concentration N for the specific size and charge combination is given by equation

$$N_k = \frac{x_k}{eQ_{DMA}} \qquad [2]$$

where e is the elementary charge and Q_{DMA} is the DMA sample flow rate. Instead of the ELPI flow rate, the

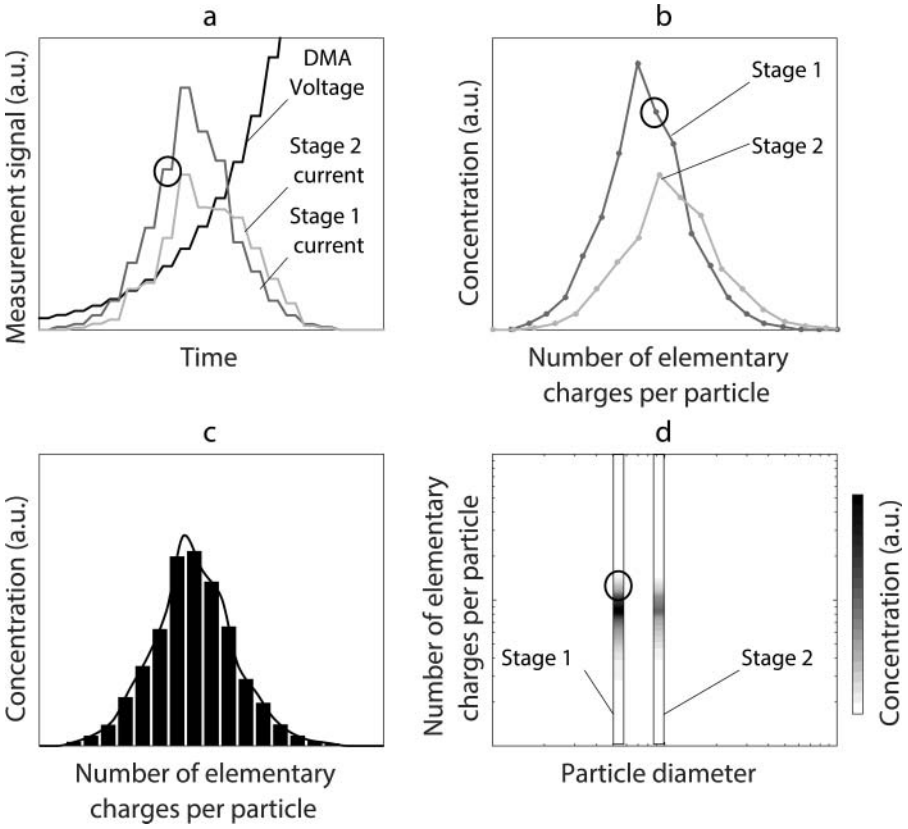

Figure 2. Example of the measurement data (a), results after the calculation (b), integrated charge distribution (c) and three-dimensional charge-size distribution (d). Only two impactor stages, 1 and 2, are shown. Data from (b) is either summed to produce an integrated charge distribution over the entire size distribution, (c) or particle concentrations are shown as a function of both particle size and charging state (d).

sample flow of the DMA is used in the equation because it defines the amount of particles entering the measurement system. The presented calculation is conducted for all of the measurement points (DMA voltages) separately, and as a result, the particle charging state is obtained for each of the impactor stages (see example in Figure 2b). The particle concentrations acquired are presented as arbitrary units because a zero-width DMA transfer function is used to simplify the calculation. In further analysis the results are combined into a single charge distribution and divided into integers of elementary charge (0.5 to 1.5 are counted as 1 and so on). An example is given in Figure 2c. Another option is to present the results in a three-dimensional figure. In this case, particle concentration is shown as a function of both mobility diameter, based on selected particle sizes, and the particle charging state (Figure 2d).

The calculation requires the selection of the particle sizes of index k, which has not yet been discussed. A straightforward solution is to use the mean diameters of the impactor stages to solve the group of equations, but this may result in unstable computational results especially when the useful signal is concentrated on only a few stages. To remedy this, at the first stage, the measured data from the entire measurement is analyzed by checking which of the impactor stages collect charge during the entire measurement. The size range used in the calculation is then limited to cover these stages. First, the maximum charge values over an entire measurement for all of the stages are searched. Then, the stages are selected for which the stage maximum value is more than 10% of the highest value over an entire measurement. To capture all of the required signal, adjacent stages are also considered. The size range used in the calculation is then selected logarithmically so that the first and last sizes are the mean diameters of the adjacent stages. For instance, if the 10% limit is exceeded for stages 5, 6, and 7, the size range is a logarithmic series from the mean diameter of stage 4 to the mean diameter of stage 8, with 14 different particle sizes. The limitation of the size range affects the solution through changes in the collection efficiency terms $a_{k,m}$.

Measurements

The measurement setup is described in Figure 3. The mobility classification is achieved using a 280 mm long Vienna type DMA (Winklmayr et al. 1991) operated

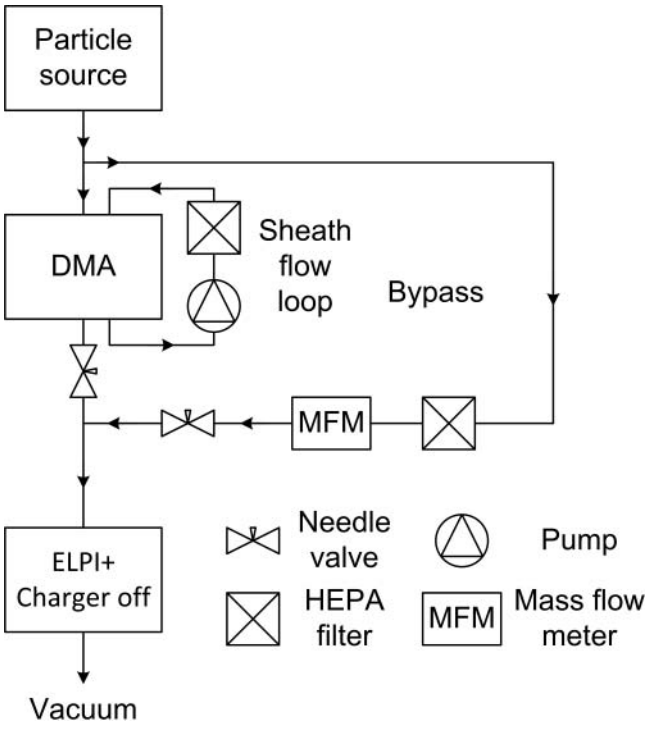

Figure 3. Measurement setup.

with a closed sheath flow loop. A sample to sheath flow ratio of 1/10 was used. The ELPI+ (Dekati Ltd., Finland) requires a sample flow of 10 l/min, which is far higher than the DMA inlet flow (2 l/min in all charge distribution measurements). As shown in Figure 3, the setup has an additional bypass loop to ensure that the inlet flow rate stays constant if the DMA flows are changed. The flow rate through this bypass loop is adjusted with needle valves, and the particles are removed using a HEPA filter. The ELPI+ was operated with the charger and the ion trap switched off, and the particles were collected in the impactor into aluminum foil collection substrates, which were covered by a thin layer of vacuum grease (Apiezon L, M&I Materials Ltd., UK).

The measurement routine consisted of scanning the DMA voltage and measuring the particles with the ELPI+. The DMA voltage was logged directly by the ELPI+ analog input channel to assemble all of the data into a single file. One measurement point consisted of 10 s stabilization and 10 s measurement periods. There were 20 measurement points, resulting in a total time of 400 s for one charge distribution. Data processing was conducted in a Matlab environment (Matlab 2015a, Mathworks Inc., MA, USA).

To study the performance of the developed method, laboratory measurements were conducted using particles of a known size, charging state and material properties. Singly charged particles were used to test that the method is capable of estimating low numbers of elementary charges per particle. The singly charged particles were generated by the Singly Charged Aerosol Reference (SCAR; Yli-Ojanperä et al. 2010). This is a reliable reference method because practically all particles are singly charged (Högström et al. 2011). The particles were composed of an approximately 10 nm NaCl or Ag seed particle surrounded by liquid diethylhexyl sebacate (DEHS). Size distributions were acquired by measuring the total electric current from the ELPI (charger and ion trap switched off) during the DMA scan. Because particles were known to be singly charged, there was a one-to-one correspondence between the total electric current and the particle number concentration in this special case. The size distributions, measured using the DMA, are shown in Figure S1a (see the SI). The generated particle sizes were 50, 100, 200, and 500 nm, with rather narrow size distributions, the Geometric Standard Deviations (GSD) ranged between 1.06 and 1.15. Because the particle sizes are significantly larger than the seed particle size, the seed particle has a minimal effect on the density. Thus, the particle density was approximated by the bulk density value of pure DEHS, which is 0.914 g/cm^3.

The method was also tested with the same narrow size distributions of particles with higher charge levels. Particles were generated by the SCAR and then neutralized using a Kr-85 aerosol neutralizer (3077A, TSI Inc., Shoreview, MN, USA) followed by an electrostatic precipitator and finally charged by corona-based diffusion chargers. The ELPI+ charger was selected to provide higher charge levels. Järvinen et al. (2014) report the charging efficiency of this charger over a wide particle size-range. The charger was operated at the standard corona discharge current value of 1 μA. In addition, another charger based on Medved et al.'s (2000) design was used to produce charged particles. This mixing-type diffusion charger is used in electrical aerosol instruments (Electrical Aerosol Detector, Model 3070A, and Nanoparticle Surface Area Monitor, Model 3550, TSI Inc., MN, USA). Qi et al. (2009) and Kaminski et al. (2012) have characterized the charger, the latter reporting particle charge distributions. The charger in this study was operated using the same flow rates (1.5 L/min aerosol and 1.0 L/min ion jet flows) and the same 1 μA corona current as in Kaminski et al. (2012).

The developed charge measurement method was also subjected to wide particle size distributions of charged particles. Particles were generated by atomizing DEHS from solutions at different concentrations (1%, 10%, and 100% by volume). HPLC-grade 2-propanol was used as a solvent in the case of the 1% and 10% solutions. The wide size distributions generated by atomizing DEHS solutions are shown in Figure S1b. The distributions

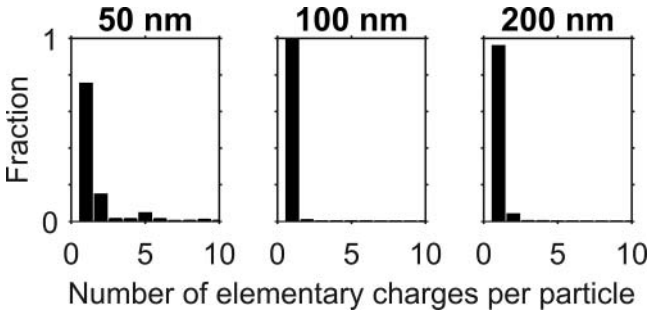

Figure 4. Charge distributions from singly charged particles of different sizes. The fraction is calculated from the charged particles only.

range to super-micron diameter and were measured using a standard ELPI+. The median mobility diameters according to lognormal fitting are 135, 224, and 430 nm for 1%, 10%, and 100% DEHS solutions. The GSD's for the atomized particle size distributions range between 2.0 and 2.4. After the generation, the aerosol was diluted with filtered air and neutralized by alpha radiation neutralizer (Am-241, 29.6 MBq, residence time 1.9 s). The final charging was performed by the same ELPI+ charger as in the previous measurements and using the same 1 μA corona current.

Results

For singly charged particles the calculation was performed as in Figure 2c, by calculating the charging state over the entire size distribution. The particles were mostly detected to carry one elementary charge by the developed method (Figure 4). At the 50 nm particle size, small amounts of other charge levels were detected, especially doubly charged particles. This effect likely arises from the low electric currents measured and from the narrow size distribution detected only by two ELPI channels. In the case of the 100 and 200 nm particles, the calculated fraction of particles with more than one elementary charge was minimal, less than 5%, which implies that the method is suitable for singly charged particles. The charge distribution for singly charged 500 nm particles is not shown because the particle concentrations were too low for the calculation.

The higher charge levels, produced by a separate ELPI+ charger installed in line, were studied with the same distributions presented in Figure S1a. The results for the unipolar diffusion charged aerosol are presented in Figure 5. Modal values of 2, 5, 10 and 36 elementary charges were observed, while the particle diameters were 50, 100, 200, and 500 nm. If a lognormal fitting is conducted for the charge distributions, median values of 2.41, 5.09, 10.5, and 37.1 are obtained. The corresponding Pn-values, penetration multiplied by the number of elementary charges per particle, for the ELPI+ charger used were 1.75, 4.08, 9.54, and 29.3 (Järvinen et al. 2014). The Pn-values include the particle losses and should be somewhat lower than the presented charge number values. Taking this into account, the values from the developed method match the Pn-values well. The measured values and the reference values for the test measurements are shown in Table 1.

The charge distributions after the mixing-type charger were tested using 100 and 200 nm narrow particle size distributions, similar to those shown in Figure S1a. The charge distributions are presented in Figure 6 accompanied by the results from the Kaminski et al.'s (2012) empirical model. The developed charge measurement method produces mode values of 3 and 8 and median values of 3.2 and 7.0 elementary charges per particle for 100 and 200 nm particles. These median values are calculated by fitting a lognormal function to the final charge distributions. In comparison, a similar fitting method gives 2.67 and 5.83 elementary charges per particle median values according to the model by Kaminski et al. (2012). Average values for the same particle sizes using a simple power equation by Kaminski et al. (2012) are 2.9

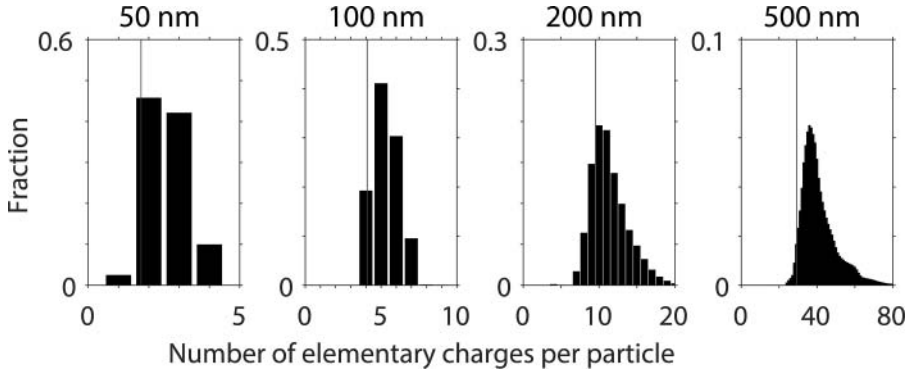

Figure 5. Charge distributions of unipolarly diffusion charged particles. The particles were charged by a separate corona charger similar to the one used in the ELPI+. The vertical line represents the charger Pn-value at the corresponding particle size.

Table 1. Measured and reference charge distribution parameters for the ELPI+ and the mixing-type chargers. The *n* refers to the number of elementary charges per particle. For the ELPI+ charger, separate values for narrow (N) and wide (W) size distributions are presented.

	ELPI+							Mixing-type					
	n mode		*n* median			*n* GSD							
d_p (nm)	N	W	N	W	*n* ref[a]	N	W	*n* mode	*n* median	*n* ref[b]	*n* ref[c]	*n* GSD	*n* GSD ref[c]
50	2	2	2.41	1.92	1.75	1.31	1.38						
100	5	4	5.09	4.57	4.08	1.21	1.36	3	3.18	2.90	2.67	1.40	1.46
200	10	10	10.5	9.82	9.54	1.22	1.25	8	6.98	6.31	5.83	1.35	1.40
500	36	33	37.1	34.7	29.3	1.18	1.20						

[a]Pn-value, Pn = 68.531·D_p(μm)$^{1.225}$ (Järvinen et al. 2014).
[b]Average, n = 0.0167·D_p(nm)$^{1.12}$ (Kaminski et al. 2012).
[c]Median from lognormal fit (Kaminski et al. 2012).

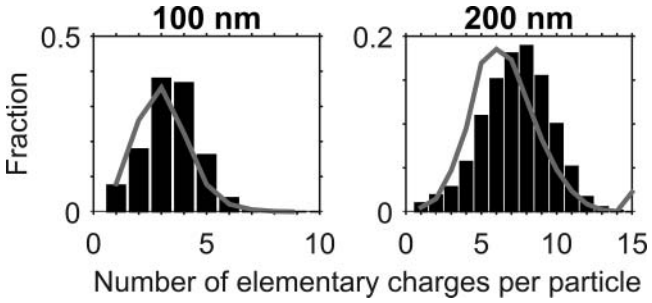

Figure 6. Charge distributions of unipolarly charged particles after the mixing-type charger. The bar plot is the distribution according to the developed method, and the line represents results from the semi-empirical model by Kaminski et al. (2012).

and 6.3. Thus, the values from the developed charge measurement method are slightly higher than those predicted by the model, which is also shown in Figure 6. The GSD values according to the charge measurement method are 1.40 and 1.35, and the corresponding values from the model are 1.46 and 1.40, which indicates that the width of the charge distribution is detected quite well by the developed method in comparison to the model.

Typical particle size distributions are rather wide compared to the test aerosols shown in Figure S1a. To study more realistic measurement application, wide distributions were generated by atomizing DEHS (size distributions in Figure S1b). This aerosol was neutralized and then charged using the same ELPI+ charger as in the case of the narrow size distributions. This type of measurement generates a three-dimensional output, in which particle number concentration is presented as a function of particle size and charging state. In Figure 7, the results for three different particle size and charge distributions are given. The pattern observed in Figure 7 closely resembles the Pn-curve of the ELPI+ charger (Järvinen et al. 2014), which is also plotted in the figure, from 30 nm up to a 1 μm particle size. This result confirms that the method is capable of measuring the charging state of wide particle size distributions and performs well in wide size range from tens of nanometers up to a micrometer.

To more closely study the charge-size distribution of Figure 7, specific particle sizes were selected, and the charge distributions are shown for these selected particle sizes in Figure 8. Because the selected particle sizes are

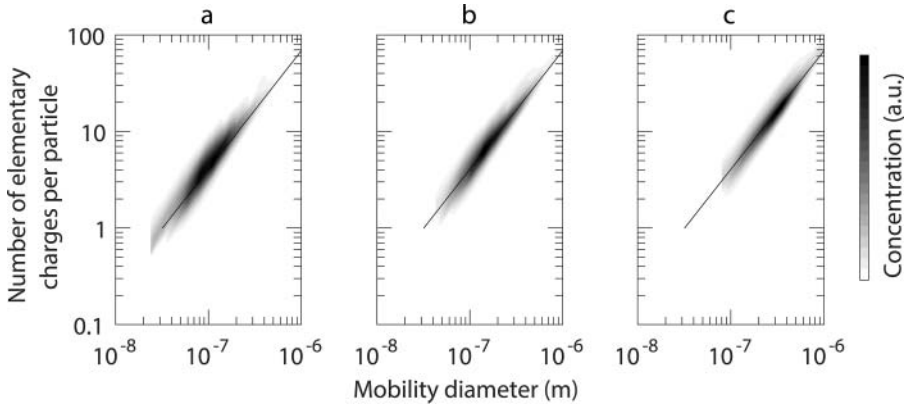

Figure 7. Charge-size distributions after the ELPI+ corona charger in the case of three wide size distributions generated by atomizing 1% (a), 10% (b), and 100% (c) DEHS solutions. The line in the figure represents part of the Pn-curve of the ELPI+ corona charger (Järvinen et al. 2014).

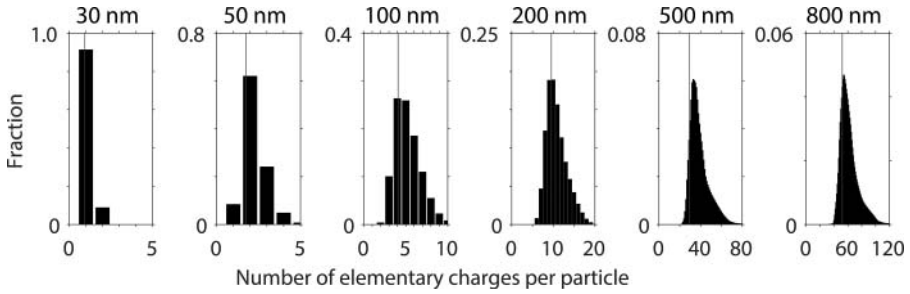

Figure 8. Charge distributions of unipolarly diffusion charged particles from wide size distributions. The charge distributions presented are cross-sections from the charge-size distributions presented in the Figure 7 at the selected particle sizes. The vertical line represents the charger Pn-value at the corresponding particle size.

not the specific sizes used in the calculation, the results are based on the interpolation of the distribution. To compare the values, the same particle sizes were selected as in Figure 5, which were supplemented by additional 30 nm and 800 nm sizes. The 30, 50, and 100 nm charge distributions were calculated as cross-sections from Figure 7a, and the 200 nm charge distribution from Figure 7b. The two largest charge distributions, 500 and 800 nm, were calculated from Figure 7c. The modal values in Figure 8 are 1, 2, 4, 10, 33, and 54 elementary charges per particle, and the median values of 1.29, 1.92, 4.57, 9.82, 34.7, and 56.6 were achieved through lognormal fitting. The Pn-values for the same particle sizes are 0.93,1.75, 4.08, 9.54, 29.3, and 52.1 (Järvinen et al. 2014). The charge values obtained from the wide size distribution are actually closer to the Pn-values than those obtained from the narrow size distributions shown in Figure 5. In general, the charge distributions from the wide size distributions are in good agreement with those measured from the narrow size distributions (Table 1).

Discussion and conclusions

While calculating the charge-size distribution results presented in this study, a zero-width DMA transfer function was used for simplicity. In the experiments, a sample to sheath flow ratio of 1/10 was used. At this flow ratio, the DMA transfer function is narrow compared to the particle size range collected by individual ELPI impactor stages, which justifies the use of the zero-width DMA transfer function approximation. Should the ratio be increased for a better signal to noise ratio, it might be necessary to include the actual DMA transfer function in the calculation.

The accuracy of the developed charge measurement method depends, among other things, on how accurately the density or effective density of the particles is known. In the case of liquid particles, the bulk density of the liquid can usually be used as an accurate estimate of the particle density. Estimating the effective density of solid particles may result in large errors. According to the equations used to calculate the charge-size distributions, an error in effective density produces an error in the charge results. The magnitude of the error depends on the particle size. For example, if the effective density is half or twice the real value, the error would be +226% or −72% at the 30 nm particle size and +77% or −50% at the 300 nm particle size. However, an estimate of the effective density of the particles as a function of particle size can be determined experimentally, using, for instance, the tandem DMA-ELPI setup (Maricq and Xu 2004) or the tandem setup with multiple charge correction (Bau et al. 2014). These tandem setups are almost the same as in this charge measurement method, only a neutralizer is added in front of the DMA. Another option is to use the parallel DMA-ELPI measurement setup presented by Ristimäki et al. (2002). Based on Ristimäki et al.'s (2002) and Bau et al.'s (2014) results, the accuracy of the reported effective density values is approximately ±20%. In the case of 30 nm particles, a ±20% error in the effective density causes +49% or −28% errors in the charge level. If the particle size is 300 nm, the error in the charge level decreases to +22% or −16%.

It is common that the particle effective density changes according to particle size. For agglomerated particles, the density is the highest for the smallest (primary) particles, while the density lowers as the agglomerates come larger. If the effective density has such a strong dependency on particle size, this charge measurement method should be used with caution. A strong change in effective density widens the particle size range collected by the individual impactor stages in mobility space, which reduces the accuracy of the final charge distribution. In the case of a small change in effective density, the constant effective density that is currently used in the calculation can be replaced by a particle size dependent density profile.

In conclusion, a DMA-ELPI charge measurement method was developed and found to produce similar values with the references used. The singly charged particles were mostly detected to carry a single elementary charge by the developed method. Values for the unipolarly

diffusion charged particles were mostly the same as those reported in the literature. The method was also found to work for wide particle size distributions generated by the atomizer. Both wide and narrow size distributions produced comparable charge levels when particle charging was achieved using the same ELPI+ charger. In the case of the mixing-type charger, the measurement method produced slightly higher charge levels than Kaminski et al.'s (2012) model, but the widths of the charge distributions were almost the same.

The size and charge range in this study is difficult for the conventional tandem DMA methods, due to the second DMA's multiple charging issues. The developed method does not suffer from this issue, because the size classification does not depend on the particle charge level.

The measurement is rather fast compared to the tandem DMA methods and could likely be tuned for faster total measurement time. By optimizing tubing between the DMA and the ELPI, stabilization could perhaps be reduced to 5 s, and the measurement period of 5 s would most likely be enough to acquire a stable signal. These modifications might enable halving the total measurement time, but this has not been tested yet. Note that although it is not reported here, it is of course possible to measure both polarities in sequence using a bipolar voltage supply for the DMA.

The main advantage of the developed measurement method is that it is suitable for a wide particle size range of approximately 30 nm up to a micrometer and for high charge levels, which have been problematic for previously used methods. The measurement is truly two-dimensional and generates particle charge-size distribution, in which particle concentration is seen as a function of both particle size and charging state.

Acknowledgments

The authors thank Dr.-Ing. Christof Asbach from Institut für Energie- und Umwelttechnik e. V. (IUTA) for providing the mixing-type charger used in this study.

Funding

The authors acknowledge Dekati Ltd. for financing this study under the project name CHARM.

References

Balachandran, W., Machowski, W., Gaura, E., and Hudson, C. (1997). Control of Drug Aerosol in Human Airways Using Electrostatic Forces. *J. Electrostat.*, 40–41:579–584.

Bau, S., Bémer, D., Grippari, F., Appert-Collin, J.C., and Thomas, D. (2014). Determining the Effective Density of Airborne Nanoparticles Using Multiple Charging Correction in a Tandem DMA/ELPI Setup. *J. Nanopart. Res.*, 16:2629.

de La Verpilliere, J. L., Swanson, J., and Boies, A. M. (2015). Unsteady Bipolar Diffusion Charging in Aerosol Neutralisers: A Non-Dimensional Approach to Predict Charge Distribution Equilibrium Behaviour. *J. Aerosol Sci.*, 86:55–68.

Emets, E.P., Kascheev, V.A., and Poluektov, P.P. (1991). Simultaneous Measurement of Aerosol Particle Charge and Size Distributions. *J. Aerosol Sci.*, 22:389–394.

Fierz, M., Meier, D., Steigmeier, P., and Butscher, H. (2014). Aerosol Measurement by Induced Currents. *Aerosol Sci. Technol.*, 48:350–357.

Fissan, H., Neumann, S., Trampe, A., Pui, D.Y.H., and Shin, W. G. (2007). Rationale and Principle of an Instrument Measuring Lung Deposited Nanoparticle Surface Area. *J. Nanopart. Res.*, 9:53–59.

Forsyth, B., Liu, B.Y.H., and Romay, F.J. (1998). Particle Charge Distribution Measurement for Commonly Generated Laboratory Aerosols. *Aerosol Sci. Technol.*, 28:489–501.

Fuchs, N.A. (1963). On the stationary charge distribution on Aerosol Particles in a Bipolar Ionic Atmosphere. *Geofis. Pura Appl.*, 56:185–193.

Hansen, P.C. (1998). Rank-deficient and discrete ill-posed problems: numerical aspects of linear inversion. Society of Industrial and Applied Mathematics, Philadelphia.

Hewitt, G.W. (1957). The Charging of Small Particles for Electrostatic Precipitation. *Trans. Am. Inst. Elect. Engrs*, 76:300–306.

Hirsikko, A., Yli-Juuti, T., Nieminen, T., Vartiainen, E., Laakso, L., Hussein, T., and Kulmala, M. (2007). Indoor and Outdoor Air Ions and Aerosol Particles in the Urban Atmosphere of Helsinki: Characteristics, Sources and Formation. *Boreal Env. Res.*, 12:295–310.

Högström, R., Yli-Ojanperä, J., Rostedt, A., Iisakka, I., Mäkelä, J.M., Heinonen, M., and Keskinen, J. (2011). Validating the Single Charged Aerosol Reference (SCAR) as a Traceable Particle Number Concentration Standard for 10 nm to 500 nm Aerosol Particles. *Metrologia*, 48:426–436.

Intra, P., and Tippayawong, N. (2011). An Overview of Unipolar Charger Developments for Nanoparticle Charging. *Aerosol Air Qual. Res.*, 11:187–209.

Järvinen, A., Aitomaa, M., Rostedt, A., Keskinen, J., and Yli-Ojanperä, J. (2014). Calibration of the New Electrical Low Pressure Impactor (ELPI+). *J. Aerosol Sci.*, 69:150–159.

Jayaratne, E.R., Ling, X., and Morawska, L. (2014). Observation of Ions And Particles Near Busy Roads using a Neutral Cluster And Air Ion Spectrometer (NAIS). *Atmos. Environ.*, 84:198–203.

Johnson, T., Caldow, R., Pöcher, A., Mirme, A., and Kittelson, D. (2004). A New Electrical Mobility Particle Sizer Spectrometer for Engine Exhaust Particle Measurements. *SAE Technical Paper*, 2004–01-1341.

Kaminski, H., Kuhlbusch, T., Fissan, H., Ravi, L., Horn, H.-G., Han, H.-S., Caldow, R., and Asbach, C. (2012). Mathematical Description of Experimentally Determined Charge Distributions of a Unipolar Diffusion Charger. *Aerosol Sci. Technol.*, 46:708–716.

Keskinen, J., Pietarinen, K., and Lehtimäki, M. (1992). Electrical Low Pressure Impactor. *J. Aerosol Sci.*, 23:353–360.

Kim, S.H., Woo, K.S., Liu, B.Y.H., and Zachariah, M.R. (2005). Method of Measuring Charge Distribution Of Nanosized Aerosols. *J. Colloid Interface Sci.*, 282:46–57.

Kulvanich, P., and Stewart, J. (1987). An Evaluation of the Air Stream Faraday Cage in the Electrostatic Charge Measurement of Interactive Drug System. *Int. J. Pharm.*, 36:243–252.

Kuuluvainen, H., Karjalainen, P., Bajamundi, C.J.E., Maunula, J., Vainikka, P., Roppo, J., Keskinen, J., and Rönkkö, T. (2015). Physical Properties of Aerosol Particles Measured from a Bubbling Fluidized Bed Boiler. *Fuel*, 139:144–153.

Kwok, P. C. L., and Chan, H.-K. (2008). Effect of Relative Humidity on the Electrostatic Charge Properties of Dry Powder Inhaler Aerosols. *Pharm. Res.*, 25:277–288.

Lee, E.S., Xu, B., and Zhu, Y. (2012). Measurements of Ultrafine Particles Carrying Different Number of Charges in on- and Near-Freeway Environments. *Atmos. Environ.*, 60:564–572.

Lähde, T., Rönkkö, T., Virtanen, A., Schuck, T.J., Pirjola, L., Hämeri, K., Kulmala, M., Arnold, F., Rothe, D., and Keskinen, J. (2009). Heavy Duty Diesel Engine Exhaust Aerosol Particle and Ion Measurements. *Environ. Sci. Technol.*, 43:163–168.

Maricq, M.M. (2004). Size and charge of soot particles in rich premixed ethylene flames. *Combust. Flame*,137:340–350.

Maricq, M.M., and Xu, N. (2004). The Effective Density and Fractal Dimension of Soot Particles from Premixed Flames and Motor Vehicle Exhaust. *J. Aerosol Sci.*, 35:1251–1274.

Maricq, M.M. (2005). The Dynamics of Electrically Charged Soot Particles in a Premixed Ethylene Flame. *Combust. Flame*, 141:406–416.

Maricq, M.M. (2006). On the Electrical Charge Of Motor Vehicle Exhaust Particles. *J. Aerosol Sci.*, 37:858–874.

Marjamäki, M., Keskinen, J., Chen, D.-R., and Pui, D. Y. H. (2000). Performance Evaluation of the Electrical Low-Pressure Impactor (ELPI). *J. Aerosol Sci.*, 31:249–261.

Medved, A., Dorman, F., Kaufman, S., and Pocher, A. (2000). New Corona-Based Charger for Aerosol Particles. *J. Aerosol Sci.*, 31:S616–S617.

Murtomaa, M., and Laine, E. (2000). Electrostatic Measurement On Lactose-Glucose Mixtures. *J. Electrostat.*, 48:155–162.

Qi, C., Asbach, C., Shin, W.G., Fissan, H., and Pui, D.Y.H. (2009). The Effect of Particle Pre-Existing Charge on Unipolar Charging and Its Implication on Electrical Aerosol Measurements. *Aerosol Sci. Technol.*, 43:232–240.

Ristimäki, J., Virtanen, A., Marjamäki, M., Rostedt, A., and Keskinen, J. (2002). On-line measurement of size distribution and effective density of submicron aerosol particles. *J. Aerosol Sci.*, 33:1541–1557.

Rostedt, A., Arffman, A., Janka, K., Yli-Ojanperä, J., and Keskinen, J. (2014). Characterization and Response Model of the PPS-M Aerosol Sensor. *Aerosol Sci. Technol.*, 48:1022–1030.

Simon, X., Bau, S., Bémer, D., and Duquenne, P. (2015). Measurement of Electrical Charges Carried by Airborne Bacteria Laboratory-Generated Using a Single-Pass Bubbling Aerosolizer. *Particuology*, 18:179–185.

Tiitta, P., Miettinen, P., Vaattovaara, P., Laaksonen, A., Joutsensaari, J., Hirsikko, A., Aalto, P., and Kulmala, M. (2007). Road-Side Measurements of Aerosol and Ion Number Size Distributions: A Comparison with Remote Site Measurements. *Boreal Env. Res.*, 12:311–321.

Vishnyakov, V.I., Kiro, S.A., Oprya, M.V., and Ennan, A.A. (2016). Charge Distribution of Welding Fume Particles after Charging by Corona Ionizer. *J. Aerosol Sci.*, 94:9–21.

Wang, S.C., and Flagan, R.C. (1990). Scanning Electrical Mobility Spectrometer. *Aerosol Sci. Technol.*, 13:230–240.

Wiedensohler, A. (1988). An Approximation of the Bipolar Charge Distribution for Particles in the Submicron Size Range. *J. Aerosol Sci.*, 19:387–389.

Winklmayr, W., Reischl, G.P., Lindner, A.O., and Berner, A. (1991). A New Electromobility Spectrometer for the Measurement of Aerosol Size Distributions in the Size Range from 1 to 1000 nm. *J. Aerosol Sci.*, 22:289–296.

Yli-Ojanperä, J., Mäkelä, J.M., Marjamäki, M., Rostedt, A., and Keskinen, J. (2010). Towards Traceable Particle Number Concentration Standard: Single Charged Aerosol Reference (SCAR). *J. Aerosol Sci.*, 41:719–728.

Yli-Ojanperä, J., Ukkonen, A., Järvinen, A., Layzell, S., Niemelä, V., and Keskinen, J. (2014). Bipolar Charge Analyzer (BOLAR): A New Aerosol Instrument for Bipolar Charge Measurements. *J. Aerosol Sci.*, 77:16–30.

Zhuang, Y., Jin Kim, Y., Gyu Lee, T., and Biswas, P. (2000). Experimental and Theoretical Studies of Ultra-Fine Particle Behavior in Electrostatic Precipitators. *J. Electrostat.*, 48:245–260.

Supplemental Information

Particle charge-size distribution measurement using a differential mobility analyzer and an electrical low pressure impactor

Järvinen A., Heikkilä P., Keskinen J., Yli-Ojanperä J.

Aerosol Physics Laboratory, Department of Physics, Tampere University of Technology
P.O. Box 692, FI-33101 Tampere, Finland

The measurement of the charge distribution is based on the combination of the DMA and the ELPI. The first instrument, DMA, selects the electrical mobility of the particles. The mean mobility of the particles penetrating the cylindrical DMA is

$$Z^* = \frac{\left(Q_{sh} + Q_{ex}\right)}{4\pi LV} \ln\left(\frac{r_2}{r_1}\right), \qquad \text{[S1]}$$

where Q_{sh} and Q_{ex} are the sheath and excess flows, L is the length of the classifying section, V is the voltage of the center rod and r_2 and r_1 are the outer and inner radii of the classifying section (Knutson and Whitby 1975). To simplify the calculations, a zero-width transfer function is assumed. In typical aerosol measurements, the charging state of the aerosol flowing into the DMA is well defined, and the classifying voltage is used to select the particle diameter penetrating the DMA. In this charge measurement application, the desired value is, however, the number of elementary charges per particle, which is accessible through the electrical mobility. The electrical mobility for a particle is defined by equation

$$Z = \frac{neC_c\left(d_p\right)}{3\pi\eta d_p}, \qquad \text{[S2]}$$

where n is the number of elementary charges per particle, e is the elementary charge, C_c is the slip correction factor (Allen and Raabe 1985), η is the viscosity of the carrier gas and d_p is the particle mobility diameter (Flagan 2001).

By combining Equations S1 and S2, the number of elementary charges per particle is solved by equation

$$n = \frac{Z^* \cdot 3\pi\eta d_p}{eC_c\left(d_p\right)}. \qquad \text{[S3]}$$

The Z^* contains only constants and the DMA voltage, which must be logged in the measurement setup. The particle mobility diameter d_p is a term that must be measured by another instrument. To achieve a wide size range and reduce the time needed to accomplish the measurement, the ELPI is used to measure the size distribution. The size classification of the ELPI is based on the impactor, which results that the size measured by

the ELPI is the aerodynamic diameter of the particle. The diameter of the particle d_p and the aerodynamic diameter d_a are linked together by equation

$$d_a = d_p \left(\frac{C_c}{C_{c,a}} \right)^{1/2} \left(\frac{\rho_p}{\rho_0} \right)^{1/2} , \qquad [S4]$$

where $C_{c,a}$ is the slip correction factor for the aerodynamic diameter, ρ_p is the density of the particle and ρ_0 is the density of 1000 kg/m^3 (Baron and Willeke 2001). If not already known, the (effective) density can be measured using the tandem DMA-ELPI method (Maricq and Xu 2004; Bau et al. 2014) or the parallel DMA-ELPI method (Ristimäki et al. 2002).

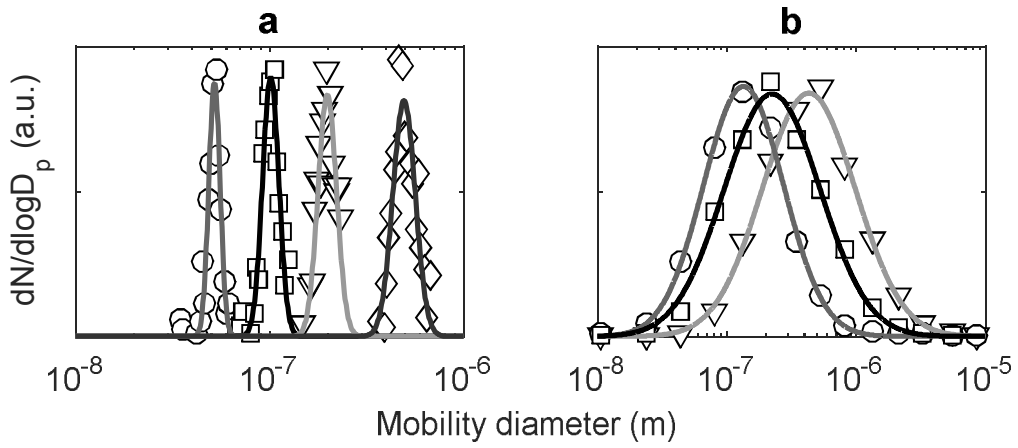

Figure S1. Normalized particle size distributions used in test measurements, including lognormal fits. The narrow size distributions generated by the SCAR are shown in subfigure (a) and the wide size distributions from the atomizer in subfigure (b). All size distributions were used separately to test the charge measurement method, although they are combined into same figures.

References

Allen, M.D., and Raabe, O.G. (1985). Slip Correction Measurements of Spherical Solid Aerosol Particles in an Improved Millikan Apparatus. *Aerosol Sci. Technol.*, 4:269-286.

Baron, P.A., and Willeke, K. (2001). Aerosol Fundamentals, in Aerosol Measurement: Principles, Techniques, and Applications, Second Edition, P. A. Baron and K. Willeke, eds, John Wiley and Sons, New York, 45-60.

Bau, S., Bémer, D., Grippari, F., Appert-Collin, J.C., and Thomas, D. (2014). Determining the effective density of airborne nanoparticles using multiple charging correction in a tandem DMA/ELPI setup. *J. Nanopart. Res.*, 16:2629.

Flagan, R.C. (2001). Electrical Techniques, in Aerosol Measurement: Principles, Techniques, and Applications, Second Edition, P. A. Baron and K. Willeke, eds, John Wiley and Sons, New York, 537-567.

Knutson, E.O., and Whitby, K.T. (1975). Aerosol classification by electric mobility: apparatus, theory, and applications. *J. Aerosol Sci.*, 8:443-451.

Maricq, M.M., and Xu, N. (2004). The effective density and fractal dimension of soot particles from premixed flames and motor vehicle exhaust. *J. Aerosol Sci.*, 35:1251-1274.

Ristimäki, J., Virtanen, A., Marjamäki, M., Rostedt, A., and Keskinen, J. (2002). On-line measurement of size distribution and effective density of submicron aerosol particles. *J. Aerosol Sci.*, 33:1541-1557.

Paper III

Yli-Ojanperä J., Ukkonen A., Järvinen A., Layzell S., Niemelä V., and Keskinen J. (2014). Bipolar Charge Analyzer (BOLAR): A New Aerosol Instrument for Bipolar Charge Measurements, Journal of Aerosol Science, 77, 16-30.

Journal of Aerosol Science 77 (2014) 16–30

Contents lists available at ScienceDirect

Journal of Aerosol Science

journal homepage: www.elsevier.com/locate/jaerosci

Bipolar Charge Analyzer (BOLAR): A new aerosol instrument for bipolar charge measurements

Jaakko Yli-Ojanperä [a,*], Ari Ukkonen [b], Anssi Järvinen [a], Steve Layzell [c], Ville Niemelä [b], Jorma Keskinen [a]

[a] Tampere University of Technology, Department of Physics, P.O. Box 692, FIN-33101 Tampere, Finland
[b] Dekati Ltd., Tykkitie 1, FIN-36240 Kangasala, Finland
[c] GlaxoSmithKline, 980 Great West Road, Brentford, Middlesex TW8 9GS, United Kingdom

ARTICLE INFO

Article history:
Received 16 April 2014
Received in revised form
1 July 2014
Accepted 3 July 2014
Available online 23 July 2014

Keywords:
Charge measurement
Charge-to-mass ratio
Pharmaceutical
Inhaler
BOLAR
Bipolar Charge Analyzer

ABSTRACT

The Bipolar Charge Analyzer (BOLAR, Dekati Ltd.) is a new commercial instrument developed to characterize bipolar charge and charge-to-mass ratio of powders and inhaled aerosols as a function of particle size. The instrument combines aerodynamic size classification with electrostatic precipitator based bipolar charge measurement. As a result bipolar charge and charge-to-mass ratios are obtained for 5 size fractions between zero and 11.6 μm. In this study we present the operation concept, design and the performance characteristics of the BOLAR. The instrument was calibrated using monodisperse particles in laboratory conditions. The performance of the instrument in inhaler measurement was tested by measuring aerosol produced by a dry powder inhaler (DPI). The DPI was found to produce noticeable levels of positively and negatively charged particles. For a single size fraction the largest observed positive and negative values were +300 pC and −200 pC, respectively, although the net charge was close to zero. By analyzing the mass of the particles collected by the individual parts of the BOLAR the size fractioned charge-to-mass ratios were calculated for the tested inhaler. The largest values were approximately ±20 pC/μg which was obtained for particles having a mean diameter of 1.8 μm. The number of elementary charges per particle ranged from ±500 up to ±8000 depending on the particle size.

1. Introduction

Electrostatic forces acting on charged aerosol particles are important in aerosol technology. Intentional processes causing a net charge on a particle are, for example, diffusion, field and flame charging (Hinds, 1998). Charging processes are widely exploited in electrostatic precipitators that are often used in air-cleaning applications, in aerosol classification devices, such as Differential Mobility Analyzers (DMA; Knutson & Whitby, 1975) and in electrical detection of the particles (e.g. Electrical Low-Pressure Impactor; ELPI, Keskinen et al., 1992 and Differential Mobility Spectrometer; Biskos et al., 2005). Other, potentially useful, not so well-characterized, charging processes are triboelectrification and surface charging. These are usually related to how the aerosol is generated. Atomizers, nebulizers and various dry powder dispensers that are often used in medical applications are known to be affected by these types of charging mechanisms. On one hand, the charge caused by

* Corresponding author. Tel.: +358 503004985.
E-mail address: jaakko.yli-ojanpera@tut.fi (J. Yli-Ojanperä).

http://dx.doi.org/10.1016/j.jaerosci.2014.07.004
0021-8502/

the generator may cause undesired effects such as particle losses inside aerosol transport tubing. On the other hand, a correct amount of charge may enhance particle collection at the intended target and suddenly become a desirable effect, which could be the case for inhalation-powders.

Until now, inhalable medicines have mainly been used for treating respiratory diseases such as asthma. In the future, they will be used for systemic drug delivery as well. Pulmonary drug delivery has several advantages over other drug administration forms. It offers faster onset of action and the same treatment is achieved with smaller drug doses compared to other methods, and thus with less side effects (Karner & Urbanetz, 2011). In order to use inhalers as routine treatment devices several requirements must be met, which all need experimental verification. Firstly, the inhaler must release the prescribed dose from shot to shot in a repeatable manner. Secondly, the drug aerosolization process should be insensitive to the breathing capability of the patient. Thirdly, the aerodynamic particle size of the drug particles must be between 0.5 and 5 μm in order to be deposited to the alveolar region, where the systemic absorption is most effective (Labiris & Dolovich, 2003; Telko et al., 2007; Karner & Urbanetz, 2011). In this size range the particle deposition in the lungs occur by diffusion, interception and inertial impaction, but in some cases the dominant deposition mechanism has been found to be electrostatic deposition (Balachandran et al., 1997; Kulon & Balachandran, 2001). This is due to the fact that the applied particle generators, such as dry powder inhalers and nebulizers, produce bipolarly charged aerosols (Balachandran et al., 1997). The previously mentioned studies suggest that the deposition of the drug aerosol in the lung depends on the charge of the individual particles, not on the net charge. The drug delivery could be further improved by utilizing the electric charge of the individual particles (Murtomaa et al., 2004; Hashish & Bailey, 1991; Fleming et al., 1997). Consequently, it would be highly beneficial to be able to tailor the charge of the individual particles coming out of different types of inhalers to an appropriate level. To accomplish this, reliable measurement techniques capable of measuring size and charge distributions of the drug aerosol particles are needed.

Recently, electrical measurement techniques and their applicability for the measurement of the drug aerosols have been thoroughly evaluated by Hoe et al. (2011). There are several important requirements for a charge measurement device targeted for inhaler measurements. One of these requirements is the measurement of aerodynamic particle size at least with some size resolution between 0.5 and 5 μm. Faraday cup aerosol electrometers applied for example by Kulvanich and Stewart (1987) and also Murtomaa & Laine (2000) fails to meet this requirement. This is also true for the Bipolar Charge Measurement System (BCMS, Balachandran et al., 2003), which has the benefit of being able to measure the bipolar electrical mobility distributions of drug aerosols. The second requirement is that the device should independently and simultaneously measure positively and negatively charged particles, since inhalers tend to produce bipolarly charged aerosols. This requirement rules out the widely applied ELPI (Kwok & Chan, 2008; Adi et al., 2010) and the relatively new Electrical Next Generation Impactor introduced by Hoe et al. (2009). Both of these impactors measure the net charge of the particles as a function of the particle size and allow further analysis of the collected samples, which is a desirable feature in pharmaceutical industry. At least two devices meet all the above requirements. These are the modified Phase Doppler Particle Analyzer (PDPA, Beleca et al., 2009) and the Electrical Single Particle Aerodynamic Relaxation Time analyzer (E-SPART, Mazumder et al., 1991) applied to inhaler measurements by e.g. Saini et al. (2007). These devices measure both the charge (positive and negative) and the size of the particles and thus provide valuable information about drug aerosols. Unfortunately, neither of the devices can be directly connected to the output of an inhaler. This is because the operation of the devices is based on a single particle analysis, which requires small input particle number concentration and small inlet flow rate ($\sim$1 L/min), while the flow rates drawn from inhalers typically range from 30 up to 90 L/min. The last requirement is that the device should analyze the whole aerosol sample coming out from an inhaler and allow, for example, chemical, size classified analysis of the collected samples. To summarize, no instrument that would offer a complete solution to the charge measurement needs of the pharmaceutical industry exists.

In this paper we introduce the first commercially available instrument, which is specifically designed to meet as many of the requirements discussed in the previous paragraph as possible. The device is manufactured by Dekati Ltd. (Finland) and designed in close co-operation with GlaxoSmithKline (United Kingdom), Aerosol physics laboratory of Tampere University of Technology and Finnish Meteorological Institute. Starting from the operation concept and calibration of the device, a thorough description of the instrument is presented. We further demonstrate how this new instrument, called the Bipolar Charge Analyzer (BOLAR) can be applied to testing of the performance of various inhalers and present the first bipolar, size classified Dry Powder Inhaler (DPI) test results, including charge-to-mass ratios of the particles as a function of the particle size. Finally, the results of the BOLAR instrument in Dry Powder Inhaler (DPI) measurements are compared to results of other instruments in terms of net charge of the particles.

2. Concept and device

2.1. Concept of operation

The fundamental problem related to inhaler studies with the existing aerosol instruments is that they cannot provide both bipolar charge and size information. For example, the electrical low pressure impactor (ELPI) can provide the size and net charge information, but it does not provide the bipolar charge information. On the other hand, an electrostatic precipitator (ESP) can provide the bipolar charge information but no information on the size of the particles. Let us consider what would happen if we place an impactor in front of an ideally operating ESP and a particulate filter just after it.

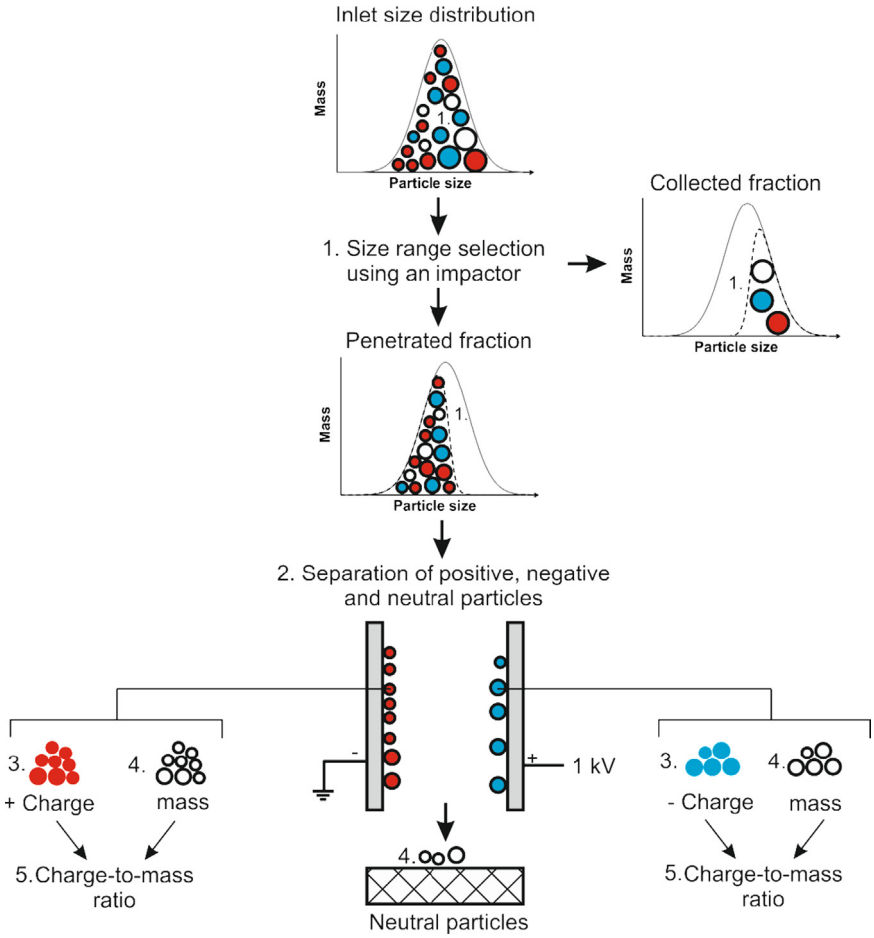

Fig. 1. Illustration of the measurement concept of the Bipolar Charge Analyzer. The instrument uses an impactor, an electrostatic precipitator and a particulate filter in series, which enables the determination of the bipolar charge and charge-to-mass ratios for an unknown inlet aerosol.

The operation of such a measurement setup, later on called the Bipolar Electrical Collection Unit (BECU), is illustrated in the Fig. 1. Let us use the setup for measuring an unknown input aerosol and perform the following steps (denoted using corresponding number in Fig. 1) in the numbered order.

1. size range selection using an impactor,
2. separation and collection of positive, negative and neutral particles,
3. charge measurement of positive and negative particles,
4. mass measurement of positive, negative and neutral particles,
5. calculation of the charge-to-mass ratios.

With this setup and process steps, we end up determining the bipolar charge and charge-to-mass ratios of the input aerosol for a size range that begins from the lower size end of the input distribution and ends at the cut diameter of the impactor. By changing the cut point, the bipolar charge and charge-to-mass ratios can be determined for any given fraction of the inlet size distribution. If we conduct another measurement with an impactor that has a larger cut point and subtract the corresponding charge and mass results from the previously obtained values, the result is the bipolar charge and charge-to-mass ratios for particles having size between the cut points of the impactors. So, having multiple BECUs with different cut points in parallel, allows the determination of the bipolar charge size distribution and charge-to-mass ratios for both polarities as a function of the particle size. This is the operation concept of the BOLAR.

In the BOLAR instrument there are 5 bipolar electrical collection units and an additional sampling port in parallel configuration (6 in total). All the collection units have different cut points in their pre-separator impactor, but otherwise the units are identical. Thus, the particles collected and analyzed by the bipolar collection tubes derive from different particle size range and represent one-sixth of the aerosol that enters into the BOLAR.

Let n denote the number of the collection unit and $n=1$ correspond to the unit having the smallest cut point in the pre-separator impactor. Let $D_{50,n}$ be the cut point of the corresponding collection unit. By combining the measurement results

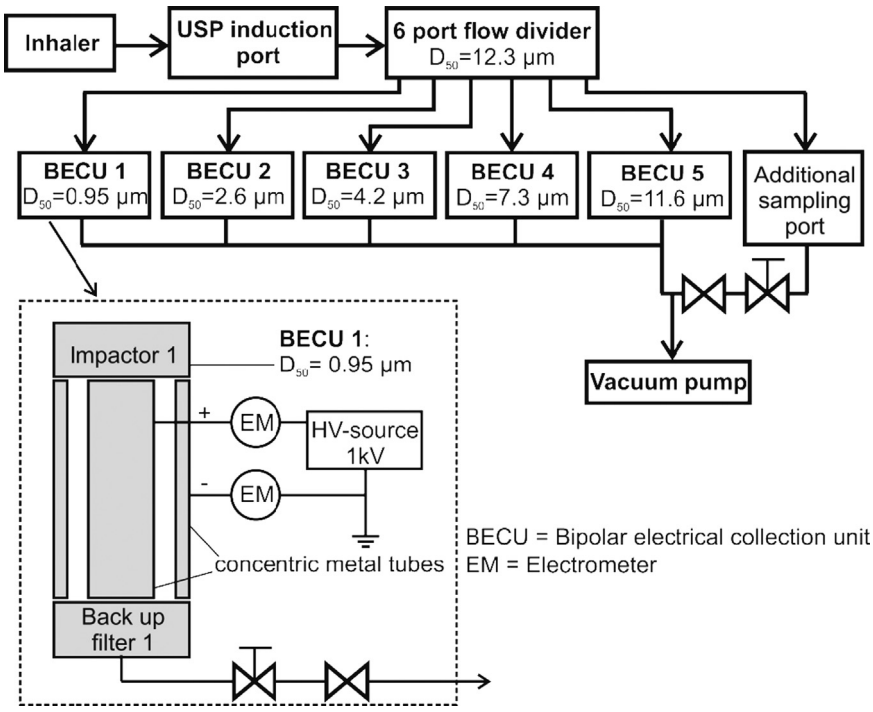

Fig. 2. Operation diagram of the Bipolar Charge Analyzer (BOLAR). The main components of the instrument are the five parallel bipolar electrical collection units, which are denoted as *BECUs*. The *BECUs* are otherwise identical, but the cut points of the impactors, and thus the analyzed particle size ranges, are different.

from two successive collection units the measurement size range of the instrument can be divided into five size fractions according to the following equation:

$$\Delta D_n = \begin{cases} 0 < D_{p,a} < D_{50,n} & \text{for } n = 1 \\ D_{50,n-1} < D_{p,a} < D_{50,n} & \text{for } n = 2, \ldots, 5 \end{cases}, \tag{1}$$

where $D_{p,a}$ is the aerodynamic particle size. For each of the size ranges, there are three important quantities to be calculated: Charge-to-mass ratios for the positively and the negatively charged particles and the charge-to-mass ratio calculated from the net charge of the particles. For a single collection unit, the ratios present the average values for particles that are smaller than the cut point of the pre-separator impactor. Charge-to-mass ratios (Q/m) for positive and negative particles are obtained using Eq. (2)

$$\frac{Q}{m}(\Delta D_n, i) = \begin{cases} \frac{Q_{n,i}}{m_{n,i}^{electrode}} & \text{for } n = 1 \\ \frac{Q_{n,i} - Q_{n-1,i}}{m_{n,i}^{electrode} - m_{n-1,i}^{electrode}} & \text{for } n = 2, \ldots, 5 \end{cases}, \tag{2}$$

where i is the polarity of the particles, i.e. *positive* or *negative*, $Q_{n,i}$ and $m_{n,i}$ are the charge and mass determined from the respective collection electrode of the collection unit n for particles having the selected polarity i. The particles collected by the other electrode and by the backup filter are not taken into account in this calculation. However, they are taken into account while the charge-to-mass ratio is calculated based on the net charge of the particles according to Eq. (4). By denoting

$$m_n = m_{n,positive}^{electrode} + m_{n,negative}^{electrode} + m_n^{backup\ filter}, \tag{3}$$

the expression for the charge-to-mass ratio calculated from the net charge information for a certain size range reduces to

$$\frac{Q}{m}(\Delta D_n) = \begin{cases} \frac{Q_{n,positive} + Q_{n,negative}}{m_n} & \text{for } n = 1 \\ \frac{(Q_{n,positive} + Q_{n,negative}) - (Q_{n-1,positive} + Q_{n-1,negative})}{m_n - m_{n-1}} & \text{for } n = 2, \ldots, 5 \end{cases}. \tag{4}$$

As a result of Eqs. (2) and (4) the charge-to-mass ratios of the input aerosol can be presented as a function of the aerodynamic particle size.

2.2. Instrument

The main components of the instrument (see Fig. 2) are a 6 port flow divider, 5 bipolar electrical collection units, an additional sampling port for size distribution or mass analysis, and a vacuum pump. By starting the vacuum pump and opening the solenoid valves located between the vacuum pump and the collection units, the drug is aerosolized inside an inhaler and is delivered through a United States Pharmacopeia induction port (USP induction port) into the flow divider at a nominal flow rate of 60 L/min. The largest particles are collected by the impactor located inside the flow divider. Ideally, the flow divider divides the aerosol evenly between 6 outlet branches. From 5 of the outlet ports the aerosol is delivered to sampling port specific electrical collection units and the remaining outlet port is reserved for additional measurements (e.g. filter based mass analysis). The flow rates of the outlet ports are tuned using adjustable valves acting as critical flow orifices (CFOs) which are followed by the solenoid valves and the vacuum pump. The instrument can be used as a standalone instrument or via a computer interface. As described in the previous Section, the 5 electrical collection units are the most important components relative to the operation of the BOLAR.

Each of the electrical collection units consist of a pre-separator impactor, an annular slit type electrostatic precipitator named as a bipolar electrical collection tube and a backup filter, which are all electrically insulated from each other and from other system components (e.g. from the flow divider). The pre-separator impactor passes through particles that are smaller than the cut point, which then enter the bipolar electrical collection tube. In the collection tube a 1 kV voltage difference is applied between the inner and outer collection electrodes. Ideally, all positively and negatively charged particles are collected onto different electrodes and measured separately using electrometers. The collection tube is followed by a backup filter, which collects the rest of the particles. In actual inhaler test measurements the electric current signals from the collection electrodes are integrated over a time interval, which is enough for the entire aerosol from a single inhaler shot to pass through the tubes and for electrometer signals to go back to zero level. As a result, both the positive and the negative charge carried by the particles in a size range defined by the pre-separator impactor are obtained. The BOLAR instrument is designed so that the particles collected by each of the components, such as the flow divider, pre-separator impactors, electrical collection tubes and backup filters can be extracted separately for further analysis, e.g. chemical or mass analysis. Thus, by analyzing the mass of the particles collected by the collection electrodes, charge-to-mass ratios for both positively charged and for negatively charged particles can be calculated.

2.3. Instrument design

The design of a new instrument, such as the BOLAR, is in most cases a compromise between many affecting properties, such as performance, usability, size and weight of the instrument. In this section, the design parameters of the main components of the BOLAR instrument which are essential for the operation of the instrument are described. The main components of the instrument are the 6 port flow divider (preceded by the USP induction port) and the 5 bipolar electrical collection units, which all consist of a pre-separator impactor, a bipolar electrical collection tube and a backup filter.

2.3.1. Flow divider and impactors

In the flow direction, the first component after the USP induction port is the 6 port flow divider. The flow divider has two main functions, namely to remove the largest particles (aerodynamic diameter $> 12.3\ \mu m$) from the aerosol before it enters the collection units using a pre-separator impactor, and to divide the remaining aerosol evenly between the 6 outlet branches. The pre-separator impactor and all the other impactor stages which are installed in the collection units were designed to meet two very important requirements. The stages were designed to have minimal particle bounce from the collection substrate, which is particularly important while collecting solid particles (May, 1945; Dzubay et al., 1976; John, 1995). In addition, the stages were designed to allow the collection of relatively large amount of particles (mass) onto the substrate without causing any significant changes to the cut points. The particle bounce is minimized using three different techniques. Firstly, the nozzle velocities (and Reynolds numbers) were designed to be small. At a certain aerodynamic particle size the velocities are about half of the corresponding values of the electrical low pressure impactor (ELPI; Keskinen et al., 1992). Secondly, the collection substrates are coated with liquid, typically either polyethylene glycol or silicon oil.

Table 1
The specifications of the impactor stages. Nominal flow rates of the stages are 10 L/min except for the pre-separator impactor. Cut points are experimentally determined values.

Stage	Nozzle diameter (mm)	Number of nozzles	Velocity (m/s)	Cut point (μm)	Reynolds number	Jet-to-plate distance (mm)	Nozzle throat length (mm)
1	0.45	70	15.0	0.95	441	1.3	1.3
2	1.3	24	5.2	2.60	446	3	3.5
3	2	16	3.3	4.17	434	4	5.4
4	3.45	10	1.8	7.29	403	6.9	6.9
5	5.55	6	1.1	11.6	417	11.1	11.1
Pre-separator	25	1	2.0	12.3	3300	40	75

Table 2
Specifications of the collection tubes. E_{50} corresponds to a particle size having n elementary charges and is collected at 50% efficiency.

Flow rate	10	L/min
r_1	0.0575	m
r_2	0.0605	m
L	0.2	m
E_{50} (1 elementary charge)	0.261	μm
E_{50} (74 elementary charges)	11.6	μm
Voltage	1000	V
Reynolds number	30	
Flow velocity	0.15	m/s

Thirdly, collection units from 1 to 4 use more than one impactor stages in cascade as follows. Unit 1 uses impactor stages 1, 2, and 4, unit two uses stages 2, 3 and 4, unit three uses 3, 4 and 5, unit four uses stages 4 and 5, and unit five uses stage 5 (see Table 1 for cut points). Using impactor stages with descending cut points in cascade configuration minimizes the particle size range collected by the individual stages and in this way reduces the probability of particle bounce. In order to make sure that the impactor stages can collect relatively large amount of particles, jet-to-plate distances were selected to be between 2 and 3 times larger than the corresponding nozzle diameters (Marple & Liu, 1974).

In the design process, the cut points were first estimated based on the results of Flagan (1982), Biswas & Flagan (1984), and Hering (1987), which are summarized by Hillamo & Kauppinen (1991). In the design, 0.208 was used as a Stokes number for all the impactor stages. As the BOLAR is intended to be used for Dry Powder Inhaler (DPI) and Metered Dose Inhaler (MDI) studies the nominal cut points of the pre-separator impactor and other impactor stages were designed to be comparable with the inlet and the impactor stages of the Next Generation Impactor at 60 L/min flow rate (NGI; Marple et al., 2003). Table 1 presents the properties of all the impactors of the BOLAR. Definition of the parameters presented in Table 1 can be found, for example, from Marple & Liu (1974).

2.3.2. *Electrical collection tubes*

A single electrical collection unit consists of two concentric tubes, which have a voltage difference between them. Aerosol flows through the space between the tubes and the particles that carry net electrical charge (either positive or negative) are collected onto the inner and outer tubes due to electric field. In terms of the size and the performance of the BOLAR instrument, the bipolar electrical collection tubes are the most crucial components. Ideally, the collection tubes would collect all the charged particles, even those that have only 1 elementary charge, up to 11.6 μm which is the cut point of the impactor on top of the tube 5. By modifying the existing instrument design, which easily fits to a 1 by 1 by 1 m box, this would require nearly 30 m long collection tubes. That is if only the lengths of the tubes were changed. Obviously, collection tubes of this length are not practical and compromises between the performance and the overall size of the instrument had to be made. The specifications of the electrical collection tubes are presented in Table 2.

The lengths of the electrical collection tubes (L) are equal. The difference between the outer radius of the inner tube (r_1) and the inner radius of the outer tube (r_2) is 3 mm and the voltage difference is 1 kV. The distance between the tubes was kept small in order to maximize the collection efficiency. For the particles that have one elementary charge, the particle size having 50% collection efficiency (E_{50}) is 0.261 μm. As an example, for 11.6 μm particles the required number of elementary charges corresponding to E_{50} and E_{100} values are 74 and 150. In comparison, the average charge of the 11.6 μm particles produced by the ELPI unipolar diffusion charger is more than 7 times larger (1100) and the Rayleigh limit is about five orders of magnitude larger. The important question related to the BOLAR is whether the collection efficiencies of the collection units are sufficient for the inhaler measurements as the 100% collection of the largest particles requires 150 elementary charges. According to Balachandran et al. (1997), the effect of the image charge deposition of the particles inside the human respiratory track can be seen when the particles have 200 or more elementary charges (2.2 μm particles). In this respect, the BOLAR is sensitive enough to be used in inhaler studies. In addition, it should be kept in mind that all of the electrical collection units are followed by the backup filters, which collect the rest of the particles.

3. Calibration

3.1. *Experimental*

The penetration efficiency of the flow divider at 30, 60 and 90 L/min flow rates and the collection efficiencies of the impactors and the bipolar electrical collection tubes at 10 L/min were measured using liquid monodisperse di-octyl sebacate (DOS; 97% purity, density=0.914 g/cm^3) particles. The particles were generated either with a modified Vibrating Orifice Aerosol Generator (VOAG, original instrument presented by Berglund and Liu, 1973) or with the Singly Charged Aerosol Reference (SCAR, Yli-Ojanperä et al., 2010). The penetration efficiency of the flow divider and the collection efficiencies of the impactor stages from 2 to 5 were measured using the VOAG as an aerosol generator. Collection efficiencies of the bipolar electrical collection tubes and the impactor 1 were measured using the SCAR as an aerosol generator. In all of the experiments, the pressure and the temperature at the inlet of the calibrated component were close to 1013 mbar and 22 °C.

The instrument response was measured as electric current signals using electrometers. Therefore, for each of the particle sizes, the measurement routine consisted of one measurement period with particle flow in the system preceded and followed by a particle free electrometer zero level measurement. The actual average signal currents were calculated by subtracting the average value of the zero level current signals from the average signal that was obtained with particle flow inside the system.

The modified VOAG was based on model Model 3050 (TSI Inc.). Modifications included a high pressure syringe pump (Nexus 6000, Chemyx Inc.), a new 20 μm orifice (Lenox Laser Corp.), a signal generator and a pulse counter. The solutions were prepared by dissolving a known volume of DOS in chromatography grade 2-propanol with reported evaporation residue (VWR International LLC). The initially highly positively charged droplets generated by the VOAG were charge conditioned either with a unipolar diffusion charger of the ELPI or with an induction ring (Reischl et al., 1977). After the charge conditioning, the droplets were brought to a dilution chamber where the aerosol was diluted at flow rates ranging from 20 to 100 L/min. As a result, the 2-propanol evaporated from the particles. The resulting aerosol was then introduced into the device under calibration (i.e. the flow divider or an impactor) either directly or through a high efficiency particle filter, which provided particle free air flow for the zero level measurements. An Aerodynamic Particle Sizer (APS 3321, TSI Inc.) was used in parallel with the instrument being calibrated to monitor that the VOAG was working properly and that the aerosol was monodisperse. The particle size was calculated according to Berglund & Liu (1973) including the non-volatile impurity concentration. The obtained physical diameter was converted to aerodynamic diameter by applying the bulk density of DOS (0.914 g/cm^3).

The SCAR is a rather new instrument that uses a novel concept presented by Uin et al. (2009) for the generation of singly charged, monodisperse particles in a wide particle size range. In the SCAR 10–12 nm NaCl seed particles are first generated using a tube furnace. The aerosol is neutralized using a ^{85}Kr-neutralizer (3077A, TSI Inc.) and classified using a Differential Mobility Analyzer (DMA; Model 3085, TSI Inc.). The resulting monodisperse and singly charged particles are grown by condensing DOS vapor onto the particles, without changing the charge of the particles. As a result, singly charged, much larger particles are generated. The particle size can be controlled by changing temperature settings of the instrument. In the experiments conducted using the SCAR, the particle free air for the instruments was produced by setting the DMA voltage to zero. The particle size distribution was measured using a Differential Mobility Particle Sizer (DMPS) consisting of a DMA 3071 (TSI Inc.) and of a CPC 3025A. The mode of the particle size distribution was used as the particle size of the calibration.

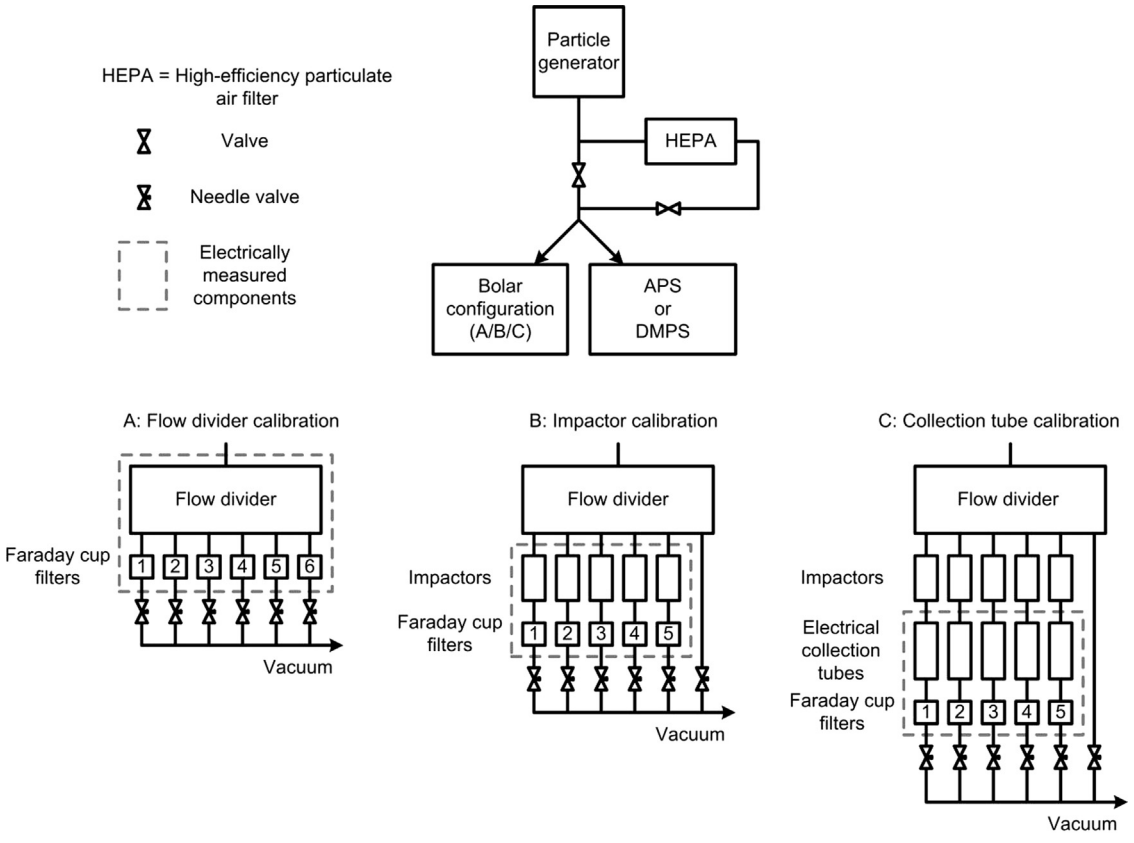

Fig. 3. Calibration setups used in the calibration of the BOLAR instrument. Particle generator was either the VOAG or the Singly Charged Aerosol Reference. Both generators produced unipolarly charged particles. Different configurations of the BOLAR are denoted as A, B and C.

The DMA was operated at 0.25 sample and 1 l/min sheath flow rates and it was calibrated using 0.496 μm poly styrene lattice particles (PSL). The obtained electrical mobility diameter was converted to aerodynamic diameter using the density of DOS (0.914 g/cm^3).

In the experiments, the BOLAR was used in three different configurations, which are shown as A, B and C in Fig. 3 as part of the calibration setups.

In the flow divider penetration efficiency measurements conducted using the VOAG (configuration A) the bipolar electrical collection units were replaced with six Faraday cup aerosol electrometers and also the electrically insulated flow divider was connected to an electrometer. All of the electric current measurements were conducted using ELPI electrometers and software. The flow rate of each of the flow divider outlets and corresponding filters were controlled by needle valves and in turn set to 5, 10 or 15 L/min, corresponding to an inlet flow rate of 30, 60 or 90 L/min respectively. The flow measurements were performed at the inlet conditions using a laminar flow element (FCO332-2W, Furness Control Ltd). The collection efficiency of the flow divider, $E_{divider}$, is calculated using the following equation

$$E_{divider} = \frac{I_{divider}}{\sum_{n=1}^{6} I_{FCn} + I_{divider}}, \tag{5}$$

where $I_{divider}$ is the electric current measured from the flow divider and I_{FCn} is the electric current from the corresponding Faraday cup aerosol electrometer. The cut point of the flow divider and also the cut points of the impactor stages were defined by fitting *s*-curves to the measurement points according to Winklmayr et al. (1990) and Dzubay and Hasan (1990)

$$E = \left(1 + \left(\frac{D_{50}}{D_{p,a}}\right)^{2s}\right)^{-1}, \tag{6}$$

where $D_{p,a}$ is the aerodynamic particle diameter, D_{50} is the aerodynamic cut point and s describes the steepness of the collection efficiency curve. Finally, the penetration efficiency, $P_{divider}$, was calculated as

$$P_{divider} = 1 - E_{divider}. \tag{7}$$

Collection efficiencies of the impactor stages and the bipolar electrical collection tubes were measured in separate experiments using configurations B and C presented in Fig. 2. The main difference compared to the configuration A is that in this case, the generated aerosol was guided to one impactor stage or to one bipolar electrical collection tube at a time (flow rate = 10 L/min), which was then calibrated completely before guiding the aerosol to another impactor or collection unit. This was performed in order to maximize the electrical current signals during the calibrations. In impactor calibrations, the BOLAR was modified so that all the impactors were immediately followed by a Faraday cup aerosol electrometer (FCAE). The electric current signals were measured using the internal electrometers of the BOLAR. The collection efficiency of the stage n, E_n, was calculated using equation

$$E_n = \frac{I_n}{I_n + I_{n,FCAE}}, \tag{8}$$

where I_n is the electric current from the impactor stage n and $I_{n,FCAE}$ is the current from the corresponding FCAE. The cut points were evaluated similarly to the flow divider cut point.

The collection efficiencies of the electrical collection tubes were calibrated using singly charged particles generated with the SCAR. In theory, inner and outer electrodes should have equal particle collection characteristics. Therefore, it was decided that it is sufficient to calibrate all the five outer electrodes and one inner electrode. In the experiments, plus or minus 1 kV voltage difference was applied between the electrodes. The impactors located before the tubes were grounded and the backup filters of the BOLAR were modified so that they could be used as FCAEs during the experiments. The electric current signals produced by the collected unipolarly charged particles were measured from the inner and the outer electrode and from the backup filters of the BOLAR instrument with ELPI electrometers. The collection efficiency for a certain particle size was calculated as a ratio of the electric current measured by the collection tube and the total current entering into the tube (FCAE + collection tube).

3.2. Results

3.2.1. Flow divider

The penetration of the particles through the flow divider is presented in Fig. 4 as a function of the aerodynamic particle size for 30, 60 and 90 L/min flow rates. The lines present the *s*-curves that were fitted to the measured penetration efficiency values.

At the lower size end of the measurement range, the penetration efficiencies is nearly 100% at all tested flow rates. At the nominal flow rate of 60 L/min, the cut point of the flow divider is 12.3 μm and at the highest flow rate it is 10.3 μm. Aerodynamic cut diameters (D_{50}) and curve steepness values (s) are presented in Table 3.

At all three flow rates, the steepness of the collection efficiency curves are rather small, compared to the steepness values of the impactor stages which will be presented later on. In addition to removing the largest particles from the aerosol, the flow divider should transport the remaining particles evenly between all of the outlet ports. This was studied at the same

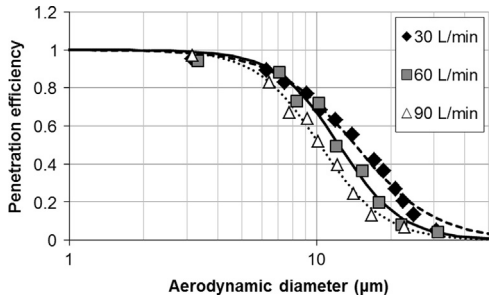

Fig. 4. Penetration efficiency of the flow divider at three different flow rates.

Table 3
Cut diameters D_{50} and curve steepness values s for the flow divider for different flow rates.

	30 L/min	60 L/min	90 L/min
D_{50} (μm)	14.3	12.3	10.3
s	1.33	1.72	1.69

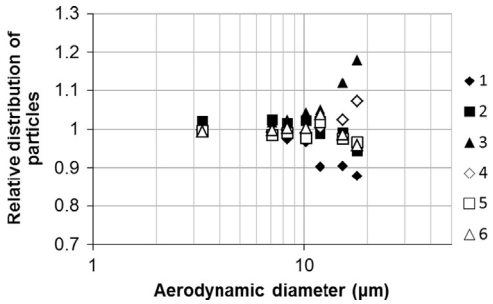

Fig. 5. Deviations of the signals of the individual outlet ports from the six port average signal value at the nominal flow rate of 60 L/min.

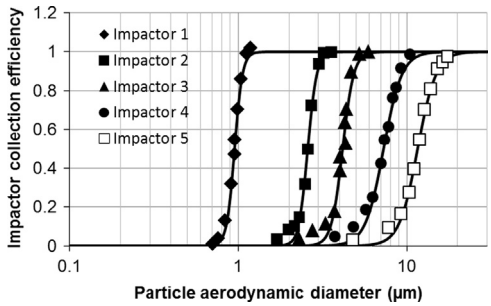

Fig. 6. Collection efficiencies of the impactor stages at 10 L/min flow rate. The solid lines present the s-curves that were fitted to the experimental values.

time with the flow divider penetration experiments by comparing the electric currents measured from the Faraday-cup filters which were connected to the outlet ports. The relative deviations of the signals of the individual outlet ports from the six port average signal values at the nominal flow rate are shown in Fig. 5.

In general, the deviations from the average values are increasing towards larger particle sizes and remain mainly below 5% up to the cut point of the flow divider. This indicates that the symmetry is very good in the whole operating particle size range of the BOLAR. The reason why the deviations appear to increase towards larger particle sizes could partly be in the flow divider design itself. However, the main reason for the increase is simply that the electric signal currents measured from the FCAEs decrease substantially as the particle size increases. In other words, the amount of particles penetrating the divider is decreasing because of the collection efficiency of the divider resulting in smaller electric currents and to lower signal to noise ratios. Thus, the measurement at very small signal levels represents the worst case of the flow divider performance for corresponding particle sizes. For the flow rates of 30 L/min and 90 L/min the relative difference in the outlet port signals is about the same as for the nominal flow rate.

Table 4
Cut diameters D_{50} and curve steepness values s for the impactor stages at 10 L/min flow rate.

Impactor	Experimental cut point D_{50} (μm)	Steepness s
1	0.95	9.39
2	2.60	8.22
3	4.17	6.64
4	7.29	4.06
5	11.57	4.02

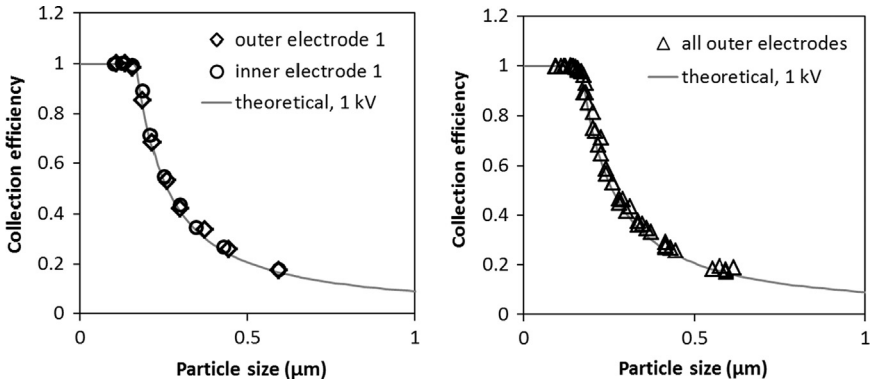

Fig. 7. Singly charged particle collection efficiency of the outer and the inner electrode of the unit 1 (left) and for all the outer electrodes (right). Theoretical values are presented as a solid line.

3.2.2. Impactors

The impactor calibration results are presented in Fig. 6. In the figure *s*-curves are fitted through the measurement points. The aerodynamic cut diameters were defined by a linear fit through the experimental efficiency values close to 0.5. The cut diameters and steepness values are presented in Table 4.

Based on Fig. 6, the collection efficiency curves are much steeper than the efficiency curve of the flow divider. In addition, the steepness values are close to the values reported for the ELPI (Marjamäki et al., 2005).

3.2.3. Electrical collection units

Calibration results for the electrical collection units for singly charged particles are shown in Fig. 7. The left figure presents the results for both of the collection electrodes of the BECU1. The right hand figure presents the results for all the outer collection electrodes of the units from 1 to 5. The theoretical efficiency values are calculated assuming a constant velocity over the space between the electrodes and by using the parameters that were presented in Table 2. Based on the results, outer and inner electrodes have similar collection efficiencies. This applies to all the outer electrodes as well. In addition, all of the experimental results agree well with the theoretical values presented for singly charged particles in Table 5. In practise, this means that the operation of the collection units meet the design criteria presented in Section 2.3.

4. Test measurements with a DPI inhaler

4.1. Experimental

As the first practical application, the BOLAR was used to determine the bipolar charge size distribution and charge-to-mass ratios for an aerosol produced by one DPI loaded with lactose particles. The inhaler was connected to the BOLAR using a standard USP inlet. The additional sampling port of the flow divider was equipped with a modified ELPI, which had the same impactor cut points as the pre-separator impactors of the BECUs of the BOLAR and a backup filter. This allows a direct comparison of the measured net charge size distributions and mass size distributions. Before the measurements, the flow rates of the BECUs and that of the modified ELPI (i.e. reference impactor) were adjusted to 10 L/min (total flow rate 60 L/min). All experiments were conducted at normal laboratory conditions ($T \approx 23$ °C, $P \approx 1$ atm, $RH \approx 50\%$).

The measurement routine was the following. At the beginning, there was no flow through the BOLAR instruments, i.e. the solenoid valves between the BECUs and the vacuum pump were closed. At this stage, the inhaler was loaded. By pressing a single button, the following actions took place. The valves were opened and consequently the flows were turned on. The inhaler was actuated and the electrical signals from the BECUs and from the modified ELPI were recorded for as long as it took for them to go back to the values that correspond to their zero levels. The whole measurement routine took approximately 60 s and during this time the electrometer offset levels were measured before and after the inhaler was

Table 5
Experimentally determined particle diameters corresponding to 50% collection efficiency for singly charged particles. Theoretical value for the 50% collection efficiency is 0.261 μm.

Tube	Particles collected to electrode	E_{50} (μm)
1	Outer	0.271
1	Inner	0.271
2	Outer	0.270
3	Outer	0.279
4	Outer	0.276
5	Outer	0.272

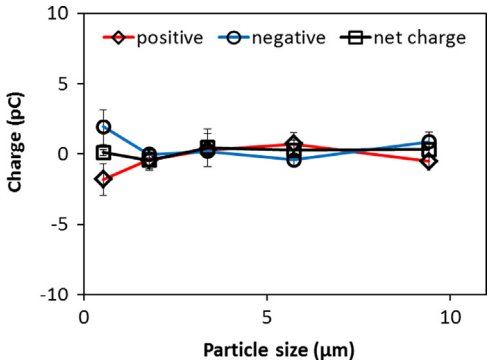

Fig. 8. Bipolar charge size distribution for an empty inhaler, i.e. for zero input. The results indicate that when the charge levels in the order of 10 pC and larger can be measured with reasonable accuracy.

actuated. The electric current signals were integrated over the measurement period to obtain the amount of electric charge collected by the electrodes of the bipolar electrical collection units. The above routine was repeated six times in order to ensure the statistical confidence for the average charge values calculated from the six repetitions and to make sure that the particle mass collected onto electrodes of BECUs was large enough to be analyzed. After the six repetitions the instrument was carefully dismantled and the particle mass collected by the impactors, the electrodes of the collection units, and by the backup filters was removed by washing down with de-ionized water. This was also conducted for the stages of the modified ELPI. The mass of the samples were determined using High Performance Liquid Chromatography (HPLC). Based on the above results, the charge size distribution and the charge-to-mass ratios were calculated according to equations presented in Section 2.1. Based on the preliminary tests conducted before the actual experiments, more than 20 DPI actuations (12 mg each) can be measured without any significant changes in the electrical measurement signals and in the performance of the device in general.

4.2. Results

Before the BOLAR was applied for measuring the bipolar charge size distribution from a DPI loaded with lactose, its operation was tested in an actual measurement configuration using an empty inhaler. The purpose of this experiment was to evaluate the lower detection limit of the charge measurement and to make sure that with zero input the results are zero as well. In electrical measurements, especially if flows are turned on and off during the measurement cycle this may not be the case. Figure 8 presents the average results of three repetitions and associated standard deviations for the bipolar collection tubes.

The results indicate that charge levels in the order of 10 pC and larger can be measured with reasonable accuracy. The results are very close to zero as they should be. The raw electric current signals of the collection tubes in one actuation of an inhaler are shown in Fig. 9. After a couple of seconds, the aerosol reaches the collection tubes which are seen as a rapid increase in the signal values. This is followed by somewhat slower decrease of the signals towards the zero. Both the rise and the decrease of the signals occur within 20 s. The largest positive and negative signal peaks correspond to the electric current signals of the negative and the positive electrode of the collection unit 5 and the smallest peaks correspond to the unit 1. In the example of the Fig. 9 all signal values were between 10 and 60 pA. As described in the previous section, the total charge of the collected particles is then obtained by integrating the electric current signals over the measurement period. This is conducted for each actuation of the inhaler and after the measurements, average values of the charge are calculated for each tube.

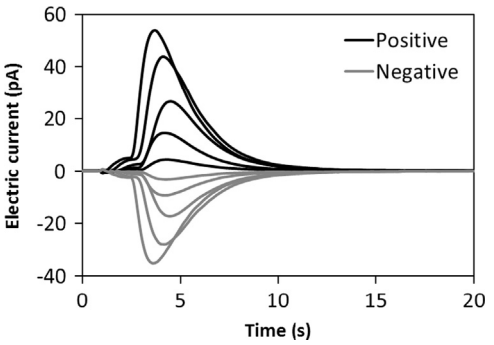

Fig. 9. Raw electrical current signals of the collection tubes from a single actuation of a dry powder inhaler (DPI). The largest positive and negative signal peaks correspond to current signals of the negative and positive electrode of the collection unit 5 and the smallest peaks correspond to unit 1.

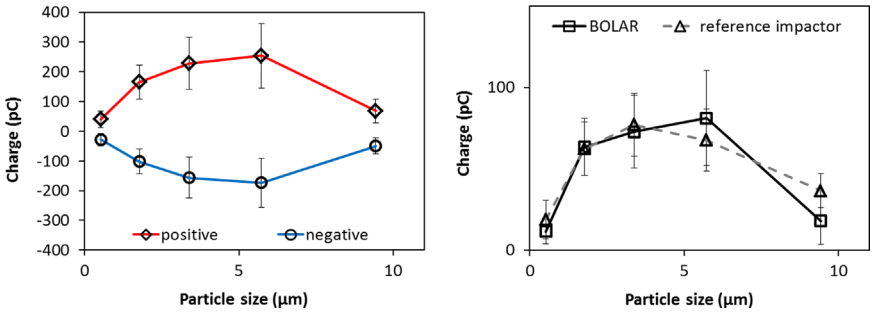

Fig. 10. Average charge size distribution and the associated standard deviation calculated from six consecutive actuation of a DPI loaded with lactose (left). Comparison of the average net charge size distributions obtained using the BOLAR instrument and the reference impactor having the same cut points as the BOLAR.

At this point, it is important to clarify that all of the results calculated from the measurements conducted using the BOLAR are to represent the results of a single inhaler actuation. In practice, this means that all the charge and mass measurement results are multiplied by the number of sampling ports (6) in the flow divider. In addition, the results from the mass analysis are divided by the number of repetitions (N), i.e. number of inhaler actuations, in the measurements.

The charge of the particles in each size range and for both polarities is calculated using the following equation:

$$Q(\Delta D_n, i) = \begin{cases} 6Q_{1,i} & \text{for } n = 1 \\ 6(Q_{n,i} - Q_{n-1,i}) & \text{for } n = 2, \ldots, 5 \end{cases}, \tag{9}$$

where $Q_{n,i}$ is the average charge value in N repetitions; n is the number of the collection unit and i is the polarity of the particles (i.e. positive or negative). The average bipolar charge size distribution and the associated standard deviations obtained for the applied DPI using the BOLAR are shown in Fig. 10. The right hand figure shows the net charge size distribution obtained using the BOLAR and the reference impactor. Based on the results, the bipolar charge levels of the particles range from -200 pC to $+300$ pC, and are much larger than the net charge of the particles in the corresponding size ranges. The standard deviation of the results is not related to the operation of the BOLAR, instead it implies that the operation of the DPI varies from one actuation to another actuation. The net charge size distributions obtained using the BOLAR and the reference impactor are quite close to each other. However, some differences in the two measurement channels corresponding to largest particle size ranges can be seen. This could be related to small differences in the impactor cut points or flow rates.

After the charge measurements, the BOLAR instrument was dismantled and the particle masses collected by the individual parts of the instrument were determined using HPLC. The mass results representing a single inhaler actuation were calculated according to Eq. (10)

$$m(\Delta D_n, i) = \begin{cases} \frac{6m_{1,i}}{N} & \text{for } n = 1 \\ \frac{6(m_{n,i} - m_{n-1,i})}{N} & \text{for } n = 2, \ldots, 5 \end{cases}, \tag{10}$$

where i is the polarity of the particles and N is the number of repetitions in the measurements. Mass size distributions corresponding to positive, negative and net charge of the particles measured after six consecutive actuation of a DPI loaded with lactose are presented in Fig. 11. Comparison of the mass size distributions obtained using the BOLAR instrument and the reference impactor, which had the same cut points as the BOLAR impactors is shown on the right hand side.

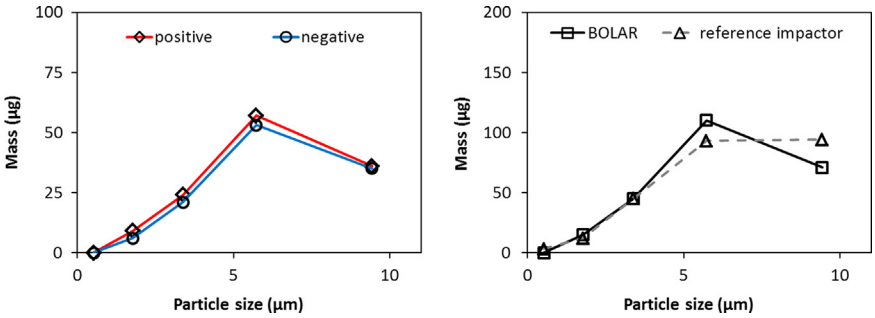

Fig. 11. Mass size distributions measured after six consecutive actuations of a DPI loaded with lactose (left). Comparison of the mass size distributions obtained using the BOLAR instrument and the reference impactor having the same cut points as the BOLAR.

Table 6
Mass collected by the impactors, outer and inner collection tubes, and back up filters during a single actuation of the DPI. The mass collected by the backup filters is very small compared to the mass collected by the other parts of the instrument.

	BECU 1	BECU 2	BECU 3	BECU 4	BECU 5	Unit
Impactor	513	467	402	339	275	µg
Outer tube	0	9	33	90	126	µg
Inner tube	0	6	27	80	115	µg
Back up filter	0	0	1	3	5	µg

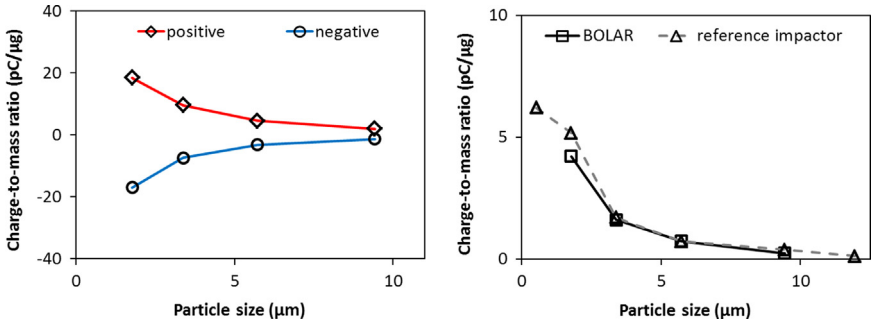

Fig. 12. Charge-to-mass ratios as a function of the particle size for the positively and negatively charged particles (left). Comparison of the charge-to-mass ratios calculated based on the net charge obtained using the BOLAR and the reference impactor (right).

The particle mass collected by the collection tubes of the BECU1 was below the lower detection limit of the applied HPLC mass analysis method and are shown as zero in Fig. 11. For the studied DPI, the mass size distributions of the positively and negatively charged particles were almost identical. The reason for the difference in the net charge measurement results obtained using the BOLAR and the reference impactor is most likely the same as in the case of Fig. 10. Besides the mass size distributions, it is both important and interesting to see how much particle mass is collected by different impactors, collection tubes and back up filters of the BOLAR. The results from the mass measurement are shown in Table 6.

The most important thing to notice from the Table 6 is that the masses collected by the backup filters are very small compared to the masses collected by the collection tubes. In the worst case, it means that a small fraction of the charged particles do not have enough charge to be collected by the collection tubes. In the best case, it means that all of the charged particles were collected and there were a few percent of neutral particles in the aerosol. Another observation is that according to the total masses calculated from the columns, the aerosol is divided quite evenly between the different BECUs.

After conducting all the above, charge-to-mass ratios for both polarities were calculated according to Eqs. (2) and (4) that were presented in Section 2.1. The charge-to-mass ratios calculated based on the bipolar and net charge of the particles are presented in Fig. 12.

According to the results, the charge-to-mass ratios were between 19 and 1 pC/µg for positively and between −17 and −1 pC/µg for negatively charged particles depending on the size of the particles. The results obtained using the BOLAR and the reference impactor were found to agree quite well at all particle sizes. By using the arithmetic mean diameter of each measurement channel as the average size of the particles and the bulk density of the lactose (1.525 g/ml) the collected particle masses were converted to number of collected particles. By dividing the charge measurement results of the Fig. 10 by the corresponding number of particles, an estimate of the number of elementary charges per particle was calculated.

Starting from the size range collected by the BECU2 and proceeding towards the largest particles (BECU5), the number of elementary charges increased from ± 500 to ± 8000. These values are very close to what one would obtain by using a unipolar diffusion charger.

The exact comparison of the results obtained for the DPI using the BOLAR to the results obtained using other instruments is very difficult. No other instrument capable of analyzing the whole aerosol population coming out from an inhaler, and being able to measure the bipolar charge size distributions and bipolar charge-to-mass ratios exists. In addition, the aerosols and charge generated by different types of inhalers and by different powders (in our case lactose only) inside the inhalers are likely to be different. Using the E-spart analyzer, Saini et al. (2007) obtained bipolar and net charge based charge-to-mass ratios of ± 2 pC/μg and 0.2 pC/μg for metered dose and dry powder inhalers (count mean diameter of the distribution were between 3 and 5 μm). Their results are somewhat smaller compared to this study, but within the same order of magnitude. Using an ELPI without the charger, Glover and Chan (2004) and Kwok et al. (2005) obtained bipolar charge values ranging from -1000 to 1300 pC for a metered dose inhaler which are about 5 times larger than the values reported in this study. Young et al. (2007) studied the influence of the humidity on the electric charge of the particles in a DPI. According to their results, the net charged based charge-to-mass ratio of the aerosol particles in the below 4.46 μm size range was between -10 and -30 pC/μg depending on the relative humidity. These results are also quite close to the results of this study.

5. Conclusions

In this study a new commercial aerosol instrument called the Bipolar Charge Analyzer (BOLAR) was introduced. The instrument combines aerodynamic size classification with electrostatic precipitator based bipolar charge measurement. As a result, bipolar charge size distributions and charge-to-mass ratios of powders and inhaled aerosols are obtained for 5 size fractions between zero and 11.6 μm. The main components of the instrument are a 6 port flow divider, 5 bipolar electrical collection units, and an additional sampling port for size distribution or mass analysis. Each of the electrical collection units consists of a pre-separator impactor (different cut points), annular slit type electrostatic precipitator and of a backup filter, which are electrically insulated from each other. Each of the components of the BOLAR was calibrated with monodisperse particles in laboratory conditions.

The performance of the instrument was tested by measuring the charge size distributions and charge-to-mass ratios produced by a dry powder inhaler (DPI) loaded with lactose particles. The DPI was found to produce noticeable levels of positively and negatively charged particles. For a single size fraction the largest observed positive and negative values were $+300$ pC and -200 pC, while the net charge was close to zero. For charge-to-mass ratios, the largest value was approximately ± 20 pC/μg which was obtained for particles having a mean diameter of 1.8 μm. The number of elementary charges per particle varied between ± 500 and ± 8000 depending on the particle size. In conclusion, the BOLAR can be applied successfully for the measurement of the bipolar charge size distributions and charge-to-mass ratios from inhalers. Compared to other instruments the results were found to be in the same order of magnitude. Although the operation of the BOLAR was demonstrated using inhaler test measurements, the instrument can be applied to the bipolar charge size distribution and charge-to-mass ratio measurements in other application areas as well.

Acknowledgment

The authors dedicate this work to Dr. Patricia K.P. Burnell from GlaxoSmithKline, who sadly passed away in the autumn of 2009. Pat was the inspiration and driving force behind developing the BOLAR instrument.

The development of the instrument involved several people at GlaxoSmithKline, Dekati, TUT, and Finnish Meteorological Institute (FMI) at various phases of work who the authors wish to acknowledge. Especially the early contributions of Ms. Anna Frey and Mr. Timo Mäkelä from the Finnish Metrology Institute and the contribution of Mr. David Prime from GlaxoSmithKline are recognized. This study was funded by Tekes (Grant No. 1811/31/06) – the Finnish Funding Agency for Technology and Innovation as well as by the Cluster for Energy and Environment (CLEEN, MMEA) (Grant No. 427/10).

References

Adi, H., Kwok, P.C.L., Crapper, J., Young, P.M., Traini, D., & Chan, H.-K. (2010). Does electrostatic charge affect powder aerosolisation. *Journal of Pharmaceutical Sciences*, *99*, 2455–2461.

Balachandra, W., Kulon, J., Koolpiruck, D., Dawson, M., & Burnel, P. (2003). Bipolar charge measurement of pharmaceutical powders. *Powder Technology*, *135*, 156–163.

Balachandran, W., Machowski, W., Gaura, E., & Hudson, C. (1997). Control of drug aerosol in human airways using electrostatic forces. *Journal of Electrostatics*, *40–41*, 579–584.

Beleca, R., Abbod, M., Balachandran, W., &Miller, P.R. (2009). In: *Proceedings of the Electrosatics Joint Conference.* Boston, MA, USA.

Berglund, R.N., & Liu, B.Y.H. (1973). Generation of monodisperse aerosol standards. *Environmental Science and Technology*, *7*, 147–153.

Biskos, G., Reavell, K., & Collings, N. (2005). Description and theoretical analysis of a differential mobility spectrometer. *Aerosol Science and Technology*, *39*, 527–541.

Biswas, P., & Flagan, R.C. (1984). High-velocity inertial impactors. *Environmental Science and Technology*, *18*, 611–616.

Dzubay, T.G., & Hasan, H. (1990). Fitting multimodal lognormal size distributions to cascade impactor data. *Aerosol Science and Technology*, *13*, 144–150.

Dzubay, T.G., Hines, L.E., & Stevens, R.K. (1976). Particle bounce errors in cascade impactors. *Atmospheric Environment*, *100*, 229–234.
Flagan, R.C. (1982). Compressible flow inertial impactors. *Journal of Colloid and Interface Science*, *87*, 291–299.
Fleming, J.S., Hashish, A.H., Conway, J.H., Hartley-Davies, R., Nassim, M.A., Guy, M.J., Coupe, J., Holgate, S.T., Moore, E., Bailey, A.G., & Martonen, T.B. (1997). A technique for simulating radionuclide images from the aerosol deposition pattern in the airway tree. *Journal of Aerosol Medicine*, *10*, 199–212.
Glover, W., & Chan, H.K. (2004). Electrostatic charge characterization of pharmaceutical aerosols using electrical low-pressure impaction (ELPI). *Journal of Aerosol Science*, *35*, 755–764.
Hashish, A.H., & Bailey, A.G. (1991). Electrostatic enhancement of particle deposition in the lung when using jet and ultrasonic nebulisers. *Institute of Physics Conference Series*, *118*, 45–50.
Hering, S.V. (1987). Calibration of the QCM impactor for stratospheric sampling. *Aerosol Science and Technology*, *7*, 257–274.
Hillamo, R.E., & Kauppinen, E.I. (1991). On the performance of the berner low pressure impactor. *Aerosol Science and Technology*, *14*, 33–47.
Hinds, W.C. (1998). *Aerosol Technology. Properties, Behavior, and Measurement of Airborne Particles* 2nd ed.). John Wiley & Sons Inc.: New York483.
Hoe, S., Young, P.M., & Traini, D. (2011). A review of electrostatic measurement techniques for aerosol drug delivery to the lung: implications in aerosol particle deposition. *Journal of Adhesion Science and Technology*, *25*, 385–405.
Hoe, S., Young, P.M., Chan, H., & Traini, D. (2009). Introduction of the electrical next generation impactor (eNGI) and investigation of its capabilities for the study of pressurized metered dose inhalers. *Pharmaceutical Research*, *26*, 431–437.
John, W. (1995). Particle-surface interactions: charge transfer, energy loss, resuspension, and deagglomeration. *Aerosol Science and Technology*, *23*, 2–24.
Karner, S., & Urbanetz, N.A. (2011). The impact of electrostatic charge in pharmaceutical powders with specific focus on inhalation-powders. *Journal of Aerosol Science*, *42*, 428–445.
Keskinen, J., Pietarinen, K., & Lehtimäki, M. (1992). Electrical low pressure impactor. *Journal of Aerosol Science*, *23*, 353–360.
Knutson, E.O., & Whitby, K.T. (1975). Aerosol classification by electric mobility: apparatus, theory, and applications. *Journal of Aerosol Science*, *6*, 443–451.
Kulon, J., & Balachandran, W. (2001). The measurement of bipolar charge on aerosols. *Journal of Electrostatics*, *51–52*, 552–557.
Kulvanich, P., & Stewart, J. (1987). An evaluation of the air stream Faraday cage in the electrostatic charge measurement of interactive drug system. *International Journal of Pharmaceutics*, *36*, 243–252.
Kwok, P., Glover, W., & Chan, H.-K. (2005). Electrostatic charge characteristics of aerosols produced from metered dose inhalers. *Journal of Pharmaceutical Sciences*, *94*, 12.
Kwok, P.C.L., & Chan, H.-K. (2008). Effect of relative humidity on the electrostatic charge properties of dry powder inhaler aerosols. *Pharmaceutical Research*, *25*, 277–288.
Labiris, N.R., & Dolovich, M.B. (2003). Pulmonary drug delivery. Part I: Physiological factors affecting therapeutic effectiveness of aerosolized medications. *British Journal of Clincal Pharmacology*, *56*, 588–599.
Marjamäki, M., Lemmetty, M., & Keskinen, J. (2005). ELPI response and data reduction I: Response functions. *Aerosol Science and Technology*, *39*, 575–582.
Marple, V.A., & Liu, B.Y.H. (1974). Characteristics of laminar jet impactors. *Environmental Science and Technology*, *8*, 648–654.
Marple, V.A., Roberts, D.L., Romay, F.J., Miller, N.C., Truman, K.G., Oort, M.V., Olsson, B., Holroyd, M.J., Mitchell, J.P., & Hochrainer, D. (2003). Next generation pharmaceutical impactor (a new impactor for pharmaceutical inhaler testing). Part I: Design. *Journal of Aerosol Medicine*, *16*, 283–299.
May, K.R. (1945). The cascade impactor: an instrument for sampling coarse aerosols. *Journal of Scientific Instruments*, *22*, 187–195.
Mazumder, M.K., Ware, R.E., Yokoyama, T., Rubin, B.J., & Kamp, D. (1991). Measurement of particle size and electrostatic charge distributions on toners using E-SPART analyzer. *IEEE Transactions on Industry Applications*, *27*, 611–619.
Murtomaa, M., & Laine, E. (2000). Electrostatic measurement on lactose–glucose mixtures. *Journal of Electrostatics*, *48*, 155–162.
Murtomaa, M., Mellin, V., Harjunen, P., Lankinen, T., Laine, E., & Lehto, V.P. (2004). Effect of particle morphology on the triboelectrification in dry powder inhalers. *International Journal of Pharmaceutics*, *282*, 107–114.
Reischl, G., John, W., & Heigwer, W. (1977). Uniform electrical charging of monodisperse aerosols. *Journal of Aerosol Science*, *8*, 55–65.
Saini, D., Biris, A.S., Srirama, M.K., & Mazumder, M.K. (2007). Particle size and charge distributions analysis of pharmaceutical aerosols generated by inhalers. *Pharmaceutical Development and Technology*, *12*, 35–41.
Telko, M.J., Kujanpää, J., & Hickey, A.J. (2007). Investigation of triboelectric charging in dry powder inhalers using electrical low pressure impactor (ELPI™). *International Journal of Pharmaceutics*, *336*, 352–360.
Uin, J., Tamm, E., & Mirme, A. (2009). Electrically produced standard aerosols in wide size range. *Aerosol Science and Technology*, *43*, 847–853.
Winklmayr, W., Wang, H.-C., & John, W. (1990). Adaptation of the twomey algorithm to the inversion of cascade impactor data. *Aerosol Science and Technology*, *13*, 322–331.
Yli-Ojanperä, J., Mäkelä, J.M., Marjamäki, M., Rostedt, A., & Keskinen, J. (2010). Towards traceable particle number concentration standard: single charged aerosol reference (SCAR). *Journal of Aerosol Science*, *41*, 719–728.
Young, P.M., Sung, A., Traini, D., Kwok, P., Chiou, H., & Chan, H.-K. (2007). Influence of humidity on the electrostatic charge and aerosol performance of dry powder inhaler carrier based systems. *Pharmaceutical Research*, *24*, 963–970.

Paper IV

Järvinen A., Keskinen J., and Yli-Ojanperä J. (2018). Extending the Faraday Cup Aerosol Electrometer Based Calibration Method up to 5 µm. Aerosol Science and Technology, 52, 828-840.

AEROSOL SCIENCE AND TECHNOLOGY
2018, VOL. 52, NO. 8, 828–840
https://doi.org/10.1080/02786826.2018.1472742

Extending the Faraday cup aerosol electrometer based calibration method up to 5 μm

A. Järvinen, J. Keskinen, and J. Yli-Ojanperä

Aerosol Physics, Faculty of Natural Sciences, Tampere University of Technology, Tampere, Finland

ABSTRACT

A Faraday cup aerosol electrometer based electrical aerosol instrument calibration setup from nanometers up to micrometers has been designed, constructed, and characterized. The set-up utilizes singly charged seed particles, which are grown to the desired size by condensation of diethylhexyl sebacate. The calibration particle size is further selected with a Differential Mobility Analyzer (DMA). For micrometer sizes, a large DMA was designed, constructed, and characterized. The DMA electrical mobility resolution was found to be 7.95 for 20 L/min sheath and 2 L/min sample flows. The calibration is based on comparing the instrument's response against the concentration measured with a reference Faraday cup aerosol electrometer. The set-up produces relatively high concentrations in the micrometer size range (more than 2500 1/cm^3 at 5.3 μm). A low bias flow mixing and splitting between the reference and the instrument was constructed from a modified, large-sized mixer and a four-port flow splitter. It was characterized at different flow rates and as a function of the particle size. Using two of the four outlet ports at equal 1.5 L/min flow rates, the particle concentration bias of the flow splitting was found to be less than ±1% in the size range of 3.6 nm–5.3 μm. The developed calibration set-up was used to define the detection efficiency of a condensation particle counter from 3.6 nm to 5.3 μm with an expanded measurement uncertainty ($k = 2$) of less than 4% over the entire size range and less than 2% for most of the measurement points.

ARTICLE HISTORY
Received 14 December 2017
Accepted 16 April 2018

EDITOR
Pramod Kulkarni

Introduction

Instrument calibration is one of the cornerstones of reliable measurements. In the field of aerosol measurement, accurate measurement of, for example, particle number concentration, is needed in clean rooms of production facilities, in ambient air monitoring, and in legislated vehicle engine exhaust particulate matter emission measurements (European Commission 2008; ISO 14644–1:2015; CEN/TS 16976:2016). Calibration of an aerosol instrument in a wide particle size range is a challenging task. Firstly, the particle size range in the aforementioned applications and, consequently the measurement size ranges of common aerosol instruments extend over several orders of magnitude, from nanometers up to micrometers. Secondly, the calibration often requires monodisperse particles of known size and concentration. Hence, different particle generation and reference measurement methods are required for different size ranges (Marple et al. 1991; Marjamäki et al. 2000; Yli-Ojanperä et al. 2012; Järvinen et al. 2014). Usually, the calibration of an aerosol instrument involves determination of the relationship between the measured and true values of either particle size or particle concentration. The concentration is typically expressed in terms of particle number or mass.

In a few cases, the calibration of the instrument size axis is possible without the exact knowledge of the particle number concentration, for example, impactor calibration (Kauppinen and Hillamo 1989; Keskinen et al. 1999). If it is sufficient to calibrate instrument only for a few discrete particle sizes, traceable particle size standards may be used. Typically, these are spherical polystyrene (PSL) particles, which have been characterized by microscopy, but recently, silica particles have also been introduced as a potential size standard in aerosol science (Kimoto et al. 2017). If a better size resolution than what is provided by the standard PSL spheres is needed, a different particle generation approach is required.

In sub-micrometer size range, a combination of a particle generator and a size classifier is typically used as a source of monodisperse particles. If the output size of the classifier, often a Differential Mobility Analyzer (DMA, Knutson and Whitby 1975), is calibrated against traceable size standard particles,

CONTACT J. Keskinen jorma.keskinen@tut.fi or A. Järvinen anssi.jarvinen@tut.fi Aerosol Physics, Faculty of Natural Sciences, Tampere University of Technology, P.O. Box 692, Tampere 33101, Finland.

the classifier operates as a size reference in this calibration. In the micrometer size range, generators that produce monodisperse particles and for which the particle size is determined by the operating parameters, are used as a size reference. Examples of such generators are the Vibrating Orifice Aerosol Generator (VOAG, Berglund and Liu 1973) and the recent Flow-focusing Monodisperse Aerosol Generator (FMAG, Duan et al. 2016). Another option is to collect part of the calibration particles and to use microscopy as a size reference.

Unlike the calibration of the size axis, the characterization of the instrument response (detection efficiency) as a function of number concentration and/or size requires a known input concentration. Currently, two different approaches are used as a number concentration reference in calibrations (Yli-Ojanperä et al. 2012). The first approach is a generator-type Number Concentration Standard (NCS). In this case, the generator number concentration output is derived from the operating parameters, provided that the particle losses are well known or preferably insignificant. The calibration is conducted by connecting the monodisperse output of the generator directly to the inlet of the device being calibrated. The only existing generator type of NCS is the Drop-on-Demand Inkjet Aerosol Generator (IAG) of the National Institute of Advanced Industrial Science and Technology (AIST) (Iida et al. 2014), which operates in the particle size range of 0.3–20 µm.

The second, and the most widely applied type of NCS, is the measurement instrument approach. In this approach, a particle generator produces monodisperse particles, which are led to the device under calibration and to the reference instrument having a well-characterized detection efficiency. In submicrometer size range, singly charged monodisperse particles that are extracted from a polydisperse distribution with a DMA are used in combination with a Faraday Cup Aerosol Electrometer (FCAE) as a number concentration reference (Liu and Pui 1974; Fletcher et al. 2009; Högström et al. 2014; ISO 27891:2015). The SI-traceability for the number concentration is achieved through traceable electric current and flow rate measurements. The combination of singly charged particles and FCAE is commonly used in measuring the counting efficiency curves of various Condensation Particle Counters (CPCs), especially in small particle sizes near the cut diameter. Multiple charging is insignificant in bipolar charging at the smallest particle diameters (Fuchs 1963; Wiedensohler 1988); therefore, mobility classification combined with FCAE enables accurate calibrations below 30 nm. Above this, the multiple charging limits the precision. However, there are methods to limit this issue, for instance, an additional aerodynamic size selection (Romay-Novas and Pui 1988; Hillamo and Kauppinen 1991; Owen et al. 2012) or modifications of the La Mer generator (Sinclair and La Mer 1948), which produce singly charged particles (Uin et al. 2009; Yli-Ojanperä et al. 2010; Yli-Ojanperä et al. 2012). In 2012, Yli-Ojanperä et al. successfully applied a modified La Mer generator and a DMA for producing singly charged calibration aerosol and for conducting a FCAE-based number concentration calibration up to 1 µm. Provided that, the modified La Mer generator is capable of producing particles larger than 1 µm, the upper size limit of this calibration method could be increased by constructing a larger DMA. A new DMA is needed as conventional DMAs operated at very low polydisperse and sheath flow rates, 0.2 L/min and 2.0 L/min, respectively, can classify singly charged particles only up to approximately 1 µm. In a CPC calibration, the total output flow rate required by the CPC and the reference instrument is usually 2 L/min or larger. Therefore, the DMA output flow of 0.2 L/min is diluted by a factor of 1/10, which results in a low output number concentration. By operating the DMA with lower than standard sheath flow rate, it is possible to extend the size range slightly (e.g., Järvinen et al. 2014; Yli-Ojanperä et al. 2014), but when high flow and relatively high number concentration of monodisperse particles are required, a large size DMA (e.g., Uin et al. 2011) becomes essential.

In principle, the available calibration methods cover the entire size range from nanometers up to micrometers, but the calibration concentrations and the availability of the calibration methods, especially in the micrometer range, are very limited. So far, the only published traceable number concentration standard in the micrometer size range with uncertainty less than 5% is the IAG of AIST, which is limited to about 50 1/cm^3 number concentration (Iida et al. 2014). A calibration method producing higher number concentrations in the micrometer size range, which has not been available, would be useful in CPC and Optical Particle Counter (OPC) calibrations, and especially in calibrations of charger-based instruments, such as the Electrical Low Pressure Impactor (ELPI, Keskinen et al. 1992; Marjamäki et al. 2000, or ELPI+, Järvinen et al. 2014).

Micrometer-sized particles are affected by inertial deposition in the bends of the flow channel. In calibration applications, flow splitters potentially induce particle losses due to inertial deposition (e.g., Gupta and McFarland 2001). Uneven particle losses between the flow splitter ports result in a concentration bias between the instrument under calibration and the reference. This bias might be significant both for the smallest nanoparticles and for the micrometer-sized particles, easily up to several percentage in some cases (Li et al. 2014). Bias values of this magnitude are unwanted and need to be compensated, which is not an easy task. Compensation of high bias values using calculated correction factors is neither a good practice nor does necessarily provide correct results. In addition, the bias depends on the particle size and flow rates. Thus, the concentration bias should be minimal and experimentally evaluated. The procedure for the evaluation of bias is presented in Yli-Ojanperä et al. (2012) and in ISO 27891:2015.

In this article, we introduce a new Faraday cup aerosol electrometer-based instrument calibration setup, utilizing singly charged particles, a new custom-made large particle DMA, and a carefully designed low particle bias flow mixing and splitting setup. The size range of the calibration setup ranges from nanometers to micrometers. To verify the operation of the new calibration setup, we characterize the particle generator output, the large DMA transfer function, and how well the calibration aerosol can be divided between the instrument under calibration and FCAE acting as a reference, that is, the bias of the flow splitting. Finally, the potential of the developed setup is demonstrated by determining the counting efficiency of a CPC in the size range of 3.6 nm–5.3 µm.

Calibration setup

The developed aerosol instrument calibration setup is a modification of a setup, which was previously introduced by Yli-Ojanperä et al. (2012). The particle generation scheme follows the principle by Uin et al. (2009) used in the Single Charged Aerosol Reference (SCAR, Yli-Ojanperä et al. 2010). In this case, we have taken the SCAR (Yli-Ojanperä et al. 2010; Högström et al. 2011; Yli-Ojanperä et al. 2012) as our basis, which is further developed for larger µm-sized particles, by developing a new particle growth unit to withstand higher temperatures, a new DMA to classify larger particles as well as a new flow mixing and splitting setup to provide equal output concentrations also in the µm-sizes. These developments are discussed in more detail after the general description of the setup.

General description of the setup

The particle generation setup is shown in Figure 1a along with different measurement configurations. The particle generation resembles the principle of the La Mer generator (Sinclair and La Mer 1948), where small primary particles are grown by condensable material, in this case diethylhexyl sebacate (DEHS). As a first stage in the setup, the primary aerosol is generated by introducing a nitrogen flow of 2.5 L/min into a tube furnace containing silver at 1180 °C temperature. After the furnace, cooling initiates nucleation of silver resulting in an approximately 10 nm particle mode. This primary aerosol is further diluted with nitrogen and a flow of 2 L/min is taken for the following stages. In addition to dilution flow adjustment, a dilution bridge is used to control the concentration. The silver particles are then charge conditioned in a Kr-85 neutralizer (Model 3077A, TSI Inc., Shoreview, MN, USA). As the particles are small, approximately 10 nm, the particles receive only a single elementary charge, positive or negative, or they are neutral. The fraction of particles with multiple elementary charges is minimal. The positively charged 10 nm particles are selected in a DMA (Model 3085, TSI Inc.), which is operated in a closed sheath flow loop configuration, sheath 20 L/min and sample 2 L/min. The seed particles are then introduced into a particle growth unit, which grows particles with DEHS to the desired size (a more detailed description is given later). In the original SCAR, the particle sizes were smaller and homogenous nucleation of the DEHS could be mostly avoided (Yli-Ojanperä et al. 2010). As micrometer-sized particles are produced by condensation, the high DEHS vapor concentration results in homogenous nucleation. These nucleated particles are neutral, and they are removed by a second DMA.

The second DMA removes the neutral nucleated particles and enables particles/no particles signal, which is used to compensate the electrometer zero level in calibration measurements. In the developed setup, the particle size ranges from approximately 3.0 nm (if the silver primary distribution is used) to 5.3 µm, and cannot be covered by a single DMA. Thus, three different DMAs are used, one at a time. The smallest particles, up to 40 nm, are classified using a nano-DMA (Model 3085, TSI Inc.). In the size range between 40 and 250 nm, a medium length Vienna-type DMA with a 280 mm long classification

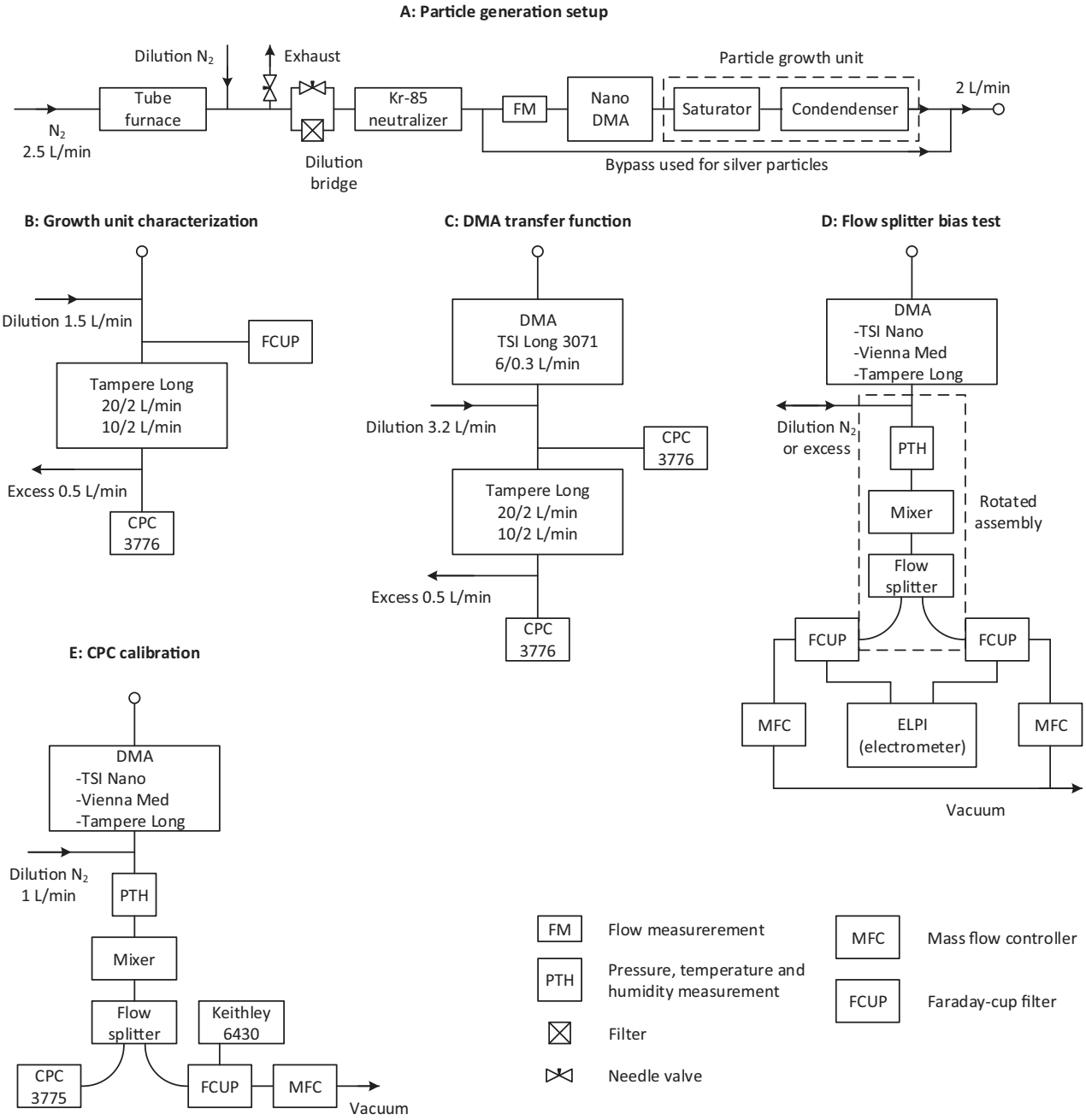

Figure 1. Measurement setups. The particle generation setup (a) remained the same during all measurements. The instrument setups (b–e) were varied depending on the measurement interest. Setup (b) was used to characterize the particle growth unit, (c) the DMA transfer function, (d) the flow splitter bias, and (e) was used in the CPC calibration.

section is used. The particle sizes above 250 nm are classified with the new large DMA: Tampere Long DMA, described later in more detail.

After the DMA, the flow rate of the calibration aerosol is matched with the instruments by diluting or by removing the extra flow. Then, pressure, temperature, and humidity are measured from the line with a PTH-sensor (PTU303, Vaisala Oyj, Vantaa, Finland), and the flow is introduced into a mixer followed by a flow splitter, see more detailed description later. The outlets of the flow splitter are connected to the instrument and the FCAE reference. The FCAE comprises a Faraday-cup filter and an electrometer (Model 6430, Keithley, Solon, OH, USA). The FCAE flow rate is controlled with a mass flow controller (Model MC-2SLPM-D/5M, Alicat Scientific Inc., Tucson, AZ, USA). The SI-traceability for the number concentration in the calibration setup

is achieved through traceable electric current and flow rate measurements.

Particle growth unit

A new particle growth unit was developed to facilitate the production of higher DEHS concentrations required for growing the particles to µm-sizes. The singly charged primary aerosol is introduced into a saturator, where the gas is saturated with DEHS. The saturator is a ceramic wick installed inside a heated stainless steel tube and impregnated with DEHS. The saturator is surrounded by a heating element and temperature is measured with a thermocouple and adjusted with a dedicated controller (E5GN, Omron, Kyoto, Japan). The saturator temperature controls the output particle size. The flow cools down to room temperature in a condenser, which is a 1 m long vertical tube with 10 mm outer and 8 mm inner diameter. When the flow cools, DEHS condenses on the singly charged silver primary particles resulting in the singly charged calibration aerosol. The DEHS vapor condenses on all available surfaces, including the walls of the condenser. To avoid excessive amounts of liquid DEHS coming from the outlet, the calibration aerosol is taken from the middle of the condenser, while the DEHS from the walls is collected into a separate bottle.

Tampere Long DMA

As singly charged micrometer-sized particles have extremely low electrical mobilities, the conventional DMAs cannot classify these particles if they are operated with high sample and sheath flows. To overcome this issue, a large-sized DMA was constructed. The Tampere Long DMA comprises a tangential particle inlet, similar to Vienna DMAs (Winklmayr et al. 1991), followed by a 1.7 m long classification section with 72 mm inner and 80 mm outer radius. The flow channels are rounded to minimize large particle losses. Aluminum was chosen as a main construction material as it is easily machined, lightweight, and adequately resists corrosion. In addition, aluminum precision cylinder tubes are available, and the outer tube was constructed from this type of tube. The electrical insulators are made of polyethylene, which is a combination of decent mechanical properties and a good chemical resistance. As significant amounts of DEHS enter the DMA due to the large particle size, chemical resistance is required. The advantage of DEHS as a particle material is that it dissolves into ethanol and 2-propanol. The DMA was designed so that the cleaning is as easy as possible by opening the upper part of the DMA and flushing the internal parts with the solvent, 2-propanol or ethanol, which is then collected into a bottle from the excess and monodisperse outlets. The solvent is then dried by flushing the DMA with clean air or nitrogen. For singly charged particles, the maximum classified particle sizes are approximately 2.5 µm and 5.3 µm at 20 L/min and 10 L/min sheath flow rates, respectively.

The commonly used calculation of the DMA outlet mobility (Knutson and Whitby 1975) does not include gravity, which produces slow downward velocity especially at micrometer sizes. As the calibration sizes are extending into micrometers, gravity was taken into account. The effect of gravity is corrected using a method, where the particle terminal velocity due to gravity is added to the velocity resulting from the flow rate (Uin et al. 2011). The effect of gravity is rather small, less than 2% for the particle size of 5.3 µm at 10 L/min sheath flow.

Mixer and flow splitter

An equal particle concentration is required for both the reference and the instrument under calibration. This may be challenging for the smallest particles and especially for large µm-sized particles (Li et al. 2014). An option to ensure equal concentrations after flow splitting is to use a static flow mixer before the flow splitter (e.g., Yli-Ojanperä et al. 2012). For coarse particles, high flow velocities in sharp turns cause inertial deposition. This can be avoided with a large cross-sectional area and long mixing element length. For the new setup, a large-sized 12-element stainless steel static mixer (FMX8412S, Omega Engineering Ltd., Manchester, UK) was selected. This was modified by inserting a conical piece inside after the mixing elements to minimize particle losses. The static mixer is followed by a 280 mm long tube (15.7 mm inner diameter) to stabilize the flow before the 4-port flow splitter (Model 3708, TSI Inc.). The FCAE and the instrument under calibration are connected symmetrically to the flow splitter with 6 mm outer and 4 mm inner diameter stainless steel tubing with equal length and bending radius.

Characterization of the calibration setup

A variety of test measurements were conducted to evaluate the new components of the developed

calibration setup, including the particle growth unit output, transfer function of the Tampere Long DMA, and mixer and flow splitter bias. Furthermore, the setup was used to calibrate the detection efficiency of a CPC in the size range between 3.6 nm and 5.3 µm. All measurement configurations used in this study are presented in Figure 1.

Particle growth unit

The particle growth unit was characterized with 2 L/min flow rate, which is the same as the outlet flow rate of the DMA classifying silver primary particles. The objective was to find the relationship between the outlet size distribution and the saturator temperature. In this case, the focus was on larger particles, and the growth unit was studied in the size range from 350 nm to 5.3 µm. The measurement setup for the growth unit characterization is presented in Figure 1b. The size distributions were measured with the Tampere Long DMA by scanning the classifying voltage over the size distribution and measuring the concentration by a CPC (Model 3776, TSI Inc.). The response of this CPC 3776 was defined in the corresponding size range against the FCAE, and the results were used to correct the CPC readings.

DMA transfer function

The DMA transfer function can be tested with monodisperse particles of a known charge level. The concentration of 1 µm size standard particles (Product number 72938, Sigma-Aldrich Inc., St. Louis, MO, USA), atomized from ultra-pure water solution, and charge conditioned in a neutralizer was applied as a first attempt, but the resulting number concentration was too low for analyzing the transfer function. However, these size standard particles were used to check that the calculated DMA size matched the standard size, which was the case. Higher concentrations were achieved by measuring the transfer function of the Tampere Long DMA with monodisperse 400 nm singly charged DEHS particles. These particles were generated using the developed particle growth unit. As the distribution from the growth unit is not monodisperse, a DMA (Model 3071, TSI Inc.) was used to select a narrow size range after the growth unit as illustrated in Figure 1c. This DMA was operated with 6 L/min sheath and excess flows in addition to 0.3 L/min sample and monodisperse flows. This flow ratio of 20 produces a narrow size distribution, which simplifies the calculation of the transfer function. The particle concentrations were monitored with 2 CPCs (both Model 3776, TSI Inc.), one before the Long DMA and one after the Long DMA. Both CPCs were operated with 1.5 L/min sample flows. Additional dilution and excess flows were used to balance the DMA sample flow to 2 L/min. The measurement of the transfer function was conducted by scanning the Long DMA voltage over the monodisperse size distribution. Transfer function was measured with 20 and 10 L/min sheath flow rates, while the sample flow was maintained at 2 L/min.

Mixer and flow splitter tests

The flow splitting was studied with two identical FCAEs, by measuring the concentration bias between the two FCAEs as presented in Figure 1d. Equal flow rates were drawn through these FCAEs, using mass flow controllers (MC-2SLPM-D/5M and MC-5SLPM-D/5M, Alicat Scientific Inc.) and both mass flow controllers were calibrated with the same separate flow meter (M-2SLPM-D/5M, Alicat Scientific Inc.) to ensure maximum accuracy. The electric currents from the FCAE Faraday-cup filters were measured with a multichannel electrometer (ELPI, Dekati Ltd., Kangasala, Finland). The two electrometer channels of the ELPI used in the electric current measurements were calibrated with the same electric current calibrator.

The most challenging cases in the flow splitting are the smallest and the largest particle sizes. The smallest particles are prone to diffusion losses and the largest particles are prone to inertial losses. As the inlet tubing (length and bending radius) and flow rates for the device under calibration and for the reference instrument are identical, the bias due to diffusion losses should not depend on the absolute flow rate as far as the flows stay laminar. In this article, the FCAE flow rates are between 0.50 and 2.00 L/min. Consequently, the flows remain laminar as the maximum Reynolds number is 710. Bias due to inertial losses on the other hand may change noticeably due small differences of any kind in the flow lines. Therefore, the flow splitter bias was characterized using the largest easily produced particle size of 5.3 µm at different flow rates. In addition, the flow splitting was characterized for the CPC calibration setup as a function of particle size, at the same size range used in the CPC calibration and at the same 1.5 L/min flow rate.

CPC calibration

The developed setup was applied in the calibration of a CPC (Model 3775, TSI Inc.) from 3.6 nm up to

5.3 µm using the setup illustrated in Figure 1e. Both the CPC and the FCAE were operated at 1.5 L/min flow rates. The lowest size range was covered by the silver primary particles ranging from 3.6 nm to 15 nm. The growth unit was used for particle sizes above 15 nm. The 15 nm size was measured with both silver and DEHS particles to see if there was a difference between the two particle materials. The entire size range is too wide to be covered with a single DMA. Thus, a set of three different DMAs was used for size ranges that were presented in the Calibration setup section earlier. The DMAs were operated with 2 L/min sample and 20 L/min sheath flows in a closed loop configuration, except the largest particle sizes above 2.5 µm, where the sheath flow was reduced to 10 L/min. The same high voltage power supply (HCP 1,25-12500 MOD, FuG Elektronik GmbH, Schechen, Germany) was used with all three DMAs. The reference particle concentration was adjusted between 4000 and 14,000 1/cm^3. For two smallest and largest particle sizes, this concentration level was not reached and the concentrations were slightly lower. Each measurement point comprised 2 min particle measurement period repeated for 10 times. The particle free period to check the electrometer zero level was maintained for 2 min between the particle measurement periods and before and after the entire sequence. From these 2 min periods, 1 min was used to wait for stabilization and 1 min was used to calculate the average electric currents.

Results and discussion

Particle growth unit

The growth unit operation was tested as a function of the saturator temperature. The outlet particle size distributions, for different saturator temperatures, are shown in Figure 2, including 2-part Gaussian fits. In this case, particles were detected with a calibrated CPC. The CPC counting efficiency decreases above 2 µm particle sizes, which is corrected in the figure. The growth unit also works at lower temperatures, but the distributions are not shown here as the main focus is on µm-sized particles. The output concentration remains high up to a saturator temperature of 190 °C, producing approximately 1.5 µm particles, but decreases above this. The concentration increase at 210 °C temperature in Figure 2 is observed because between 190 and 210 °C temperatures the first stage dilution was minimized to maximize the output concentration. Note that, in Figure 2, the *y*-axis is the measured number concentration, which also represents the maximum possible concentration when the setup is used to calibrate instruments in case of three large sizes while primary dilution was minimized. The concentration could be increased if the distance between the first DMA and the saturator was shortened to minimize seed particle losses, or if the particle generation could be located above the DMA. In current setup, particles are subjected to gravitational losses as they are brought from the level of the laboratory table up to the DMA inlet close to the ceiling.

The modal diameters from the fits are shown as a function of the saturator temperature in Figure 2. The fit predicts a steady increase in particle diameter for increased saturator temperature. However, in practice, the particle diameter levels and does not increase above 260 °C temperatures, limiting the particle diameter to approximately 5–6 µm. The growth unit produces particle distributions with geometric standard deviations between 1.10 and 1.17 within the tested size range.

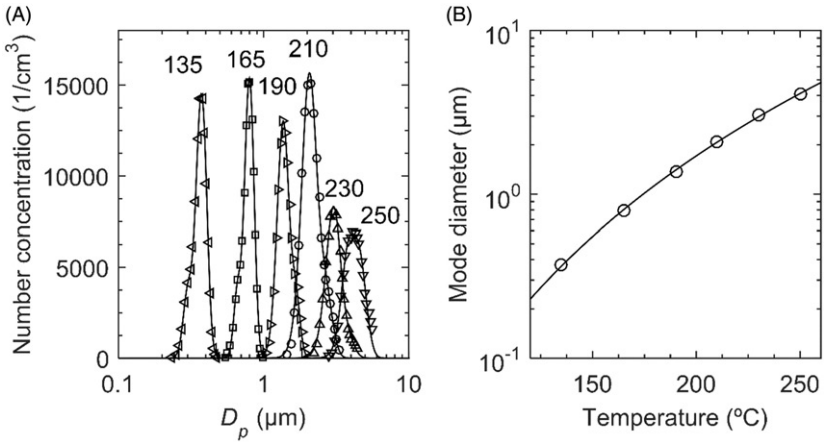

Figure 2. Growth unit size distributions for different saturator temperatures (°C) (a) and mode diameters as a function of temperature (b). The symbol D_p refers to the particle mobility diameter.

DMA transfer function

The DMA transfer function was tested using singly charged DEHS particles, which were first classified with a commercial DMA (Model 3071, TSI Inc.) operated with 6 L/min sheath and 0.3 L/min sample flows. Because of the narrow input distribution and constant concentration at inlet of the Tampere Long DMA, the transfer function was calculated straight from the CPC concentration measured after the Tampere Long DMA. The transfer function for 20 L/min and 10 L/min sheath flows in conjunction with 2 L/min sample flows is shown in Figure 3, including 2-part Gaussian fits. In case of the 20 L/min sheath, the transfer function width (Full Width Half Maximum, FWHM) is 0.434×10^{-9} m^2/Vs and the peak mobility is 3.45×10^{-9} m^2/Vs producing resolution of 7.95. The obtained resolution value for 20/2 flow configuration is somewhat lower than the theoretical maximum of 10. However, the obtained resolution value is acceptable for a large DMA compared with previous devices. For instance, Uin et al. (2011) reported a β-value of 0.17 for a large-sized DMA, which corresponds a resolution of 5.88. The measured transfer function differs in some degree from the typical triangular shape, especially at the lower mobilities. The reason for this difference is unknown, but it may originate from small deviations from the design values, especially in terms of concentricity. For the 10 L/min sheath flow, the width increases as expected, and is 0.767×10^{-9} m^2/Vs, while the peak mobility is 3.42×10^{-9} m^2/Vs. These values produce a resolution of 4.45, which is closer to the theoretical maximum of 5 for 10/2 flow configuration. The transfer function resembles the triangular shape in this case, indicating that the width of the transfer function originates more from the flow configuration than other factors.

Mixer and flow splitter tests

High-quality flow splitting between the instrument under calibration and the reference instrument is essential. This was studied by measuring the bias β between two flow splitter ports, including the stainless steel tubing installed after the splitter. The bias is derived, for instance, in Yli-Ojanperä et al. (2012) or in ISO 27891:2015. Two equal FCAEs were used as detectors in this bias measurement. First, the detection efficiency is calculated for the FCAE 2, while the

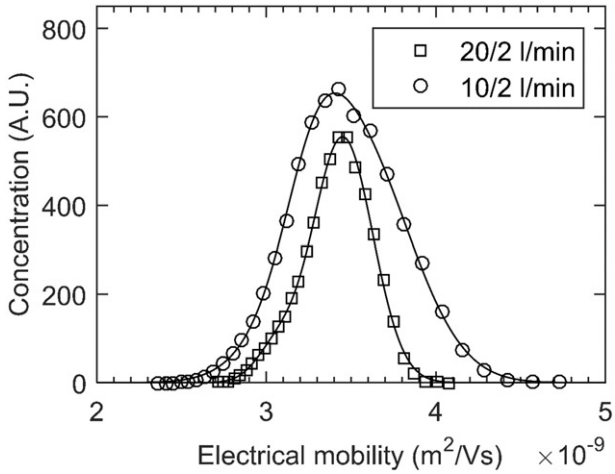

Figure 3. Tampere Long DMA transfer function for 20 L/min and 10 L/min sheath flows and 2 L/min sample flow rates.

FCAE 1 is considered as the reference. The detection efficiency η takes a form of

$$\eta = \frac{C_2}{C_1} = \frac{I_2}{I_1}\frac{Q_1}{Q_2}, \tag{1}$$

where C refers to particle concentration, I is the electric current measured by the FCAE including offset correction achieved by particles on/off cycling and Q the flow rate through the FCAE. The bias β is defined through detection efficiencies by equation

$$\beta = \sqrt{\frac{\eta_a}{\eta_b}}, \tag{2}$$

where η is the detection efficiency of the instrument, and the index a refers to the standard measurement configuration and b to the configuration where the flow splitter ports are switched. The inlet port switching was conducted by rotating the entire assembly containing the PTH-measurement, mixer, splitter, and the inlet tubes (see Figure 1d).

The bias uncertainty is calculated from statistical Type-A factors and non-statistical Type-B factors. In this case, we take a different approach compared with the ISO 27891:2015 and evaluate the statistical uncertainty of the bias based on the differences in the calculated detection efficiencies in successive particle off-on-off repetitions in a single measurement. The statistical uncertainty of the detection efficiency $u_{Type\text{-}A}(\eta)$, is calculated from equation

$$u^2_{Type-A}(\eta) = \frac{\sum_{i=1}^{n}(\eta_i - \bar{\eta})^2}{n(n-1)}, \tag{3}$$

where n is the number of particle on/off cycles (10) and $\bar{\eta}$ the average detection efficiency in the corresponding measurement point. This statistical Type-A uncertainty is calculated for all the measurement

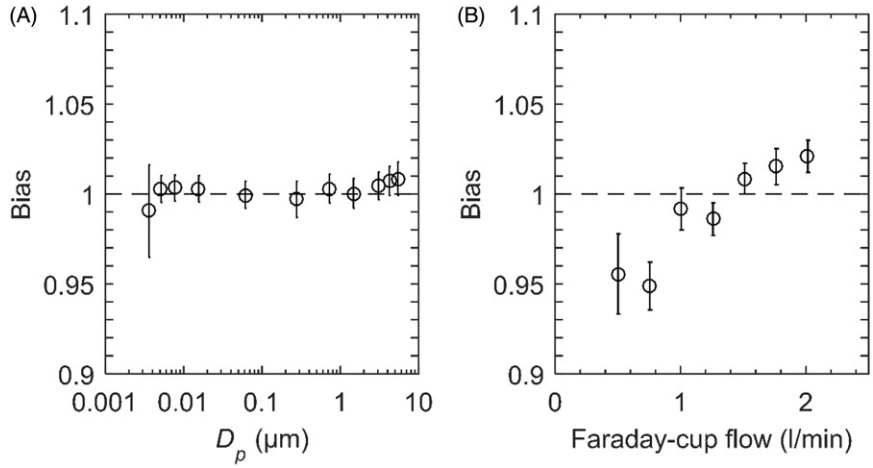

Figure 4. Flow splitter bias as a function of particle mobility diameter D_p at 1.5 L/min flow rate (a) and as a function of FCAE flow rate at 5.3 μm particle diameter (b) together with the expanded measurement uncertainties (coverage factor $k = 2$).

points and for both the normal and switched configuration separately. As a result, two series of uncertainty values are obtained, $u^2_{Type\text{-}A}(\eta_a)$ and $u^2_{Type\text{-}A}(\eta_b)$.

The non-statistical Type-B uncertainty $u_{Type\text{-}B}(\eta)$, caused by the measurement uncertainties of the instruments used, is calculated from the uncertainties of the electric current and flow measurement with equation

$$u_{Type-}B^2(\eta) = \eta^2\left(\left(\frac{u(Q_1)}{Q_1}\right)^2 + \left(\frac{u(Q_2)}{Q_2}\right)^2 + \left(\frac{u\left(\frac{I_2}{I_1}\right)}{\frac{I_2}{I_1}}\right)^2\right), \quad (4)$$

where $u(I_2/I_1)$ is the uncertainty of the proportional current measurement, $u(Q)$ the uncertainty of the flow measurement, and the indices 1 and 2 refer to corresponding FCAEs. Equation (4) is calculated for all the measurement points of both the normal and switched configuration separately. Electrometer channels were calibrated twice, 4 months apart from each other, with the same current calibrator at 10 pA current. The difference in the I_2/I_1 ratio was below 0.01% between the measurements. As the currents measured in the actual bias measurements were lower than in the calibration, varying between 3 and 200 fA, we assigned a significantly higher standard uncertainty value of 0.25% for the I_2/I_1 ratio than we observed in the calibrations. Flow rates Q_1 and Q_2 were controlled by mass flow controllers, which were calibrated with the same flow meter during measurements. Thus, the mass flow controller repeatability 0.1% full scale as a standard uncertainty is considered as the measurement uncertainty (absolute accuracy is insignificant). Hence, the flow measurement standard uncertainty for FCAE 1 $u(Q_1)$ is 0.002 L/min (0.14%) and for FCAE 2 $u(Q_2)$ is 0.005 L/min (0.34%).

Type-A and Type-B uncertainties are combined to obtain the total uncertainty for the detection efficiency

$$u^2(\eta) = u^2_{Type-A}(\eta) + u^2_{Type-B}(\eta). \quad (5)$$

Equations (3)–(5) are calculated for both configurations (a and b) and the uncertainty of the bias is calculated from

$$u(\beta) = \sqrt{\left(\frac{1}{2\eta_b}\sqrt{\frac{\eta_b}{\eta_a}}u(\eta_a)\right)^2 + \left(\frac{1}{2\eta_b}\sqrt{\frac{\eta_a}{\eta_b}}u(\eta_b)\right)^2}, \quad (6)$$

which is multiplied by the coverage factor $k = 2$ to obtain the expanded uncertainty expressed at a 95% confidence level.

The concentration bias results are presented as a function of the particle diameter at 1.5 L/min flow rate in Figure 4a and as a function of the flow rate at 5.3 μm particle diameter in Figure 4b. In the whole measured particle size range, namely between 3.6 nm and 5.3 μm, the measured bias values are smaller than ±1% at 1.5 L/min flow rate, which is a very good result for such a wide particle size range. It is also worth mentioning that within the uncertainty limits, the bias value of the flow splitting is one, i.e., no bias in the whole size range when the flow rate is 1.5 L/min. Figure 4b shows the relative concentration bias as a function of the common flow rates of the Faraday cups for 5.3 μm particles. For this largest particle size, the measured bias values range from −5.0% to 2.1% and show clear dependency on the flow rate. The flow mixing and splitting operates very well if the flow rate is between 1 L/min and 2 L/min for each Faraday cup. The measured bias is ±1.5% in the range between 1 L/min and 1.75 L/min and increases slowly

to 2.1% at 2 L/min. These bias values are acceptable, as values of several percent have been reported previously (Li et al. 2014).

CPC calibration

The detection efficiency of the CPC 3775 η_{CPC} is calculated with equation

$$\eta_{CPC} = \frac{C_{CPC}}{\beta C_{REF}} = C_{CPC}\frac{neQ\eta_{FC}}{\beta I}, \quad (7)$$

where C_{CPC} is the concentration measured by the CPC, C_{REF} is the reference concentration from the FCAE, e is the elementary charge, and β is the bias. The number of elementary charges per particle n is 1 due to particle generation principle. The flow rate through the FCAE Q is measured by the mass flow controller, including the calibration factor, but it is converted to instrument inlet conditions using a pressure and temperature measurement, installed before the mixer. The electric current from the FCAE I includes the zero level correction (particle on/off measurement) and the electrometer calibration factor. The factor η_{FC} represents the FCAE detection efficiency, which is affected by diffusion losses in smallest particle sizes and gravitational settling in the largest particle sizes. According to Gormley and Kennedy (1949), the detection efficiency due diffusional loss is calculated for the inlet length of 63 mm and the flow rate of 1.5 L/min according to Gormley and Kennedy (1949). The lowest FCAE detection efficiency of 0.95 due diffusion loss is acquired for the smallest particle size of 3.6 nm. The detection efficiency due gravitational deposition in the inlet tube is calculated based on the same parameters according to Thomas (1958), and the minimum value of 0.992 is acquired for the largest particle size of 5.3 µm. The FCAE total detection efficiency is obtained by multiplying these two detection efficiency functions.

The uncertainty for the detection efficiency is evaluated for Type-A and Type-B factors. The Type-A analysis containing all the statistical factors is calculated from an equation

$$u^2_{Type-A}(\eta_{CPC}) = \frac{\sum_{i=1}^{n}(\eta_{CPC,i} - \bar{\eta}_{CPC})^2}{n(n-1)}, \quad (8)$$

in which, n is the number of cycles (10) and $\bar{\eta}$ is the average detection efficiency in the corresponding measurement point.

The Type-B uncertainty is mostly related to the flow measurement accuracy, but the electrometer calibration and concentration bias are also included in the uncertainty analysis. The uncertainty of the FCAE detection efficiency was evaluated by Yli-Ojanperä et al. (2012). In their approach, a symmetric rectangular probability distribution with a half width of 20% of the theoretical diffusion loss (1-η_{FC}) was used for calculating the uncertainty of the detection efficiency. Now, we apply this method for the total FCAE detection efficiency, which includes both diffusion and gravitational settling. The detection efficiency uncertainty for Type-B factors takes a form of

$$u_{Type-B}{}^2(\eta_{CPC}) = \eta^2_{CPC}\left(\left(\frac{u(Q)}{Q}\right)^2 + \left(\frac{u(\eta_{FC})}{\eta_{FC}}\right)^2 + \left(\frac{u(\beta)}{\beta}\right)^2 + \left(\frac{u(I)}{I}\right)^2\right), \quad (9)$$

in which, $u(Q)$ is the flow measurement standard uncertainty of 0.008 L/min (0.54%). The flow rate is given in the instrument inlet conditions, and this conversion requires pressure and temperature information. The uncertainties of temperature and pressure are small and not included in the evaluation. The values and associated uncertainty values of the bias $u(\beta)$ were taken from Figure 4. The current measurement standard uncertainty $u(I)$ is 0.06%, except for the smallest particle size, due to low particle concentration and challenging electrometer calibration at low currents 0.25%.

Type-A and Type-B uncertainties are combined, resulting in a total uncertainty of

$$u(\eta_{CPC}) = \sqrt{u^2_{Type-A}(\eta_{CPC}) + u^2_{Type-B}(\eta_{CPC})}, \quad (10)$$

which is multiplied by the coverage factor $k = 2$ in the final results to obtain expanded uncertainty at a 95% confidence level.

The CPC 3775 counting efficiency, including uncertainties, is shown in Figure 5. The 50% (lower) cut-size measured with silver particles is 5.1 nm. Hermann et al. (2007) have measured similar values for silver particles with two CPC 3775's, for one CPC approximately 4 nm and for the other 5 nm. The particle material changes from silver to DEHS at 15 nm particle size. This 15 nm point was measured with both materials to see if there was some material dependency. However, the detection efficiencies are almost the same for both the materials, 0.876 ± 0.012 for silver and 0.881 ± 0.012 for DEHS, which are within the uncertainty limits ($k = 2$). When the particle size increased, the CPC counting efficiency increased gradually peaking at 0.957 at 275 nm particle

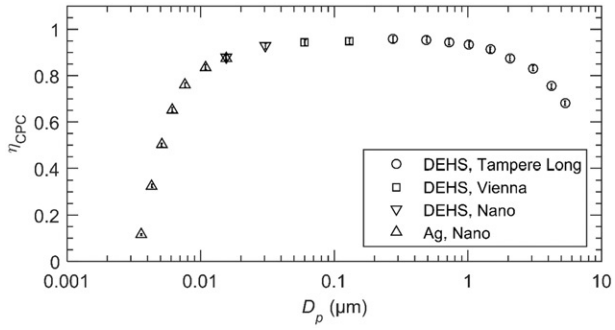

Figure 5. CPC 3775 detection efficiency η_{CPC} as a function of particle mobility diameter D_p including expanded uncertainties ($k = 2$). The measurement point particle material and the DMA type is given in the legend.

Table 1. Components of the expanded ($k = 2$) calibration uncertainties (%) for three different particle diameters.

	Particle diameter		
Uncertainty factor	3.6 nm	720 nm	5.3 µm
Type-A uncertainty (Noise)	0.36	0.04	0.25
Bias of the flow splitting	2.61	0.73	0.91
Electrometer calibration factor	0.50	0.12	0.12
Flow rate measurement	1.07	1.07	1.07
FCAE detection efficiency	1.27	0.01	0.19
Total	3.15	1.30	1.40

diameter. Above this, the detection efficiency begins to decrease gradually. At 1 µm particle diameter, the detection efficiency is is 0.93 and drops down to 0.68 at 5.3 µm particle diameter. In general, the shape of the measured detection efficiency curve resembles the detection efficiency of the CPC 3772 (TSI Inc.), which has been characterized using multiple particle generation and reference methods by Yli-Ojanperä et al. (2012).

The uncertainty components of the CPC calibration are shown in Table 1. The calibration uncertainty depends on the particle diameter. The highest expanded uncertainty value of 3.15% ($k = 2$) is obtained for the smallest particle size of 3.6 nm. In this case, the most significant component is the uncertainty of the flow splitter bias, which was measured at low particle concentrations and consequently at low current levels resulting in a rather low signal to noise ratio. The bias is also a significant uncertainty component at the largest particle size of 5.3 µm. However, above 5 nm particle sizes, the flow measurements produces the largest uncertainty component.

There are some advantages in using the FCAE as a concentration reference as in our case. The main advantage of the FCAE is that the detection efficiency does not principally depend on particle size. There are diffusion losses for nanoparticles (<10 nm) and gravitational settling for large particles in the inlet tubing, but these losses may be calculated according to Gormley and Kennedy (1949) and Thomas (1958) and compensated. The large µm-sized particles experience losses in the bends of flow lines. In CPCs, flow lines can be more complex resulting in losses for large particles. In the case of the custom made FCAE, the inlet is a short straight tube, which goes directly into the detection area. Thus, the particle losses are minimal. Another advantage is that the FCAE can operate at different inlet flow rates, allowing the same flow rate to be used for the instrument under calibration and for the FCAE, which is optimal from the bias point of view.

On the down side, the FCAE cannot detect individual particles, as particle counters. This limits the lowest possible calibration concentration in the case of FCAE acting as a reference. At 1 L/min flow rate, 1000 1/cm^3 concentration produces a current of 2.7 fA, which is low, but the calibration is still reasonable at this electric current. At the intermediate size range, the expanded uncertainty level would be less than 2% in this case, if other uncertainty factors than the signal-to-noise ratio, and the electrometer calibration factor remained constant. The calibration concentration could be reduced to some extend, perhaps down to 200 1/cm^3, if the measurement time was increased. If the number of cycles was tripled, resulting in a total calibration time of 122 min, the expanded uncertainty would be less than 3% at 1 L/min FCAE flow rate. Another option would be to utilize the bipolar calibration routine (Pihlava et al. 2016), which increases the signal to noise ratio of the electrical measurement.

Conclusions

We have introduced an aerosol instrument calibration setup based on the work by Uin et al. (2009) and Yli-Ojanperä et al. (2010) with an exceptionally wide particle size range. The setup relies on production of singly charged particles, allowing both size and concentration calibrations. The FCAE is used as a concentration reference, which allows definition of a traceable particle concentration through electric current and flow rate measurements in a wide size range. The advantages, in addition to the wide size range, are that a single particle generator covers the whole particle size range and that the particle size selection is straightforward using DMAs. The size is selected by adjusting correct saturator temperature and correct DMA settings, including selection of the DMA. As

commercial DMAs have limited size ranges, a new DMA was developed for µm-sized particles. Previously (e.g., Yli-Ojanperä et al. 2012), multiple, completely different particle generation methods and different concentration references have been required to cover the size range, which is now possible with the new setup.

The operation of the main components was tested. The particle size as a function of the growth unit saturator temperature was measured. The transfer function of the constructed Tampere Long DMA was also measured. The transfer function was not completely triangular with 20 L/min sheath and 2 L/min sample flows, but the resolution of the DMA was still at 7.95. In the number concentration calibrations, the flow splitting between the instrument and reference is important. To this end, a new flow mixing and splitting setup was designed and constructed. We measured the flow splitter bias with two identical FCAEs at equal inlet flow rates as a function of the flow rates, and observed some dependency on the flow rate at 5.3 µm particle size. The bias was also studied as a function of the particle size between 3.6 nm and 5.3 µm at 1.5 L/min inlet flow rates. The measured bias values were found to be smaller than ±1% in the whole measured particle size range at 1.5 L/min flow rate.

The setup was applied in an example calibration of the CPC detection efficiency from 3.6 nm to 5.3 µm. The size range of the developed setup was wide enough to define the cut diameter of 5.1 nm and to see the decrease in the counting efficiency above 1 µm particle sizes. The expanded uncertainties ($k = 2$) of the detection efficiencies were less than 4% through the entire size range and less than 2% between 5 nm and 5.3 µm. The smallest particle sizes are associated with the largest uncertainties, due to low particle concentrations in both bias and CPC calibration measurements, which affect especially the uncertainty of the bias. Above 5 nm particle size, the most significant uncertainty factor is the flow measurement.

In summary, the developed calibration setup is relatively easy to use and is based on the example CPC calibration it suits very well for the calibration of various CPCs and other aerosol instruments. When compared with other available methods in the µm-size range, the calibration concentrations of the developed setup are relatively high, approximately 15,000 1/cm^3 at 2 µm particle size and more than 2,500 1/cm^3 at 5.3 µm particle size, which allows calibration of low sensitivity instruments. The future tasks are to enhance the calibration setup size accuracy by calibrating classification DMAs against multiple reference sizes and to estimate the uncertainty for the output size.

Acknowledgments

Authors thank Antti Lepistö, Veli-Pekka Plym and Timo Lindqvist for manufacturing the calibration setup components.

Funding

The authors gratefully acknowledge financial support from the MMEA research program of the Cluster for Energy and Environment (CLEEN Ltd., Finland), funded by Tekes – the Finnish Funding Agency for Technology and Innovation.

References

Berglund, R. N., and Liu, B. Y. H. (1973). Generation of Monodisperse Aerosol Standards. *Environ. Sci. Technol.*, 7:147–153.

CEN/TS 16976:2016. Ambient Air – Determination of the Particle Number Concentration of Atmospheric Aerosol.

Duan, H. Romay, F. J., Li, C., Naqwi, A., Deng, W., and Liu, B. Y. H. (2016). Generation of Monodisperse Aerosols by Combining Aerodynamic Flow-Focusing and Mechanical Perturbation. *Aerosol Sci. Technol.*, 50:17–25.

European Commission (2008). Commission Regulation (EC) No 692/2008 of 18 July 2008 implementing and amending Regulation (EC) No 715/2007 of the European Parliament and of the Council on Type-approval of Motor Vehicles with Respect to Emissions from Light Passenger and Commercial Vehicles (Euro 5 and Euro 6) and on Access to Vehicle Repair and Maintenance Information. *Official Journal of the European Union*, L 199.

Fletcher, R. A., Mulholland G. W., Winchester M. R., King, R. L., and Klinedinst, D. B. (2009). Calibration of a Condensation Particle Counter Using a NIST Traceable Method. *Aerosol Sci. Technol.*, 43:425–441.

Fuchs, N. A. (1963). On the Stationary Charge Distribution on Aerosol Particles in a Bipolar Ionic Atmosphere. *Geofis. Pura Appl.*, 56:185–193.

Gormley, P. G., and Kennedy, M. (1949). Diffusion from a Stream Flowing through a Cylindrical Tube. *Proc. R. Irish Acad.*, 52:163–169.

Gupta, R., and McFarland, A. R. (2001). Experimental Study of Aerosol Deposition in Flow Splitters with Turbulent Flow. *Aerosol Sci. Technol.*, 34:216–226.

Hermann, M., Wehner, B., Bischof, O., Han, H.-S., Krinke, T., Liu, W., Zerrath, A., and Wiedensohler, A. (2007). Particle Counting Efficiencies of New TSI Condensation Particle Counters. *J. Aerosol Sci.*, 38, 674–682.

Hillamo, R., and Kauppinen E. (1991) On the Performance of the Berner Low Pressure Impactor. *Aerosol Sci. Technol.*, 14:33–47.

Högström, R., Yli-Ojanperä, J., Rostedt, A., Iisakka, I., Mäkelä, J. M., Heinonen, M., and Keskinen, J. (2011). Validating the Single Charged Aerosol Reference (SCAR)

as a Traceable Particle Number Concentration Standard for 10 nm to 500 nm Aerosol Particles. *Metrologia*, 48:426–436.

Högström, R., Quincey, P., Sarantaridis, D., Lüönd, F., Nowak, A., Riccobono, F., Tuch, T., Sakurai, H., Owen, M., Heinonen, M., Keskinen, J., and Yli-Ojanperä, J. (2014). First Comprehensive Inter-Comparison of Aerosol Electrometers for Particle Sizes up to 200 nm and Concentration Range 1000 cm^{-3} to 17 000 cm^{-3}. *Metrologia*, 51:293–303.

Iida, K., Sakurai, H., Saito, K., and Ehara, K. (2014). Inkjet Aerosol Generator as Monodisperse Particle Number Standard. *Aerosol Sci. Technol.*, 48:789–802.

ISO 14644-1:2015. Cleanrooms and Associated Controlled Environments – Part 1: Classification of Air Cleanliness by Particle Concentration.

ISO 27891:2015. Aerosol Particle Number Concentration — Calibration of Condensation Particle Counters.

Järvinen, A., Aitomaa, M., Rostedt, A., Keskinen J., and Yli-Ojanperä, J. (2014). Calibration of the New Electrical Low Pressure Impactor (ELPI+). *J. Aerosol Sci.*, 69:150–159.

Kauppinen, E. I., and Hillamo, R. E. (1989). Modification of the University of Washington Mark 5 In-stack Impactor. *J. Aerosol Sci.*, 20:813–827.

Keskinen, J., Pietarinen, K., and Lehtimäki, M. (1992). Electrical Low Pressure Impactor. *J. Aerosol Sci.*, 23:353–360.

Keskinen, J., Marjamäki, M., Virtanen, A., Mäkelä, T., and Hillamo, R. (1999). Electrical Calibration Method for Cascade Impactors. *J. Aerosol Sci.*, 30:111–116.

Kimoto, S., Dick, W. D., Hunt, B., Szymanski, W. W., McMurry P. H., Roberts, D. L., and Pui, D. Y. H. (2017). Characterization of Nanosized Silica Size Standards. *Aerosol Sci. Technol.*, 51:936–945.

Knutson, E. O., and Whitby, K. T. (1975). Aerosol Classification by Electric Mobility: Apparatus, Theory, and Applications. *J. Aerosol Sci.*, 8:443–451.

Li, L., Mulholland, G. W., Windmuller, L., Owen, M. C., Kimoto, S., and Pui, D. Y. H. (2014). On the Feasibility of a Number Concentration Calibration Using a Wafer Surface Scanner. *Aerosol Sci. Technol.*, 48:747–757.

Liu, B. Y. H., and Pui, D. Y. H. (1974). A Submicron Aerosol Standard and Primary, Absolute Calibration of the Condensation Nuclei Counter. *J. Coll. Interf. Sci.*, 47:156–171.

Marjamäki, M., Keskinen, J., Chen, D.-R., and Pui, D. Y. H. (2000). Performance Evaluation of Electrical Low Pressure Impactor (ELPI). *J. Aerosol Sci.*, 31:249–261.

Marple, V. A., Rubow, K. L., and Behm, S. M. (1991). A Microorifice Uniform Deposit Impactor (MOUDI): Description, Calibration, and Use. *Aerosol Sci. Technol.*, 14:434–446.

Owen, M., Mulholland, G., and Guthrie, W. (2012). Condensation Particle Counter Proportionality Calibration from 1 Particle·cm^{-3} to 10^4 Particles·cm^{-3}. *Aerosol Sci. Technol.*, 46:444–450.

Pihlava, K., Keskinen, J., and Yli-Ojanperä, J. (2016). Improving the Signal-to-Noise Ratio of Faraday cup Aerosol Electrometer Based Aerosol Instrument Calibrations. *Aerosol Sci. Technol.*, 50:373–379.

Romay-Novas, F., and Pui, D. Y. H. (1988). Generation of Monodisperse Aerosols in the 0.1–1.0-μm Diameter Range Using a Mobility Classification–Inertial Impaction Technique. *Aerosol Sci. Technol.*, 9:123–131.

Sinclair, D., and La Mer, V. K. (1948). Light Scattering as a Measure of Particle Size in Aerosols. *Chem. Rev.*, 44:245–267.

Thomas, J. W. (1958). Gravity Settling of Particles in a Horizontal Tube. *J. Air Pollut. Control Assoc.*, 8:32–34.

Uin, J., Tamm, E., and Mirme, A. (2009). Electrically Produced Standard Aerosols in a Wide Size Range. *Aerosol Sci. Technol.*, 43:847–853.

Uin, J., Tamm, E., and Mirme, A. (2011). Very Long DMA for the Generation of the Calibration Aerosols in Particle Diameter Range up to 10 μm by Electrical Separation. *Aerosol Air Qual. Res.*, 11:531–538.

Wiedensohler, A. (1988). An Approximation of the Bipolar Charge Distribution for Particles in the Submicron Size Range. *J. Aerosol Sci.*, 19:387–389.

Winklmayr, W., Reischl, G. P., Lindner, A. O., and Berner, A. (1991). A New Electromobility Spectrometer for the Measurement of Aerosol Size Distributions in the Size Range from 1 to 1000 nm. *J. Aerosol Sci.*, 22:289–296.

Yli-Ojanperä, J., Mäkelä, J. M., Marjamäki, M., Rostedt, A., and Keskinen, J. (2010). Towards Traceable Particle Number Concentration Standard: Single Charged Aerosol Reference (SCAR). *J. Aerosol Sci.*, 41:719–728.

Yli-Ojanperä, J., Sakurai, H., Iida, K., Mäkelä, J. M., Ehara, K., and Keskinen, J. (2012). Comparison of Three Particle Number Concentration Calibration Standards Through Calibration of a Single CPC in a Wide Particle Size Range. *Aerosol Sci. Technol.*, 46:1163–1173.

Yli-Ojanperä, J., Ukkonen, A., Järvinen, A., Layzell, S., Niemelä, V., and Keskinen, J. (2014). Bipolar Charge Analyzer (BOLAR): A New Aerosol Instrument for Bipolar Charge Measurements. *J. Aerosol Sci.*, 77:16–30.

Tampereen teknillinen yliopisto
PL 527
33101 Tampere

Tampere University of Technology
P.O.B. 527
FI-33101 Tampere, Finland

ISBN 978-952-15-4195-7
ISSN 1459-2045